HYDROLYSIS AND AQUEOUS CORROSION OF SILICATE AND ALUMINOSILICATE GLASSES VIA *AB INITIO* MOLECULAR DYNAMICS SIMULATION

A DISSERTATION IN
Physics
and
Chemistry

Presented to the Faculty of the University
of Missouri-Kansas City in partial fulfillment of
the requirements for the degree

DOCTOR OF PHILOSOPHY

by
KHAGENDRA BARAL

M.Sc., Tribhuvan University, Kathmandu, Nepal, 2007

Kansas City, Missouri
2021

HYDROLYSIS AND AQUEOUS CORROSION OF SILICATE AND ALUMINOSILICATE GLASSES VIA *AB INITIO* MOLECULAR DYNAMICS SIMULATION

Khagendra Baral, Candidate for the Doctor of Philosophy Degree

University of Missouri-Kansas City, 2021

ABSTRACT

Hydrolysis and aqueous corrosion of glass is a complex and puzzling phenomenon. Although many endeavors have been made to investigate corrosion in glass, it is still an open question with many unanswered fundamental issues. To explore the hydrolysis mechanism in glasses and provide new insights into their corrosion, single and mixed alkali ions doped silicate and aluminosilicate bulk glasses are simulated using *ab initio* molecular dynamics (AIMD). The atomic origin of the hydrolysis reaction is analyzed, and its effects on the structural, electronic, mechanical, and optical properties of the studied glasses are explored. A complete picture of interatomic bonding and charge transfer in the hydrated models is depicted and compared with dry models. A novel quantum mechanical parameter, total bond order (TBO), is introduced to characterize the internal cohesion and strength of the simulated glasses. Water in glass remains as molecular water H_2O and dissociated water OH. The ionized water attacks the silicate and aluminosilicate framework and depolymerizes it, producing Si-OH and Al-OH. The small amount of water in silicate glass enhances its mechanical strength while excess water deteriorates it.

The aqueous corrosion on a surface is investigated, further simulating the glass-water interface models of aluminosilicate glasses using AIMD. The local short- and intermediate-range order properties embedded in pair distribution function, coordination number, bond-angle, and bond-length distribution are analyzed in detail to delineate subtle variation caused due to hydrolysis. The calculated interatomic bonding and charge transfer are compared and contrasted in the bulk, surface, and interface models. The TBO is used to analyze the effect of hydrolysis on the internal cohesion of studied glasses. Furthermore, the aqueous corrosion effects of Na/K-Cl salts on aluminosilicate glass surfaces are explored. The hydrolysis increases with the increasing concentration of salts, and KCl is more detrimental to the glass network than NaCl. The results presented here provide new insight to understand the aqueous corrosion of glass surfaces and help design mechanically strong and durable glasses.

APPROVAL PAGE

The faculty listed below, appointed by the Dean of the School of Graduate Studies, have examined a dissertation titled "Hydrolysis and Aqueous Corrosion of Silicate and Aluminosilicate Glasses Via *Ab Initio* Molecular Dynamics Simulation" presented by Khagendra Baral, candidate for the Doctor of Philosophy degree, and certify that in their opinion it is worthy of acceptance.

Supervisory Committee

Wai-Yim Ching, Ph.D., Committee Chair

Department of Physics and Astronomy

Da-Ming Zhu, Ph.D.

Department of Physics and Astronomy

Paul Rulis, Ph.D.

Department of Physics and Astronomy

Zhonghua Peng, Ph.D.

Department of Chemistry

Xiaobo Chen, Ph. D.

Department of Chemistry

CONTENTS

LIST OF ILLUSTRATIONS

LIST OF TABLES

ACKNOWLEDGMENTS

I would like to express my sincere gratitude to my advisor Professor Wai-Yim Ching for his admirable co-operation and inspirable guidance throughout this work. This endeavor would not have been possible without his support.

I would like to thank Professor Da-Ming Zhu, Professor Paul Rulis, Professor Zhonghua Peng, and Professor Xiaobo Chen for kindly serving in my dissertation committee and encouraging me, providing valuable suggestions and guidance for this work. I would also like to thank Dr. Aize Li from Corning Incorporated for her help and support in our collaborative works.

I am grateful to my parents, whose love and support have significantly helped bring me to this position. They have been the constant source of inspiration throughout my life. In addition, I would like to thank my wife Ajita for her unwavering support in every aspect, and my son Kritik and daughter Kritika, whose smiles, hugs, and kisses always bring great pleasure and happiness to my life.

My special thanks go to my colleagues and all friendly and helpful members of the Electronic Structure Group for their enormous supports throughout my graduate career. In addition, I would like to express my appreciation to the school of graduate studies at UMKC for the grant support for this interdisciplinary research work. Finally, I want to thank the University of Missouri-Kansas City, the Department of Physics and Astronomy, the Department of Chemistry, the National Energy Research Scientific Computing Center, and Research Computing Resources of the University of Missouri for their support in many ways.

DEDICATION

I dedicate this work to my family.

CHAPTER 1

INTRODUCTION

The thirst for discovering new materials for the better living of humans is never satisfied. For example, even if the history of glassmaking dates back to 3600 years ago, a search for the design and development of better glasses is still going on.[1] However, developing the new materials based on trial and error is time-consuming and costly. Therefore, material scientists play a crucial role in finding and developing new materials. In this regard, laboratory experiments are essential in testing the theories, performing the experiments, and providing scientific conclusions to design and create new materials. However, the experiments are not viable in all cases or expensive and time-consuming. Moreover, in many cases, although the experiment can characterize the structure and properties of a material, it cannot provide atomistic information required for a comprehensive understanding of that material and its properties.

Alternatively, a computer simulation effectively complements the experiment and provides new findings. In many cases, the atomistic information from computer simulation helps rationalize and tailor the experimental process to propose further or new investigation. In the last few decades, computing resources have been increasing along with new computational opportunities. The introduction of high-performance computer systems and developing efficient numerical algorithms are significantly advancing the simulation field. Furthermore, the developed computational resources have empowered the computational studies to cover various topics, from microstructure to macro simulations, and in various

scientific fields such as condensed matter physics, biophysics, medical physics, astrophysics, geology, chemistry, and many more.

The two main simulation techniques used in studying the material are a classical and an *ab initio* method. The classical approach is based on the interatomic potential that describes the interactions between particles. In contrast, the *ab initio* method is based on quantum mechanics and evolved from density functional theory (DFT). In the *ab initio* method, each atom's electronic degree of freedom is used to compute the forces, making it more accurate than the classical approach. The *ab initio* methods have become increasingly popular in material science research and provided many valuable results in recent years. Many reviews and books have highlighted the importance of various *ab initio* methods to solve real-world problems in material science.[2, 3]

This study uses DFT and *ab initio* calculations to explore details of the structure and properties of silicate and aluminosilicate glasses. The main focus is to study the aqueous corrosion and durability in these glasses relevant to industrial and technological applications. The temperature-dependent properties are simulated using *ab initio* molecular dynamic (AIMD). As DFT is primarily a ground-state theory, it cannot directly simulate the temperature-dependent properties of materials. However, the dynamic behavior can be simulated within the classical mechanic's principle adopting approximation of DFT. The following subsections will introduce and discuss the types and properties of silicate and aluminosilicate glasses studied in this dissertation.

1.1. Structure of Silicate and Aluminosilicate Glasses

Silica glass (SiO_2) is an amorphous material that exhibits only short- and medium-range order properties. Its structure is well defined by a continuous random network (CRN) model as proposed by W. H. Zachariasen in his pioneering work *"The atomic arrangement in glass"*.[4] According to the CRN, the Si atom in SiO_2 is tetrahedrally coordinated by four O atoms forming SiO_4 tetrahedral units, as shown in **Figure 1**. These tetrahedra are interconnected at the corner by O called the bridging oxygen. The continuous arrangement of these tetrahedra results in the polymerized glass network. The random distribution of inter-tetrahedral angles lacks long-range order resulting in the rich intermediate-range order. After Zachariasen's work, much progress has been made in elucidating silica glass structures. Experimental methods like X-ray absorption fine structure (XAFS) [5, 6], nuclear magnetic resonance (NMR) spectroscopy [7, 8], neutron diffraction [9] in combination with molecular dynamics simulations [10, 11] have been widely used to explore the local structures of this glass. All these studies support the structure of silica glass as proposed by the CRN model.

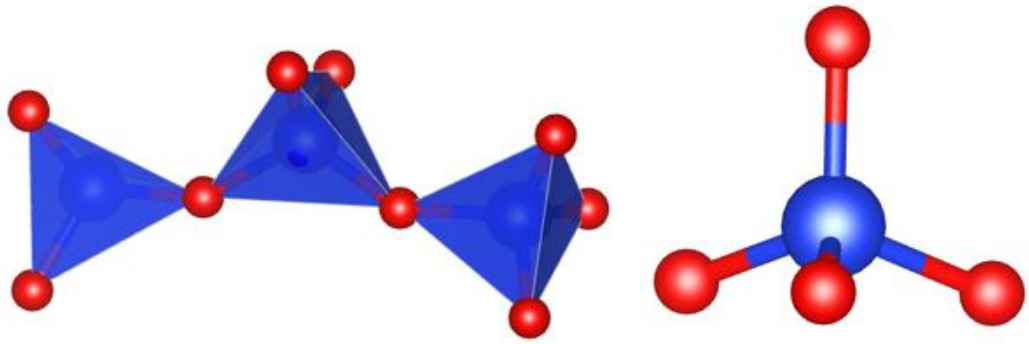

Figure 1. Geometry of SiO_4 tetrahedra in silica glass. (Si = Blue, and O = Red)

Most of the commercial and technologically important glasses are made by doping other oxides into silica as impurities. For example, SiO_2 glass doped with network modifier alkali ions finds wide application as a basis for commercially available glasses.[12] The alkali cations in silica break the Si-O-Si network and convert the bridging oxygen to a non-bridging one. Nevertheless, the backbone of the glass network remains the same. The alkali cations are weakly bonded with oxygen forming a predominantly ionic bond, as shown in **Figure 2**. The modified random network (MRN) model could explain the network of alkali doped glasses.[4] It states that the alkali silicate glass network comprises a well-polymerized silica skeleton and a depolymerized network rich in alkali ions.[13-15]

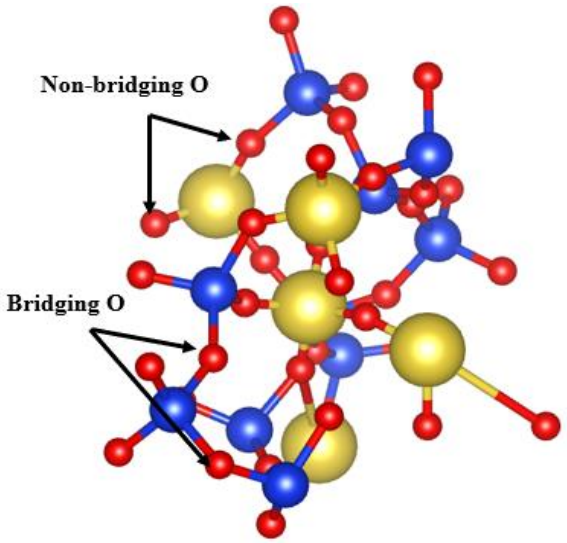

Figure 2. Structure of alkali silicate glass network. (Si = Blue, O = Red, and Alkali ion = Golden)

Alumina is a conditional glass former. Alumina doped in silica either adjusts to the network forming $[AlO4]^{-}$ tetrahedrons or acts as a network modifier being in a higher coordinated state (5 or 6).[16-18] If Al joins the network forming $[AlO_4]^{-}$ tetrahedrons, three

such tetrahedrons are interconnected, sharing one oxygen called tri-cluster O.[19-21] Although Al forms $[AlO4]^{-}$ tetrahedrons, they carry a negative charge and differ from neutral SiO_4 tetrahedra. In the case of alkali doped aluminosilicate (AS), the glass network becomes even more complex, as discussed below.

The ternary network of alkali AS is far more complicated than binary AS glass. The Si and Al still form tetrahedral units, but the alkali ions act either as a charge compensator for Al tetrahedron $[AlO_4]^{-}$ or break the network to produce non-bridging oxygen (NBO). The alkali/aluminum ratio R usually determines the roles of alkali ions, and their effect can be discussed by dividing into three regions: peraluminous (R<1), meta-aluminous (R=1), and peralkaline (R>1). In the R < 1 region, all alkali ions are used to compensate charge in Al tetrahedrons. Since alkali ions are not enough to neutralize all Al tetrahedrons, the remaining Al forms tetrahedrons producing tri-cluster O or modifies the network to adopt higher coordination. Some previous studies have shown the existence of both tetrahedral and octahedral coordinated Al, while some studies have proposed only four-coordinated Al in this region.[18, 22, 23] In the R = 1 region, enough alkali ions are present to compensate the charge in $[AlO_4]^{-}$ units, so none of them will produce NBO, indicating that the glass structure is fully polymerized. Some experimentalists support this notion.[24-26] However, some experimental studies disagree with this conclusion as they have shown the existence of NBOs for R = 1.[16, 27, 28] All these raise questions about the validity of the assertion that at R = 1, all alkali ions behave as charge compensators, and alkali AS glass is fully polymerized. In the R > 1 region, some alkali ions are used to neutralize charge in Al tetrahedrons, while the remaining ions modify the network, breaking the Si-O-Si bond and producing NBOs. Hence, for R > 1, alkali

ions act as both a charge compensator and a network modifier. The presence of NBO in alkali AS glass significantly influences their physical, transport, and thermodynamics properties, chemical durability, hardness, glass transition temperature, etc. Understanding such effects on glass properties is essential for designing better glass products. The alkali AS glasses with composition R = 1 have drawn significant attention as they exhibit a drastic change in their physical properties compared with the other two regions. In addition, the surface structure of these glasses becomes even more complex due to the presence of dangling bonds. In such models, the concentration of NBO will increase on the outer surface.[29]

1.2. Mixed Alkali Effect

Alkali-doped silicate glasses exhibit an anomalous property known as the mixed alkali effect (MAE), which yields a nonlinear variation on glass properties when two different alkali ions are present.[30-36] When one alkali replaces another in an oxide glass, several properties vary as a function of composition in a non-additive fashion. The ionic transport-related properties such as electrical conductivity, ionic diffusion coefficient, ionic mobility, and viscosity mostly exhibit pronounced MAE.[37, 38] On the other hand, the bulk thermodynamic properties like molar volume and density, mechanical properties, refractive index, thermal expansion coefficients show comparatively small MAE.[38] Despite numerous studies on MAE, its origin is still under debate.[39] Therefore, the atomistic picture of interatomic bonding is essential for understanding this phenomenon.

1.3. Hydrolysis of Bulk Silicate and Aluminosilicate Glasses

The water solubility in silicate and AS glasses has drawn significant attention as water is pervasive, and these glasses show a considerable effect of corrosion in an aqueous

environment. Water in glass, which exists as ionized water OH and molecular water H_2O, significantly affects its mechanical strength, chemical durability, and other physical and chemical properties.[40, 41] Even a trace of water in glass can cause drastic changes in properties like density, viscosity, glass transition temperature, thermal expansion coefficient, mechanical strength, and refractive index.[42-48] Hydrolysis in pure silicate and alkali silicates is well studied, which proposes that water breaks the Si-O-Si linkage producing Si-OH following the reaction:

$$Si{-}O{-}Si + H_2O \rightarrow 2Si{-}OH \quad (1.1)$$

However, the hydrolysis in a more complicated multicomponent network like AS and alkali AS glasses is comparatively less studied, and still, many things are left to be revealed. Different theories are proposed to explain the hydrolysis in these glasses. Unlike silica, whether the AS network is depolymerized or not due to hydrolysis is the subject of contention among glass researchers. Many arguments are made in support of and against the depolymerization of this glass network, which makes hydrolysis in alkali AS glasses even more controversial and intriguing. Some studies have shown due to hydrolysis, OH groups behave as bridging hydroxyls in the form of Si−OH−Al linkages and free hydroxyls as M−OH (M=Na, K), leaving the degree of network polymerization unchanged. However, this mechanism is severely criticized by other studies. They support the depolymerization of the AS framework by water and the formation of Si−OH and Al−OH species. Despite numerous studies and investigations, the structural role of water in alkali doped silicate and AS glasses remains unclear. Therefore, a definitive conclusion regarding the hydrolysis of these glasses at the atomistic level is still lacking.

1.4. Aqueous Corrosion of Aluminosilicate Glass Surfaces

Glass surface provokes a significant interest due to its disproportionality. It plays a vital role in its performance in many applications like display technology, nuclear waste glasses, etc. [49-52] Corrosion of silicate glass surfaces by water in the aqueous environment is more common.[53-56] Aqueous corrosion is slower than acidic corrosion; however, it degrades the glass network and reduces its performance. The ionized water enters the glass in the aqueous corrosion by hydrolyzing the surface. At ordinary temperatures, glass corrosion by water is slower but becomes more significant at higher temperatures.[53, 57] Aqueous corrosion of silicate glasses is a great issue in the immobilization of nuclear waste materials, bioactive glasses for biomedical application, application as glass reaction chambers, etc., and it has drawn sufficient interest in recent years.[54, 58-61]

The water can be transported in glass by two mechanisms: proton transfer, i.e., ionic diffusion between network modifying cation and hydrogen [62], and water diffusion.[63] The proton transfer can go farthest from the glass surface than water diffusion. The proton transfer is more common in silicate glass containing network modifying cations. When water reacts on the aluminosilicate surface, T-OH (T = Si, Al) are the main functional groups created, breaking the T-O-T bonding. This hydrolysis reaction is well represented by:

$$\text{T-O-T} + H_2O \rightarrow 2\ \text{T-OH} \qquad (1.2)$$

This reaction is supposed to degrade the glass network and reduce mechanical strength in silicate glass.[64, 65] The hydrolysis of the glass surface and T-OH formation increases with time and propagates into the bulk region.

The presence of leachable alkali ions makes hydrolysis of alkali aluminosilicate glass more complicated. Due to the network modifier alkali ions, the NBO sites immediately react with nearby water molecules dissociating them into H^+ and OH^-, and get hydrated. The protonation of the NBO site results in M-OH and T-OH (T=Si, Al). The M-OH later dissociates into M^+ and OH^- ions. In addition, the proton diffuses into the bulk region through discrete proton hopping between two adjacent NBO sites. Continuation of this reaction causes more water molecule dissociation on the surface and propagation of glass hydrolysis. Hence, in alkali aluminosilicate glass, in addition to the glass water reaction (1.2) mentioned above, the following ion-exchange processes is to be accounted for:

$$TO\text{-}M + H_2O \rightarrow T\text{-}OH + M\text{-}OH \quad (1.3)$$

$$M\text{-}OH \rightarrow M^+ + OH^- \quad (1.4)$$

The process of M^+ ion extracted to the liquid media from the glass matrix is leaching in the glass. The leaching of M in charge-balanced conditions will be slower as compared to M in the NBO position. Therefore, it is crucial to analyze the chemical modification of hydrated surface and cation dissociation to the solution to understand the effects of surface chemistry in silica and silica-based glasses.[66] The glass dissolution rate becomes intensive in the presence of salts like NaCl/KCl.[67]

The experimental techniques such as infrared (IR), Raman, and nuclear magnetic resonance (NMR) spectroscopy, X-ray photoelectron spectroscopy (XPS), neutron diffraction, magic angle spinning NMR, sum frequency generation, electron microprobe (EMP) analysis, Auger electron spectroscopy (AES), secondary ion mass spectroscopy (SIMS), spectroscopic ellipsometry (SE) etc., are widely used to explore the water effect in silicate glass and change

in surface chemical composition due to glass-water reaction.[42, 68-75] Vibrational spectroscopy techniques are used to investigate the surface characterization of the water absorbed layer and the polarization of water molecules [76]. Although the experimental studies are targeted to probe the characteristic changes on the glass surface aftermath reaction of water, they are unable to extract the critical information regarding the structural characterization and chemical reaction mechanism at atomistic level as the breaking of glass network, dissociation of water and recombination of O and OH groups around Si, Al and alkali ions are complex atomic process. Thus, despite intensive experimental investigations with advanced characterization, the fundamental question regarding the origin of the glass-water reaction mechanism and transport behaviors of ions in the surface and corroded regions is still unclear. Hence, a detailed understanding of hydrolysis reaction mechanism and diffusion of ions with accurate information of glass surface chemistry at an atomic level is essential to elucidate the glass corrosion behavior and its stability against the environment for the designing and to produce new glass composition with improved chemical durability and stability. In this regard, accurate theoretical simulation is a viable tool to provide deep insights and new predictions in parallel with experimental efforts. The computer simulation techniques like *ab initio* molecular dynamics (AIMD) in a limited amount and classical MD and mesoscale simulations using Kinetic Monte Carlo are widely used to study glass-water reactions.[77-84] The force field in MD simulation must be sufficiently accurate to explain the chemical reaction, dissociation, and bond formation. The used forces are either empirical force fields or calculated by quantum mechanical methods. The routinely used classical MD can handle a larger system, and for a longer time frame, however availability of empirical potentials, especially that one can

correctly express glass surface-water reaction, is still lacking. Moreover, in the case of a multicomponent complex system with mixed covalent, ionic, and hydrogen bonding, it will be even more challenging in classical MD to have a sufficiently accurate potential to describe such complex interatomic interaction. In this aspect, first-principles simulation is the only alternative to reproduce glass hydrolysis reactions and provide reliable results. The quantum mechanics-based AIMD method can achieve a high degree of numerical accuracy and simulate chemical reactions by calculating the electronic contributions of the system. Thus, AIMD is a valuable tool for studying glass corrosion in an aqueous environment and is necessary for this study to provide details of the structural and dynamic information of glass-water reactions.

1.5. Outline of Dissertation

The outline of this dissertation is as follows. Chapter 2 discusses the theoretical methods and computational packages used in this study. Chapters 3, 4, and 5 are devoted to discussing hydrolysis and aqueous corrosion mechanisms of silicate and aluminosilicate glasses. The results in this dissertation divide mainly into two parts:

Part I: This part deals with the hydrolysis of bulk alkali silicate and aluminosilicate glasses studied using *ab initio* calculations (Chapters 3 and 4). These chapters are based on our published work in alkali silicates [85, 86] and aluminosilicates glasses.[87, 88]

Part II: This part focuses on the aqueous corrosion and durability of an aluminosilicate glass surface, including the effect of Na/K-Cl salts (Chapter 5). This chapter is based on the extension of our works in aluminosilicate glasses.[87, 88]

A final synopsis is presented in chapter 6, which summarizes the results presented in this dissertation and potential future research in this direction.

CHAPTER 2

THEORY AND METHODOLOGY

This chapter discusses the details of the theoretical framework used in this study. We used DFT-based [89, 90] two *ab initio* computational packages: (i) Vienna *ab initio* simulation package (VASP) [91, 92]and (ii) Orthogonalized linear combination of atomic orbitals (OLCAO) [93]. This chapter also introduces the methodology adopted to collect and analyze the data. The use of *ab initio* calculations in this study over the classical approach ensures the accuracy and reliability of the results presented in this dissertation.

2.1. Density Functional Theory

DFT is a most popular and versatile quantum mechanical approach widely used in Physics, Chemistry, Biology, Minerology, Material Engineering, and other related areas to calculate the ground-state electronic structure and fundamental properties of materials. DFT has a primary consequence: it treats a many electrons system as a functional of ground-state electron density and gives the physical properties of that system. It is widely popular in the computational material field because of its reasonable accuracy and computational cost. Furthermore, it reduces the many-body wave function to the ground state electronic density of state, reducing the 3N (N= total number of electrons in the system) dimensionality of the problem into 3 degrees of freedom. DFT uses a wave function as a central quantity that contains all the information of a system.

The basic understanding of atoms and molecules starts from solving the non-relativistic time-independent Schrodinger equation for many-atom and many-electron system defined as:

$$\hat{H}\Psi = E\Psi \tag{2.1}$$

where, Ψ is the many-electron wave function. $\hat{H}$ is the Hamiltonian of a system with N electrons and M nuclei defined as:

$$\hat{H} = -\frac{\hbar^2}{2}\sum_{\alpha=1}^{N}\frac{\nabla_\alpha^2}{m_\alpha} - \frac{\hbar^2}{2m_e}\sum_{i=1}^{N}\nabla_i^2 + \sum_{\alpha=1}^{M}\sum_{\beta>\alpha}\frac{Z_\alpha Z_\beta e^2}{r_{\alpha\beta}} - \sum_{\alpha=1}^{M}\sum_{i=1}^{N}\frac{Z_\alpha e^2}{r_{i\alpha}} + \sum_{i=1}^{N}\sum_{i>j}\frac{e^2}{r_{ij}} \tag{2.2}$$

where, i, j refers to electrons, α , β denotes nuclei, m_e is the mass of the electron, and m_α is the mass of the nuclei. Here, the first term represents the kinetic energy of the nuclei; the second term is the kinetic energy of an electron; the third term is the repulsion potential energy between nuclei of atomic number Z_α , Z_β and the fourth term gives the potential energy for Coulomb attraction between electron and nucleus.

It is a great challenge to solve the Schrodinger equation (2.1) for a many-body system using the Hamiltonian $\hat{H}$ given by equation (2.2). So, it is necessary to introduce some approximations to solve the Schrodinger equation (2.1). The first approximation introduced is the Born-Oppenheimer approximation which treats atomic nuclei at rest and deals with the motion of electrons. Since the mass of the nuclei is much larger than that of an electron, i.e., $m_\alpha >> m_e$, the atomic nuclei move much slower than the electrons. Therefore, the motions of electrons and nuclei can be treated separately. Under Born-Oppenheimer approximation, electronic Hamiltonian of N electrons and M nuclei can be expressed as:

$$\hat{H} = -\frac{\hbar^2}{2m_e}\sum_{i=1}^{N}\nabla_i^2 - \sum_{\alpha=1}^{M}\sum_{i=1}^{N}\frac{Z_\alpha e^2}{r_{i\alpha}} + \sum_{i=1}^{N}\sum_{i>j}\frac{e^2}{r_{ij}} \tag{2.3}$$

For a system containing many electrons or molecules, equation (2.3) is still complex. Moreover, since most physical problems generally consist of many interacting electrons and ions, equation (2.3) is still unsolvable for such cases. In the early 20s, many efforts have been

made to develop the methods which can solve, at least approximately, the Schrodinger equation for the many-body systems. Some of such adopted approaches were Hartree-Fock (H-F) [94], perturbation theory [95], Green's function method [96], configuration interactions [97], etc. However, all these wave function-based methods turn out to be computationally expensive, even for a small system containing 50 atoms.[98] Thus, for a real-world problem containing a large system size, DFT is the proper choice.

The DFT has its root in the Thomas-Fermi (T-F) model, developed around the 1920s, where they approximated the electron distribution in an atom using a statistical approach. However, as no molecular binding was included in the T-F model [99], its accuracy was very low. Hence, this model was primitive in terms of quantitative predictions for solid-state Physics. However, the T-F model approximates the DFT formulation made by Hohenberg-Kohn (H-K) theorem.[89] Hence, H-K's work in 1964 was the most crucial step towards developing the DFT.[89] The modern formulation of DFT, as proposed by H-K, states that the density of particles can be treated as a basic variable based on which all properties of a system can be treated as functional. Later in 1965, Kohn and Sham (K-S) [90] published their work, which is the most modern approach to calculate the material's electronic structure properties.

The ground state energy and wave function of an electronic system is related as:

$$E\Psi = \frac{\left\langle \Psi \mid \hat{H} \mid \Psi \right\rangle}{\left\langle \Psi \mid \Psi \right\rangle} \tag{2.4}$$

where $$\left\langle \Psi \mid \hat{H} \mid \Psi \right\rangle = \int \Psi^{*} \hat{H} \Psi dx \tag{2.5}$$

and $$\hat{H} = \hat{T}_{el} + \hat{V}_{ee} + \sum_{1}^{N} V_{ext}(\vec{r}) \tag{2.6}$$

for an N electron system. Here, N and $V_{ext}(\vec{r})$ determine all ground state properties.

The H-K theorem uses potential $V(\vec{r})$ and electron density $\rho(\vec{r})$ instead of numbers of electrons N to define the character of an atom. The first H-K theorem states that "The external potential $V_{ext}(\vec{r})$ is a unique functional of electronic density $\rho(\vec{r})$". Hence, the electron density $\rho(\vec{r})$ can determine the system's ground state energy and wave function using the H-K theorem. The ground state energy of any system in the presence of external potential $V_{ext}(\vec{r})$ can be written as a function of electron density $\rho(\vec{r})$ as:

$$E_V[\rho(\vec{r})] = \int \rho(\vec{r}) V_{ext}(\vec{r}) dr + F_{HK}[\rho(\vec{r})] \tag{2.7}$$

where $F_{HK}[\rho(\vec{r})]$ is a universal functional of $\rho(\vec{r})$. It is a sum of kinetic energy $T[\rho(\vec{r})]$ and electron-electron interactional energy $V_{ee}[\rho(\vec{r})]$. $F_{HK}[\rho(\vec{r})]$ is independent of the external potential $V_{ext}(\vec{r})$. Therefore, $F_{HK}[\rho(\vec{r})]$ can be expressed as:

$$F_{HK}[\rho(\vec{r})] = T[\rho(\vec{r})] + V_{ee}[\rho(\vec{r})] \tag{2.8}$$

where, $$T[\rho(\vec{r})] = \left\langle \Psi_0 \mid \hat{T} \mid \Psi_0 \right\rangle \tag{2.9}$$

and $$V_{ee}[\rho(\vec{r})] = \left\langle \Psi_0 \mid \hat{V}_{ee} \mid \Psi_0 \right\rangle \tag{2.10}$$

We can simplify

$V_{ee}[\rho(\vec{r})]$ as,

$$V_{ee}[\rho(\vec{r})] = J[\rho(\vec{r})] + E_{ncl}[\rho(\vec{r})] \tag{2.11}$$

with $$J[\rho(\vec{r})] = \frac{1}{2} \iint \frac{\rho(\vec{r})\rho(\vec{r}')}{|\vec{r} - \vec{r}'|} d\vec{r} d\vec{r}', \tag{2.12}$$

In equation (2.11) $J[\rho(\vec{r})]$ is a classical Coulomb repulsion part, and E_{ncl} is a non-classical term that contributes to electron-electron interaction and is the central part of 'exchange-correlation energy'. This non-classical term is a very elusive but quite important quantity.

The second H-K theorem relates minimum ground state energy with system electron density. It states that "The energy functional $E_V[\rho(\vec{r})]$ assumes its minimum value as ground state energy E_0 for the correct ground-state electron density $\rho_0(\vec{r})$ ":

i.e $$E_0 = \int \rho_0(\vec{r}) V_{ext}(\vec{r}) d\vec{r} \tag{2.13}$$

The above equation (2.7) cannot be solved until $F_{HK}[\rho(\vec{r})]$ is known. Moreover, the functionals $E_{ncl}[\rho(\vec{r})]$ and $T[\rho(\vec{r})]$ are not well defined. This makes use of DFT for many electrons problem complexes due to unsolvable quantity $F_{HK}[\rho(\vec{r})]$. The determination of ground state energy in the given external potential helps minimize the functional of three-dimensional density function, helping to find the exact form of $F_{HK}[\rho(\vec{r})]$. As the H-K theorem does not provide the solution of the functional $F_{HK}[\rho(\vec{r})]$, K-S devised a method to find $E_V[\rho(\vec{r})]$ solving the equation for electron density $\rho(\vec{r})$ which is capable of yielding an unknown functional used in approximation.

According to K-S, the kinetic energy of a real interacting reference with the same density of non-interacting reference is:

$$T_s = -\frac{1}{2}\sum_{i=1}^{N}\left\langle \Psi_i \mid \nabla^2 \mid \Psi_i \right\rangle \tag{2.14}$$

Here, the kinetic energy T_s is not the same as the true kinetic energy of the real interacting system. In terms of T_s, $F_{HK}[\rho(\vec{r})]$ can be defined as:

$$F[\rho(\vec{r})] = T_s[\rho(\vec{r})] + J[\rho(\vec{r})] + E_{XC}[\rho(\vec{r})] \tag{2.15}$$

Solving equations (2.8) and (2.15), we get,

$$E_{XC}[\rho(\vec{r})] = [T[\rho(\vec{r})] - T_s[\rho(\vec{r})]] + [V_{ee}[\rho(\vec{r})] - J[\rho(\vec{r})]] \tag{2.16}$$

Using equation (2.11), (2.16) turns as,

$$E_{XC}[\rho(\vec{r})] = [T[\rho(\vec{r})] - T_s[\rho(\vec{r})]] + E_{ncl}[\rho(\vec{r})] \tag{2.17}$$

$$E_{XC}[\rho(\vec{r})] = T_R[\rho(\vec{r})] + E_{ncl}[\rho(\vec{r})] \tag{2.18}$$

The first term of equation (2.18) ($T_R[\rho(\vec{r})]$) gives the residual part of true KE excluding the non-interacting system. Here $E_{XC}[\rho(\vec{r})]$ is the exchange-correlation energy functional, which contains-residual part of true KE, non-classical contribution of self-interaction, and the exchange and correlation effects of potential energy.

Based on equations (2.7) and (2.15), the energy functional of a real interacting system is

$$E_V[\rho(\vec{r})] = \int \rho(\vec{r}) V_{ext}(\vec{r}) dr + T_s[\rho(\vec{r})] + J[\rho(\vec{r})] + E_{XC}[\rho(\vec{r})] \tag{2.19}$$

For a non-interacting system, the energy expression contains only 2 components: the KE T_s and energy due to interaction with the external potential $V_{ext}(\vec{r})$. Thus, we can write,

$$E_V[\rho(\vec{r})] = \int \rho(\vec{r}) V_{ext}(\vec{r}) dr + T_s[\rho(\vec{r})] \tag{2.20}$$

The minimization of equation (2.20) is unconditional, so we construct a conditional minimum problem introducing a functional $G[\rho(\vec{r})]$ as:

$$G[\rho(\vec{r})] = E_V[\rho(\vec{r})] - \frac{\lambda}{2} \int |\rho(\vec{r})|^2 d\vec{r} \tag{2.21}$$

Here λ is Lagrange's multiplier with constraints. From (2.20) and (2.21) we get,

$$G[\rho(\vec{r})] = \int \rho(\vec{r}) V_{ext}(\vec{r}) dr + T_s[\rho(\vec{r})] - \frac{\lambda}{2} \int |\rho(\vec{r})|^2 d\vec{r} \tag{2.22}$$

The stationary principle for ground-state density gives:

$$\delta\left\{E_V[\rho(\vec{r})]-\lambda\left[\int\rho(\vec{r})d\vec{r}-N\right]\right\}=0 \tag{2.23}$$

Solving this equation (2.23), we get,

$$\lambda=\frac{\delta E_V[\rho(\vec{r})]}{\delta\rho(\vec{r})} \tag{2.24}$$

Equations (2.19) and (2.24) gives:

$$\lambda=V_{ext}(\vec{r})+\frac{\delta T_s[\rho(\vec{r})]}{\delta\rho(\vec{r})}+\int\frac{\rho(\vec{r}\,')}{|\vec{r}-\vec{r}\,'|}d\vec{r}\,'+V_{XC}(\vec{r}) \tag{2. 25}$$

$$\lambda=V_{eff}(\vec{r})+\frac{\delta T_s[\rho(\vec{r})]}{\delta\rho(\vec{r})} \tag{2. 26}$$

With $V_{eff}(\vec{r})=V_{ext}(\vec{r})+\int\frac{\rho(\vec{r}\,')}{|\vec{r}-\vec{r}\,'|}d\vec{r}\,'+V_{XC}(\vec{r})$ (2. 27)

Where the exchange-correlation potential, also known as K-S potential, is the functional derivative of exchange-correlation energy E_{XC} with respect to electron density $\rho(\vec{r})$ as:

$$V_{XC}(\vec{r})=\frac{\delta E_{XC}[\rho(\vec{r})]}{\rho(\vec{r})} \tag{2.28}$$

By solving N one electron Schrodinger equation for given $V_{eff}(\vec{r})$, we can get electron density $\rho(\vec{r})$ which satisfies;

$$\left[-\frac{1}{2}\nabla^2+V_{eff}(\vec{r})\right]\Psi_i(\vec{r})=\varepsilon_i\Psi_i(\vec{r}) \tag{2.29}$$

The value of wave function $\Psi_i(\vec{r})$ obtained solving (2.29) is used to determine electron density given as:

$$\rho(\vec{r})=\sum_{i=1}^{N}|\Psi_i|^2 \tag{2.30}$$

Equations (2.27) – (2.30) are K-S equations. Based on the initial guessed electron density, $\rho(\vec{r})$ we calculate the effective potential and solve the K-S equation, and then calculate $\rho(\vec{r})$ again. If it is self-consistent, the quantities force, energy, etc., are calculated. If the electron density is not self-consistent, the effective potential is recalculated, and the process is repeated. Although the K-S approach is exact, the indeterminacy of exchange-correlation functional E_{XC} makes this equation challenging to solve. Determination of this value is in focus even in modern DFT. The exchange-correlation is determined from interaction among electrons which depends on the Coulomb interaction between them and their quantum numbers. The E_{XC} can be split into the exchange and correlation parts. The exchange interaction results from the Pauli exclusion principle, which states that two electrons in the same space cannot have the same four quantum numbers. The correlation energy is related to the correlation motion between electrons of opposite spin.

One of the approximations used to solve exchange-correlation functional is local density approximation (LDA), in which density at a certain point ***r*** is used to calculate the exchange-correlation energy of that point. According to this approximation, the exchange-correlation functional is calculated as:

$$E_{XC}[\rho(\vec{r})] = \int \rho(\vec{r})\varepsilon_{XC}[\rho(\vec{r})]d\vec{r} \tag{2.31}$$

Where, ε_{XC} is the exchange-correlation energy of an electron in a homogenous electron gas of density $\rho(\vec{r})$. Eq (2.31) gives local density functional where density is used as the main parameter to compute the exchange and correlation energy.

LDA is simple, accurate, and has a low computational cost than other approximations. It is widely used in solid-state physics to describe many ground state properties of many-electron

systems. LDA is more efficient in approximating the energy of a system correctly when the density is uniform. In this study, LDA is used in OLCAO calculation.

In the scenario where density varies rapidly, LDA needs to be corrected. LDA uses an approximation that density is uniform at a point $\boldsymbol{r}$, but most real systems are spatially non-uniform. In such a situation, the spatial variation of electron density must be included in the exchange-correlation energy functional. Including the spatial variation of electron density, the exchange-correlation energy functional becomes:

$$E_{XC}^{GGA}[\rho(\vec{r})] = \int f(\rho(\vec{r}), \nabla\rho(\vec{r}))d\vec{r} \tag{2.32}$$

Where the integral is a function of local density $\rho(\vec{r})$ and its gradient. This equation (2.32) is called generalized gradient approximation (GGA). There exist different GGAs such as PBE provided by Perdew, Burke, and Ernzerhof [100], B3LYP provided by Becke's three parameters hybrid method [101], and Lee, Yang, and Par [102]. The use of PBE is more common in Physics, while B3LYP is mostly used in Chemistry. The details of two computational packages VASP and OLCAO, will be discussed in the following sections:

2.2. Vienna *Ab Initio* Simulation Package (VASP)

VASP is a quantum mechanical computational package developed by Kresse and co-workers in 1993.[91, 103] It is widely popular in first-principles and *ab initio* molecular dynamics calculation of electronic structure and dynamics properties. It is widely used in condensed matter physics and material engineering. It has high flexibility of computing capability using a different approach to solve Schrodinger equation such as DFT method using K-S equation, H-F approximation with Green functions method using Roothaan equation, solving hybrid functionals mixing H-F with DFT, and many-body perturbation theory. A

plane-wave basis set is implemented in VASP to efficiently transform Hamiltonian operations of wavefunctions between real and reciprocal space using Fast Fourier Transform (FFT). The plane-wave basis set is implemented in VASP using two techniques: the projector augmented wave method [92, 104] and the ultra-soft pseudo-potential method.[105, 106] The first method is more accurate but more expensive than the second one in terms of calculation time.

It is difficult and practically impossible to solve all-electron plane wave. The use of pseudopotential approximation makes it easier to solve this equation. The idea of using pseudopotential is it ignores some core level nodal features and focuses on the far where the chemical bonds between two atoms are formed. There are three different types of potentials used in VASP. Norm-conserving pseudopotential [107], ultra-soft Vanderbilt pseudopotential [105, 106], and projector augmented wave (PAW).[92, 104] In this study, the PAW-PBE [100] method is adopted, one of the best GGA available in VASP.

The iterative matrix diagonalization techniques such as conjugate gradient scheme [108], the blocked Davidson algorithm [109], and the residual minimization with direct inversion of the iterative subspace (RMM-DIIS) [110, 111] are supported in VASP for self-consistency cycle (SCF) calculation. This study used RMM-DISS and blocked Davidson for efficient matrix diagonalization. The RMM-DIIS is faster, whereas the blocked Davidson is stable and slow. The blocked Davidson algorithm is used in the first iteration, followed by RMM-DIIS in the combined situation. The charge density is mixed efficiently in VASP by using Broyden and Pulay mixing scheme.[112, 113]

Due to parallelization of the code, VASP is very efficient for parallel calculation, which allows the analysis of even a larger system with a few hundred or 1000 atoms. This study uses VASP for AIMD simulation, geometry optimization, and the system's elastic and mechanical properties evaluation.

2.3. *Ab initio* molecular dynamics (AIMD)

The ground state theory discussed in the previous section is routinely used in many fields for calculation. However, many real-world problems deal with finite thermodynamic conditions with finite temperature and pressure. In AIMD, the forces are calculated based on quantum mechanics. One type of the AIMD implemented is Ehrenfest molecular dynamics which solves the time-dependent Schrodinger equation, and the nuclei are propagated using classical mechanics. Being very expensive, its applicability is limited. Another better approach is to use the Born-Oppenheimer approximation, which separates the electronic degree of freedom with nuclei propagation. This approach is known as Born-Oppenheimer molecular dynamics. Here, the electronic structure is reduced by solving the time-independent Schrodinger equation self consistently. The force calculation in each step is within Pulley correlated Hellmann-Feynman theorem. The nuclei are propagated according to classical mechanics. The Born-Oppenheimer MD can be stated as follows,

$$M_I \ddot{R}_I(t) = -\nabla_I \min_{\Psi_0} \left\{ \langle \Psi_0 | H_E | \Psi_0 \rangle \right\} \tag{2.33}$$

The AIMD calculation in this study is carried under Born-Oppenheimer MD implemented in VASP. An example of the INCAR file is given in the Appendix. In this work, the AIMD simulation is carried under an NVT ensemble where the number of particles (N), volume of the system (V), and temperature of the system (T) remain constant. A choice of proper

ensemble depends on the problem at hand. The details about MD simulation are discussed in the respective chapters.

2.4. Geometry Optimization

The geometric optimization of the structure of materials is an essential step for further analysis and properties evaluation. The initial step in assessing the preferred properties of any system is that we need a realistic, near-perfect structural model. The DFT optimized structure typically differs from the available experimental structure in lattice characteristics. Hence, the initial geometric optimization is essential for further analysis of properties.

VASP mainly consists of four input files: INCAR, KPOINTS, POSCAR, and POTCAR for the simulation of any system. The INCAR file controls the parameter in the calculation. The number of K-points based on the system size is written in KPOINTS file. The POSCAR consists of the initial position and lattice vector of the system. Finally, the POTCAR is the file that includes the information of potential for all atoms in the same order as described in the POSCAR file.

2.5. Elastic and Mechanical Properties Calculation

The elastic and mechanical properties of a material are important regarding its application for various purposes. The improvements and upgrading of computational methods have made the *ab initio* calculation of mechanical properties of materials more accurate. In general, two approaches are used to calculate the mechanical properties using the *ab initio* method. The first method is based on analyzing a crystal's total energy as a function of its volume or pressure. The total energy $E(V,\varepsilon)$ of a crystal can be written as:

$$E(V,\varepsilon) = E(V_0) + V\sum_{i=1}^{6}\sigma_i\varepsilon_i + \frac{V}{2}\sum_{i,j=1}^{6}C_{ij}\varepsilon_i\varepsilon_j + ... \tag{2.34}$$

where ε_i are strain components, σ_i are stress components, and C_{ij} are the elastic tensors. The total energies obtained from the above equation for different strains can be fitted to a parabola near the minimum energy from which the elastic constants can be derived.[114] Another approach uses the *ab initio* stress-strain relationship defined by Nielsen and Martin scheme.[115] A small strain ε is applied to a fully relaxed system. Then Hook's law is solved as:

$$\sigma_i = \sum_{j=1}^{6}C_{ij}\varepsilon_j \tag{2.35}$$

Here the stress components σ_i are linearly dependent on the applied strain ε_j and elastic constants C_{ij}. Solving the above equation, the values of elastic tensors C_{ij} and their inverse compliance tensors S_{ij} can be obtained. The bulk mechanical parameters can be evaluated using the values of C_{ij}, S_{ij}, and Voight-Reuss-Hill approximation for polycrystals.[116-118] Voight's approach gives the upper limit of bulk K_{Voight} and shear G_{Voight} modulus, while Reuss approximation gives the lower limit of bulk K_{Reuss} and shear G_{Reuss} modulus.

$$K_{Voight} = \frac{1}{9}(C_{11} + C_{22} + C_{33}) + \frac{2}{9}(C_{12} + C_{13} + C_{23}) \tag{2.36}$$

$$G_{Voight} = \frac{1}{15}(C_{11} + C_{22} + C_{33} - C_{12} - C_{13} - C_{23}) + \frac{1}{5}(C_{44} + C_{55} + C_{66}) \tag{2.37}$$

$$K_{Reuss} = \frac{1}{(S_{11} + S_{22} + S_{33}) + 2(S_{12} + S_{13} + S_{23})} \tag{2.38}$$

$$G_{Reuss} = \frac{15}{4(S_{11} + S_{22} + S_{33}) - 4(S_{12} + S_{13} + S_{23}) + 3(S_{44} + S_{55} + S_{66})} \tag{2.39}$$

Hill's approximation uses the average value of the Voight and Reuss approach and gives the bulk modulus and shear modulus values.

$$K = \frac{K_{Voight} + K_{Reuss}}{2} \tag{2.40}$$

$$G = \frac{G_{Voight} + G_{Reuss}}{2} \tag{2.41}$$

From values of K and G, the Young's modulus E and Poisson's ratio η can be obtained as follows:

$$E = \frac{9KG}{3K + G} \tag{2.42}$$

$$\eta = \frac{3K - 2G}{2(3K + G)} \tag{2.43}$$

2.6. Orthogonalized Linear Combination of Atomic Orbitals (OLCAO)

The VASP simulated structures are treated further using OLACO to evaluate the electronic structure and optical properties. The OLCAO package is an in-house package developed by Professor Ching and systematically improved and refined to study the electronic structure of a complex system. The combination of two methods, VASP and OLCAO, provides the best balance and approach between accuracy, efficiency, cost and has been applied in the study of many complex systems.

The OLCAO is used to calculate the electronic structure, interatomic bonding, partial charge, and optical properties of simulated models. It is an all-electron method based on the LDA of DFT. In OLCAO, the atomic orbitals are used for the basis expansion, which suits more for the molecular wave function for a larger system. In addition, the flexible choice of basis sets: minimum basis (MB), full basis (FB), and extended basis (EB), makes OLCAO very efficient for the electronic structure calculation of materials. In combination with VASP, OLCAO has been successfully employed to study amorphous solids [119-122], liquid [123], and large and complex biological systems.[124-126] The OLCAO has been systematically upgraded and refined over the years, increasing its computational efficiency, reliability, accuracy, and range of applicability.

The OLCAO method is developed based on the traditional LCAO method with numerous modifications and extensions. In OLCAO, the solid-state wave functions $\Psi_{n\vec{k}}(\vec{r})$ are expanded in atomic orbitals with Bloch function, which consists of Gaussian Type Orbitals (GTO) and spherical harmonics for the angular momentum quantum number, which can be expressed as:

$$\Psi_{n\vec{k}}(\vec{r}) = \sum_{i.\gamma} C_{i\gamma}^{n}(\vec{k}) b_{i\gamma}(\vec{k},\vec{r}) \tag{2.44}$$

where n is the band index, i is the orbital quantum number, γ is the serial number of the atom, $\vec{k}$ is the wave vector, and $b_{i\gamma}(\vec{k},\vec{r})$ is the Bloch sum which can be written as:

$$b_{i\gamma}(\vec{k},\vec{r}) = \frac{1}{\sqrt{N}} \sum_{v} e^{i(\vec{k}.\vec{R}_v)} u_i(\vec{r} - \vec{R}_v - \vec{t}_\gamma) \tag{2.45}$$

Here $\vec{R}_v$ represents the lattice vector and $\vec{t}_\gamma$ is the position of γ^{th} atom in the cell. Here $u_i(\vec{r})$ is the linear combination of atomic orbitals. It consists of both radial and angular parts as given by:

$$u_i(\vec{r}) = \left[\sum_{j=1}^{N} A_j r^l e^{(-\alpha_j r^2)} \right] . Y_l^m(\theta, \phi) \tag{2.46}$$

Here i collectively represents the principal quantum number n and angular momentum quantum numbers (l, m). N is the number of GTOs and α_j is the set of predefined variables usually guided by past experiences, and its value lies in the geometric series of $\alpha_{\min}$ to $\alpha_{\max}$.

The first term $\left[\sum_{j=1}^{N} A_j r^l e^{(-\alpha_j r^2)} \right]$ gives the radial part of the equation, and it is a linear combination of GTO. The use of GTO simplifies the evaluation of orbital interaction integral as the product of two GTO gives a new GTO, which makes the integration and differentiation quite concise mathematically. The second term is the angular part which consists of the real spherical harmonics.

The set of atomic orbitals $u_i(\vec{r})$ in equation (2.46) includes the core, occupied valence, and additional unoccupied orbitals. Based on the nature of the material and dimension of the system, three types of basis sets: MB, FB, and EB, will be chosen. When only core and valence shell orbitals are included in the calculation, it is called MB, which is suitable especially for the large amorphous system. On the other hand, a FB set, which includes the MB plus empty orbitals of the next unoccupied shells, is more than sufficient for a smaller system to give an accurate result. In the case of spectral properties calculation, where unoccupied states of higher

energy are of interest, another level of unoccupied orbitals is added in FB to form an EB set. Hence, there is great flexibility in choosing an atomic basis set to deal with accuracy and computational time. In OLCAO, the potential is constructed based on the LDA of DFT. It solves iteratively the one-electron K-S equation given as (in atomic unit):

$$[-\vec{\nabla}^2 + V_{e-n}(\vec{r}) + V_{e-e}(\vec{r}) + V_{xc}[\rho(\vec{r})]]\Psi_{n\vec{k}}(\vec{\boldsymbol{r}}) = E_n(\vec{k})\Psi_{n\vec{k}}(\vec{\boldsymbol{r}}) \tag{2.47}$$

Where, $-\vec{\nabla}^2$ is kinetic energy, V_{e-n}, V_{e-e} and $V_{xc}[\rho(\vec{r})]$ are the electron-nuclear, electron-electron Coulomb, and exchange-correlation part of potential energy, respectively. The exchange-correlation potential $V_{xc}[\rho(\vec{r})]$ depends on electron density $\rho(\vec{r})$ defined as $\rho(\vec{r}) = \sum_{occ} |\Psi_{n\vec{k}}(\vec{\boldsymbol{r}})|^2$ using which above equation can be solved self-consistently.

In LDA approximation of DFT, the exchange and correlation part of the potential $V_{xc}(\vec{r})$ is responsible for many-electron interaction, which is obtained from the exchange-correlation functional ε_{xc} for the exchange-correlation energy $E_{xc}(\vec{r})$ written as:

$$E_{xc}(\vec{r}) = (\vec{r})\int \rho(\vec{r})\varepsilon_{xc}[\rho(\vec{r})]d\vec{r} \tag{2.48}$$

Using the local approximation, the $V_{xc}(\vec{r})$ takes the form:

$$V_{xc}(\vec{r}) = \frac{d(\rho\varepsilon_{xc}[\rho])}{d\rho} = -\frac{3}{2}\alpha\left[\frac{3}{\pi}\rho(\vec{r})\right]^{\frac{1}{3}} \tag{2.49}$$

In OLCAO under LDA, total energy of the system can be written as,

$$E_T = \sum_{n,\vec{k}}^{occ} E_n(\vec{k}) + \int \rho(\vec{r})\left(\varepsilon_{xc} - V_{xc} - \frac{V_{e-e}}{2}\right)d\vec{r} + \frac{1}{2}\sum_{\gamma,\delta}\frac{Z_\gamma Z_\delta}{\vec{R}_\gamma - \vec{R}_\gamma} \tag{2.50}$$

where, the first term represents the sum over one-electron states and the last term is the sum over the lattice. Here the factor ½ accounts for double-counting of Coulomb potential. The total energy is an important physical quantity in OLCAO, and it is used as a criterion for convergence of energy in self-consistent potential.

The OLCAO is effectively used to calculate the various electronic properties like band structure, the density of states, bond order, effective charge, dielectric function, and optical properties. The calculation of effective charge enables us to analyze the charge transfer in the system. The effective charge (Q*) is the number of electronic charges of the atom. It is calculated using the Mulliken scheme.[127-129] In the Mulliken scheme, the fractional charge $\rho^n_{i,\alpha}$ for i^{th} orbital of the α^{th} atom of normalized state $\Phi_n(\vec{r})$ with energy E_n is expressed as:

$$\sum_{i,\alpha} \rho^n_{i,\alpha} = \int |\Phi_n(\vec{r})|^2 \, d\vec{r} = 1 \tag{2.51}$$

$$\rho^n_{i,\alpha} = \sum_{j,\beta} C^{n*}_{i\alpha} C^n_{j\beta} S_{i\alpha,j\beta} \tag{2.52}$$

where n is the band index, i and j denote the orbital quantum numbers of atoms α and β respectively, $C^n_{j\beta}$ is the eigenvector coefficients of the nth state wave function and $S_{i\alpha,j\beta}$ is the overlap matrix between atoms α and β. The effective charge (Q^*_α) of each atom and bond order (BO) value $\rho_{\alpha\beta}$ between a pair of atoms are calculated based on the Mulliken scheme [128] using the following equations:

$$Q^*_\alpha = \sum_i \sum_{n,occ} \sum_{j,\beta} C^{*n}_{i\alpha} \, C^n_{j\beta} \, S_{i\alpha,j\beta} \tag{2.53}$$

$$\rho_{\alpha\beta} = \sum_{n,occ} \sum_{i,j} C_{i\alpha}^{*n} \, C_{j\beta}^{n} \, S_{i\alpha,j\beta} \tag{2.54}$$

where n is the band index, *i* and *j* denote the orbital quantum numbers of atoms α and β, respectively, $C_{j\beta}^{n}$ are the eigenvector coefficients of the n^{th} state wave function, and $S_{i\alpha,j\beta}$ is the overlap matrix between atoms α and β.

The density of states (DOS) $G(E)$ gives the number of electron states per unit energy in the material. DOS can be expressed as:

$$G(E) = \frac{\Omega}{(2\pi)^3} \frac{d}{dE} \int_{BZ} dk = \frac{\Omega}{(2\pi)^3} \int \left(\frac{dS}{|\nabla E|} \right) \tag{2.55}$$

where Ω is the volume of the unit cell, S is the overlap matrix, and the integral is over the constant energy surface on the Brillion Zone (BZ).

The inter-band optical properties of the simulated glasses are calculated in the form of the frequency-dependent complex dielectric function $\varepsilon(\hbar\omega) = \varepsilon_1(\hbar\omega) + i\varepsilon_2(\hbar\omega)$. The imaginary and real parts, $\varepsilon_2(\hbar\omega)$ and $\varepsilon_1(\hbar\omega)$ respectively, are obtained from equations:

$$\varepsilon_2(\hbar\omega) = \frac{e^2}{\pi m\omega^2} \int_{BZ} dk^3 \sum_{n,l} \left| \left\langle \psi_n(\vec{k},\vec{r}) \right| -i\hbar\vec{\nabla} \left| \psi_l(\vec{k},\vec{r}) \right\rangle \right|^2 \times f_l(\vec{k}) \left[1 - f_n(\vec{k}) \right] \delta \left[E_n(\vec{k}) - E_l(\vec{k}) - \hbar\omega \right] \tag{2.56}$$

$$\varepsilon_1(\hbar\omega) = 1 + \frac{2P}{\pi} \int_0^\infty \frac{s\varepsilon_2(\hbar\omega)}{s^2 - \omega^2} ds \tag{2.57}$$

where *l* and n represent the occupied and unoccupied states, respectively, and $f_l(\vec{k})$, and $f_n(\vec{k})$ are the Fermi distribution functions. From the value of ε_1 at the zero frequency, the refractive

index n is obtained using expression $n = \sqrt{\varepsilon_1(0)}$. The energy loss function (ELF) F(ω) is calculated from the imaginary part of (1/ε)

$$F(\omega) = IM(-\frac{1}{\varepsilon(\omega)}) = \frac{\varepsilon_2(\omega)}{\varepsilon_1^2(\omega) + \varepsilon_2^2(\omega)} \tag{2.58}$$

CHAPTER 3

UNDERSTANDING THE ATOMISTIC ORIGIN OF HYDRATION EFFECTS IN SINGLE AND MIXED BULK ALKALI-SILICATE GLASSES

3.1. Introduction

The effect of water incorporation in silica and alkali-doped glasses is an intriguing subject in geophysics and material science. The hydrolysis of silicate glass greatly affects its mechanical strength, chemical durability, and many other physical and chemical properties. Even a trace of water can cause changes in properties like density, viscosity, glass transition temperature, thermal expansion coefficient, mechanical strength, and refractive index.[43, 45-47, 130, 131] The spectra from near-infrared (IR) spectroscopy and nuclear magnetic resonance (NMR) have shown that water in a glass remains as two species, molecular water H_2O and dissolved water in the form of OH group.[42, 48, 68, 132-134] Water reacts with silica network in breaking the siloxane Si-O-Si bond and forming the silanol group Si-OH that can be represented by the well-known hydrolysis reaction: Si-O-Si + H_2O → 2Si-OH. This reaction is claimed to be responsible for reducing mechanical strength in silica as the dissociated water degrades the glass network.[64, 65] In contrast, recent studies actually show that water-soaked silica is resistant to crack growth [135], and silica glass immersed in hot water is strengthened.[136] Despite considerable effort for decades to understand the silica-water interaction, it is still an open question on the role of water in different silicate glasses, especially when doped with alkali ions. There is also a distinction between the water on the surfaces of the silicate glasses and those in bulk samples, and this difference is usually ignored in discussions.[40, 82, 137-139] For detailed knowledge of this complex interaction at the

atomic level, rigorous quantum mechanical calculations are necessary. The role played by different types of alkali ions is of paramount importance in understanding the origin of hydration in alkali-silicate glasses, which will be significantly different from hydration effect on pure silica, and for the development of stronger and more durable glass products.

Many experimental techniques such as infrared (IR), Raman and nuclear magnetic resonance (NMR) spectroscopy, X-ray crystallography, electron microscopy, neutron diffraction, and magic angle spinning NMR have been used to study the alkali silicate glasses and the effect of water content.[42, 68-74] The IR spectroscopy is widely used since IR active vibrational modes of H_2O can be easily detected. However, the breaking of silica network, the dissociation of water, and the recombination of O and OH groups around the alkali ions are complex atomic-level processes that cannot be easily elucidated by experimental means. In this regard, accurate theoretical simulation is a viable tool to provide deep insights and new predictions in parallel with experimental efforts. The simulation techniques like reverse Monte Carlo and classical molecular dynamics (MD) are routinely used, whereas *ab initio* MD (AIMD) is more limited.[77-84, 137, 140] Moreover, such studies are usually focused on the water effect at the glass surface rather than in the bulk structure. In a multicomponent complex system with mixed covalent, ionic and hydrogen bonding, classical MD faces the challenges of having the reliable potential to describe interatomic interaction. First-principles simulation is a better alternative to provide results that can clarify experimental observations and provide the missing information on specific interatomic bonding rather than simply relying on the geometric information of the structures.

Alkali-doped silicate glasses exhibit an anomalous property generally known as the mixed alkali effect (MAE), showing a nonlinear variation on glass properties when two or more types of alkali ions are present. A prominent MAE is observed on ionic motion-related properties such as electrical conductivity, dielectric loss, alkali ions diffusion, internal friction, and viscosity, exhibiting a large departure on values from simple additivity rule while a noticeable effect is observed in bulk properties like elastic moduli and refractive index.[30, 35, 38] Many previous studies on MAE are focused on properties associated with alkali ion movements [30, 35, 38, 141-143], while studies on macroscopic bulk properties are still lacking. Moreover, despite numerous studies on MAE, there is no universally accepted mechanism to explain this phenomenon, and its atomistic origin is still under debate. Therefore, the detailed picture of interatomic bonding in multi-component alkali silicate glass is essential to understand this effect which requires high-level quantum calculation.

The main goal for the present study is to provide details of the electronic structure and internal bonding and correlate them with mechanical and optical properties in seven carefully-constructed bulk models of hydrous alkali silicate glasses including pure silica, single alkali doped (Li, Na, K) and mixed alkali doped (Li+Na, Li+K, and Na+K) in order to shed some light on the MAE and compare with the results from corresponding anhydrous models.[144, 145] It should be clearly stated that this work is restricted to bulk glasses, so any comparison with results related to glass surfaces needs to be carefully scrutinized. Our main conclusion is that the hydration of bulk alkali silicate glasses increases their mechanical strength which may enhance their durability. The paper is organized in the following order. The next section begins with a brief discussion on computational methods used. The main results on the structure and

properties of the bulk hydrated alkali silicate glasses are presented and discussed in Sections 3.3 and 3.4. This is followed by a brief conclusion and plans for future direction in the last section.

3.2. Simulation Procedures and Computational Methods

3.2.1 Procedures for Model Construction

The starting model for hydrous silicate glasses is the anhydrous continuous random network model of amorphous SiO_2 (a-SiO_2).[144] The reason for choosing this unique model is that it is a near-ideal continuous random network model with no over- or under-coordinated Si or O atoms which is very challenging to construct due to difficulty in matching the strong covalent Si-O bonds across the periodic boundaries of the cell. This model has been extensively utilized in the study of silicate and related glasses.[120-122, 145-147] This is then followed by a melt-and-quench scheme based on AIMD to simulate alkali silicate glasses with 30 mol. % alkali oxide content discussed in previous work.[145] This combined process of using the near-ideal initial model and AIMD ensures our final fully relaxed model will be more accurate for this multi-component mixed glasses than those derived from classical MD. Near this composition, (33.33 mol. % of alkali oxide), the complete breaking of the silica network is possible.[148] To determine the most appropriate number of water molecules to be doped in the alkali-silicate models in the present study, we start with the near-perfect a-SiO_2 model [144] from which all the anhydrous alkali silicate models are constructed. To accommodate the added water content, the volume of the model is expanded by about 5%. Water molecules are then added to the interstitial positions of the structure such that they do not overlap with the host atoms. A series of test calculations are carried out with 3, 4, 5, 6, and 7 water molecules

with five different randomly chosen configurations and fully relaxing them using Vienna *Ab-initio* Simulation Package (VASP) [149] with no constraints to the cell volume or shape. The electronic structure and bonding for the five samples for five different numbers of water molecules are calculated and ranked according to their total energy (TE) and the total bond order density (TBOD) (see descriptions in **Section 3.4**). The hydrated pure a-SiO_2 models with the lowest TE and the corresponding TBOD values are listed in **Table 1**. It turns out that the model with the lowest energy corresponds to the one with the highest TBOD. Therefore, all the seven hydrated alkali-doped silicate glass models in this study will contain four water molecule. To check the effectiveness of the approach for model construction, we again simulated another five models for each alkali-doped model. Nearly close results on the TBOD and ground state energy values are found. So the model with the largest TBOD and lowest TE is chosen as the most representative model for each hydrated alkali-silicate glass for detailed analysis. The results of TE and TBOD for seven chosen glass samples with four water molecules each, including the pure a-SiO_2, are listed in **Table 2.** We believe that our careful and systematic step-by-step procedures described above provide us the most representative models for this very complex glass system, and it is quite distinct from the conventional approach of focusing only on one composition of one alkali atom type.

Table 1. Calculated TBOD and corresponding lowest total energy for the different number of water molecules doped a-SiO_2 glass.

Number of H_2O	TBOD	Total Energy (eV)
3-H_2O	0.02380	-0.13078389E+04
4-H_2O	0.02404	-0.13085722E+04
5-H_2O	0.02213	-0.12985547E+04
6-H_2O	0.02048	-0.12642978E+04
7-H_2O	0.02349	-0.13074594E+04

Table 2. Calculated TBOD and corresponding lowest total energy for hydrated alkali silicate glass models.

Glass Models	TBOD	Lowest total energy (eV)
SiO_2	0.02404	-0.13085722E+04
Li-Doped	0.02747	-0.11944054E+04
(Li+Na)-doped	0.02398	-0.11827821E+04
(Li+K)-doped	0.02105	-0.11803445E+04
Na-doped	0.02400	-0.11668664E+04
(Na+K)-doped	0.01998	-0.11567636E+04
K-doped	0.01877	-0.11556264E+04

3.2.2 Methods for Properties Calculation

We used two well-established density functional theory-based packages: VASP [149, 150] and the Orthogonalized Linear Combination of Atomic Orbital (OLCAO) method [93, 151] in this study. VASP is used for geometric optimization and mechanical properties evaluation of all glass models under the same set of input parameters and exchange-correlation potential. We used PAW-PBE potential with generalized gradient approximation.[100] During the unconstrained relaxation, the plane-wave cutoff energy is set at a relatively high value, 600 eV, with electronic convergence criteria of 10^{-5} eV. The force convergence limit for ionic relaxation is set at 10^{-3} eV/Å.

We calculated the mechanical properties based on the stress-strain response scheme.[152] The elastic coefficients C_{ij} are evaluated by solving the linear equation $\sigma_i = \sum_j C_{ij}\epsilon_j$ where i and j vary from 1 to 6. The stress component σ_i are obtained by applying a strain ϵ_j of ±0.5 % to the equilibrium cell. From the calculated C_{ij} values, the bulk modulus (K), shear modulus (G), Young's modulus (E), and Poisson's ratio (η) are calculated based on the Voigt–Reuss–Hill (VRH) approximations for poly-crystals.[118, 153, 154] This approach is relatively

efficient for bulk crystals or glass models, especially when a large numbers of models are to be calculated. Details of the calculation are explained in Chapter 2.

The electronic structure and bonding analysis of simulated glasses are carried out by OLCAO method using the VASP relaxed structure as input. This method is based on the local density approximation within the density functional theory. It is an all-electron method with Gaussian type orbitals forming atomic orbitals in the basis expansion for the Bloch function. The OLCAO code is extremely efficient for the electronic structure calculation of large complex systems [120, 121, 123, 155] due to the ability to evaluate all multicenter interaction integrals analytically.[93] The use of atomic orbitals enables the quantitative evaluation of bond order (BO) values $\rho_{\alpha\beta}$ between a pair of atoms α and β, and the effective charge Q_α^* based on the Mulliken scheme [127, 128] (see Chapter 2 for details). The bond order values give a quantitative measure of the bond strength between each pair of atoms. The effective charge and BO using the Mulliken scheme in the OLCAO method use the more localized minimal basis set.[93] We would like to point out that most of the simulations on glasses, especially those using MD, lack the ability to analyze the interatomic bonding in detail. They usually infer from the structures and atomic coordination in the model, which are pure geometric parameters. The summation of all bond order values in the model normalized by its volume gives us a key parameter, the total bond order density (TBOD) which can be divided into different components of the partial BOD (PBOD) according to different type of bond pairs or for bonds in different structural parts of the model. The same can be said about the sum of effective charges for each groups of atoms or their partial charges (PC) which is the deviation

of the neutral atom charge from the effective charge Q_α*. This is a step beyond the usual interpretation based on formal charges.

The OLCAO method is also effective in calculating the dielectric properties based on interband optical absorption theory in the form of frequency-dependent complex dielectric function $\varepsilon(\hbar\omega) = \varepsilon_1(\hbar\omega) + i\varepsilon_2(\hbar\omega)$. First, the imaginary part $\varepsilon_2(\hbar\omega)$ is evaluated from which the real part $\varepsilon_1(\hbar\omega)$ is derived by applying Kramer-Kronig transformation.[156] From the zero-frequency limit, $\varepsilon_1(0)$ the refractive index $n = \sqrt{\varepsilon_1(0)}$ can be estimated. Since all the matrix elements for dipole transitions using *ab initio* wave functions are explicitly included, they are quite reliable for complex non-crystalline glassy systems; even the calculations are based on a one-electron approach. This approach also does not include the vibrational effects of the molecules in the model which are usually restricted to very low energy or long wave lengths. Details of the calculation are discussed in reference.[93]

3.3 Results

3.3.1. Relaxed Structures and Coordination Numbers

The ball and stick structures of the fully relaxed seven models with periodic boundary conditions, including the pure a-SiO_2, are shown in **Figure 3**. The composition and geometrical parameters for the relaxed models are listed in **Table 3.** The silicon atoms are tetrahedrally coordinated with oxygen, and each tetrahedral are connected to each other by corner-sharing bridging oxygen. The alkali atoms are clustered around non-bridging oxygen (NBO) which are produced due to alkali doping. Both species of water, molecular water H_2O and dissociated water OH, are present in the final structures consistent with the experimental observations.[42, 68, 70] The number of dissociated water molecules are listed in **Table 4,** together with other

calculated physical properties to be described later. It can be seen that details of the hydrated alkali silicate glasses depend on the nature of the alkali ions involved.

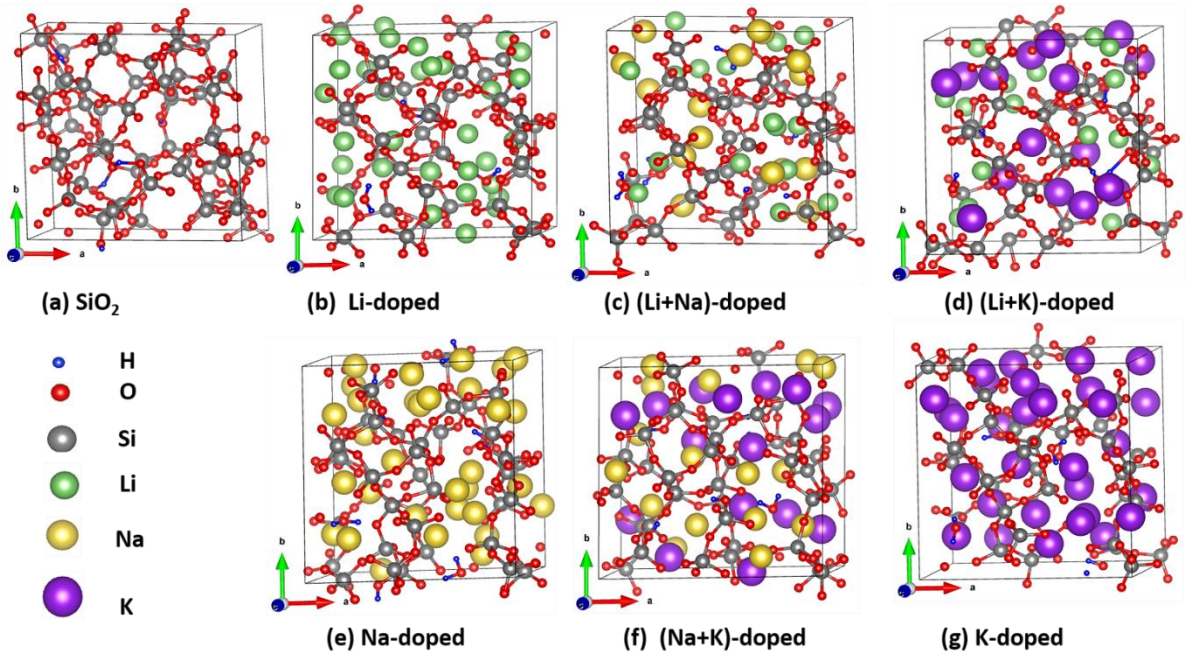

Figure 3. Ball and stick sketch of hydrated alkali silicate glass models.

Table 3. Final structural parameters and atomic composition of the seven hydrated models (Volume is in $Å^3$).

Glass Models	Si	O	H	Li	Na	K	a (Å)	b (Å)	c (Å)	α^0	β^0	γ^0	Volume
a-SiO_2	54	108	0	-	-	-	13.78	13.19	14.10	88.99	96.25	92.25	2547.35
Li-doped	38	96	8	32	-	-	13.01	13.06	12.89	88.24	87.73	88.28	2187.68
(Li+Na)-doped	38	96	8	16	16	-	13.29	13.77	13.25	89.16	88.94	90.54	2421.51
(Li+K)-doped	38	96	8	16	-	16	13.36	13.82	14.12	91.82	87.13	89.99	2600.93
Na-doped	38	96	8	-	32	-	12.95	13.51	13.32	89.38	87.41	88.39	2326.15
(Na+K)-doped	38	96	8	-	16	16	14.35	13.50	13.90	89.09	88.23	88.55	2690.42
K-doped	38	96	8	-	-	32	13.68	14.00	14.34	89.29	89.22	89.35	2747.79

Table 4. Calculated electronic structure and properties for the hydrated alkali silicate glasses. (N = Dissociated water molecules, E_g = Band gap, and n = Refractive index)

Glass Models	N	E_g	Averaged Partial Charge ΔQ (in e)						*n*
		(eV)	Si	O	H	Li	Na	K	
a-SiO_2	4	3.10	2.02	-1.00	0.45	-	-	-	1.45
Li-Doped	1	4.15	1.93	-0.98	0.38	0.54	-	-	1.49
(Li+Na)-doped	1	4.13	1.92	-0.99	0.41	0.50	0.68	-	1.44
(Li+K)-doped	2	3.87	1.89	-0.99	0.37	0.52	-	0.72	1.48
Na-doped	1	3.84	1.88	-0.99	0.36	-	0.65	-	1.48
(Na+K)-doped	3	3.05	1.88	-1.01	0.31	-	0.63	0.80	1.47
K-doped	2	2.57	1.89	-1.04	0.35	-	-	0.78	1.50

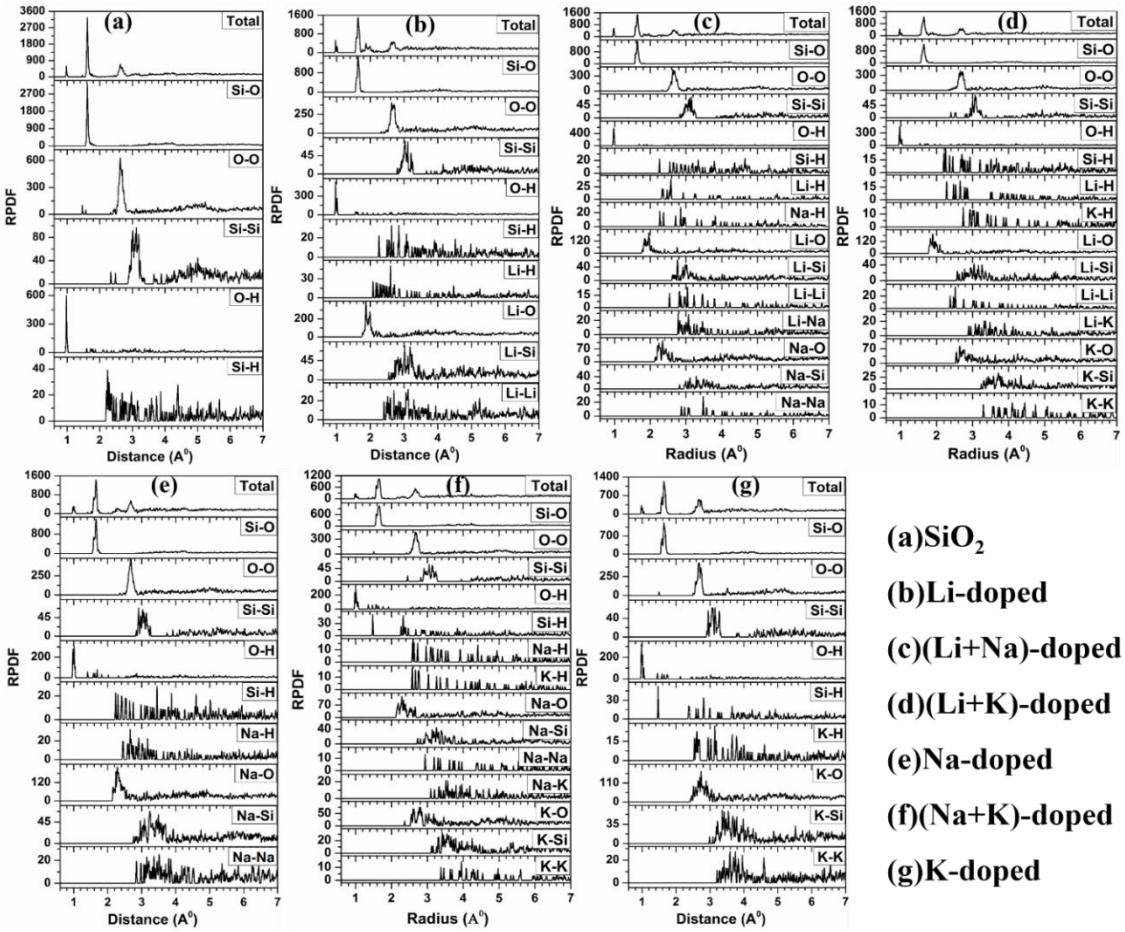

Figure 4. Radial pair distribution function for the seven hydrated glasses.

The pair distribution function (PDF) for the bulk glass model helps to capture the local environment of Si, O, and alkali ions in the presence of water. The total and pair-wise resolved PDFs for the seven hydrated glass models are shown in **Figure 4.** The averaged Si-O and O-O bond lengths (BLs) determined from peak position are 1.62 Å and 2.63 Å in hydrated silica (**Figure 4 (a)**), which are close to the values in the un-hydrated a-SiO_2 model.[144] In the case of hydrated alkali silicate glasses, the Si-O and O-O BLs are slightly increased and lie within the range of 1.64Å to 1.66Å for Si-O and 2.67Å to 2.70Å for O-O pairs, respectively. The range for the Si-Si bond can also be identified around a more broader peak centered at 3.1 Å. The small but sharp peak at 1.0 Å simply shows the O-H covalent bond in the unionized water molecules. The partial PDFs for other atomic pairs in the hydrated alkali-silicates are far more complicated with no clear peak structures except for the alkali-O pairs indicating the attachment of alkali ions to the NBOs. The averaged BLs of alkali ions with NBOs follow the order of Li-O < Na-O < K-O. It should be noted that BLs derived from PDF are solely geometrical entities and contain no information on the strength of the bond, which require quantum mechanical calculations. The partial PDF for Alkali-H, Alkali-Si, and alkali-Alkali pairs are much more difficult to disentangle due to the much more random distributions in the hydrated alkali silicate and may also depend on the water content.

The coordination number (CN) of each type of atom in glass has always been emphasized in analyzing their structures, especially for simulations using classical MD. **Table 5** lists the averaged CN for Si, O, and alkali atoms in 7 hydrated models calculated using two different cut-off distances. CN-1 uses the first minimum of the corresponding PDF for the cut-off distances as were used in all MD simulations; and CN-2 determines the cut-off distances

Table 5. Calculated coordination numbers for Si, O and alkali atoms in seven hydrated glass models according to two criteria for cutoff distance. (CN-1 = cutoff based on PDF and CN-2 = cutoff based on BO value. See text for details).

Glass Models	Atom	CN-1			CN-2		
		Cutoff (Å)	#bonds	C.N.	Cutoff (Å)	#bonds	C.N.
SiO_2	Si	1.9	213	3.944	2.6	215	3.981
	O	2.0	229	2.045	2.5	233	2.080
	Si	1.9	153	2.833	2.0	153	2.833
Li-doped	O	2.2	260	2.321	2.8	289	2.580
	Li	2.2	93	2.906	2.8	119	3.719
	Si	1.9	153	2.833	2.0	153	2.833
(Li+Na)-	O	2.6	281	2.509	3.2	309	2.759
doped	Li	2.2	49	3.062	2.5	55	3.438
	Na	2.6	58	3.625	3.2	74	4.625
	Si	1.9	151	2.796	2.0	151	2.796
(Li+K)-doped	O	2.9	281	2.509	3.4	325	2.902
	Li	2.2	48	3.000	2.6	56	3.500
	K	2.9	52	2.250	3.4	87	5.438
	Si	1.9	153	2.833	2.0	153	2.833
Na-doped	O	2.6	289	2.580	3.2	340	3.036
	Na	2.6	120	3.750	3.2	164	5.125
	Si	1.9	151	2.796	2.0	151	2.796
(Na+K)-	O	2.9	285	2.545	3.3	327	2.920
doped	Na	2.6	58	3.625	3.0	71	4.438
	K	2.9	52	3.25	3.3	82	5.125
	Si	1.9	154	2.852	2.0	154	2.852
K-doped	O	3.0	314	2.804	3.5	370	3.304
	K	3.0	140	4.375	3.5	185	5.781

according to the BL where the significant BO values are observed as shown in **Figure 11(a)** in **Section 3.4** that will be discussed in detail later. In the CN-1 scheme, when PDFs have a broad first peak with a non-zero first minimum, the cut-off distance and hence the CN cannot be precisely defined such that the first coordination shell becomes uncertain. A broad

distribution of alkali-O nearest neighbor in alkali silicate glass makes this choice even more difficult. Hence, the calculation according to the CN-2 scheme based on BO-BL distribution is more realistic in determining the CN of alkali ions. This observation can be clearly shown in the comparison of average CN between CN-1 and CN-2 in **Table 5.** The CN for Si and O are either identical or very close in CN-1 and CN-2, whereas those of alkali ions have much larger average values of CNs.

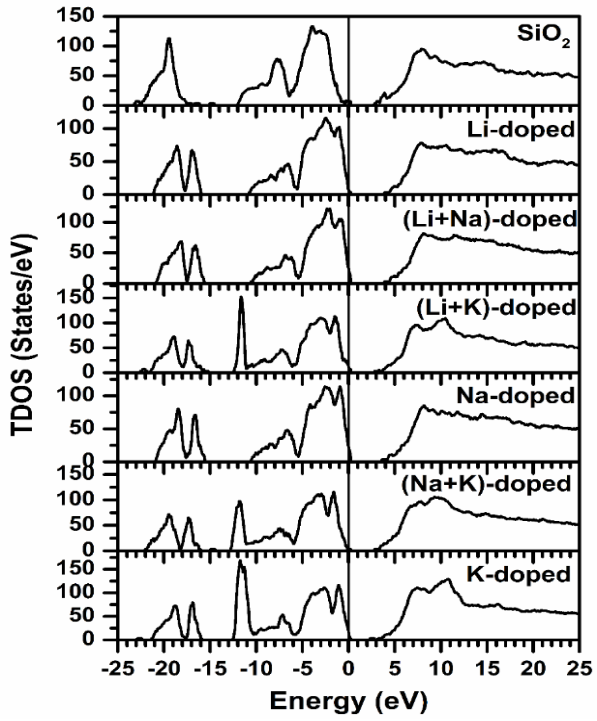

Figure 5. Calculated total density of states for the seven hydrated glass models.

3.3.2. Electronic Structure

The electronic structure of glasses is best described in terms of electron density of states. The calculated total density of states (TDOS) and atom- or component-resolved partial DOS (PDOS) provide the best summary for the electronic structures. The results for TDOS and

PDOS for hydrated alkali-silicate glasses are shown in **Figure 5** and **Figure 6,** respectively. The valance band (VB) DOS can be divided into two parts, the lower and the upper. The lower part DOS has a single prominent peak in pure silica, while in other models, it has two peaks. The upper part DOS of pure silica and Li-, Na- and (Li+Na)-doped glasses has two segments while K containing three glasses have more than two segments. The peak at -11.5 eV can be traced to the presence of the semi-core K-3p levels. The DOS features in the conduction band (CB) are mostly similar for all models. But when we move from top to bottom through different panels of **Figure 5**, we see the band gap steadily decreases. The atom resolved PDOS in **Figure 6** shows the contribution of each atom on VB and CB regions DOS in the hydrated glass models. It shows the lower part of the VB DOS is mainly from the O atom while alkali atoms contribute to the CB DOS.

The calculated band gaps for all hydrated models are plotted in **Figure 7** in the form of vertical histograms and compared with the dry models. A striking fact is the difference between hydrated and un-hydrated pure a-SiO_2 model. The hydrated model has its band gap reduced by a factor of almost 3, from 5.648 eV to 3.100 eV. The band gap generally decreases in the hydrated models as the sizes of the alkali ions increase following the order of Li-silicate > Na-silicate > K-silicate with no clear evidence of MAE. For K-doped silicate, there is a much larger decrease in the band gap when hydrated. When compared to the dry models, the band gap increases for (Li+Na)-, (Li+K)- and Na-doped models on hydration while it decreases for other models. It should be cautioned that the band gaps calculated using the DFT method are usually underestimated, and this underestimation may depend on the chemical composition,

but the observed trend should be valid since the calculations used the same method and procedure.

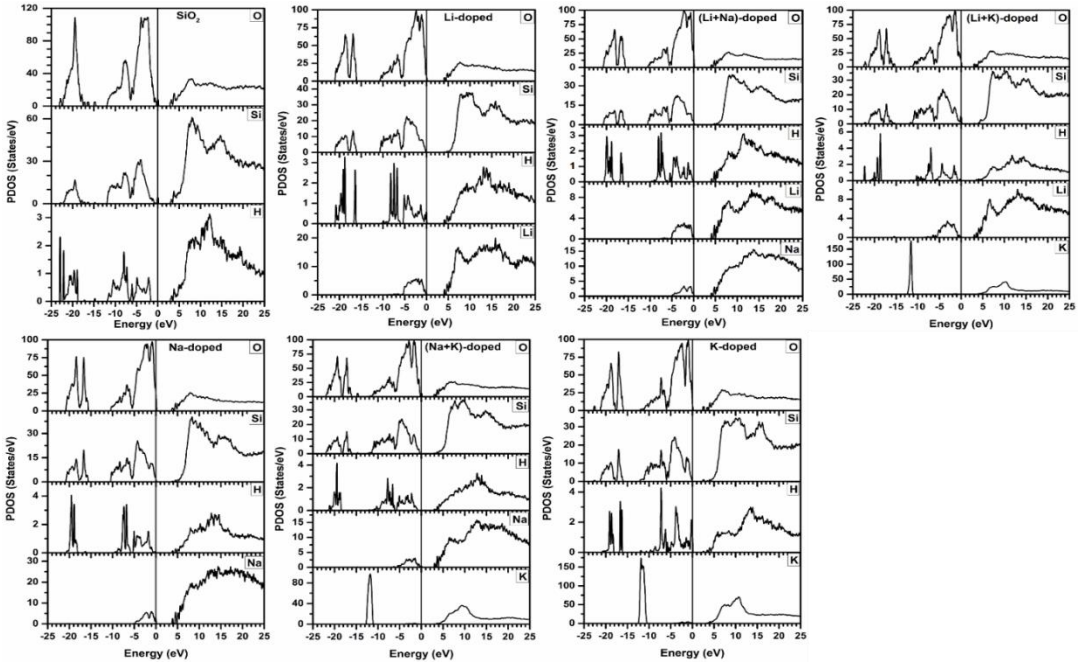

Figure 6. Calculated partial density of states for the seven hydrated glass models.

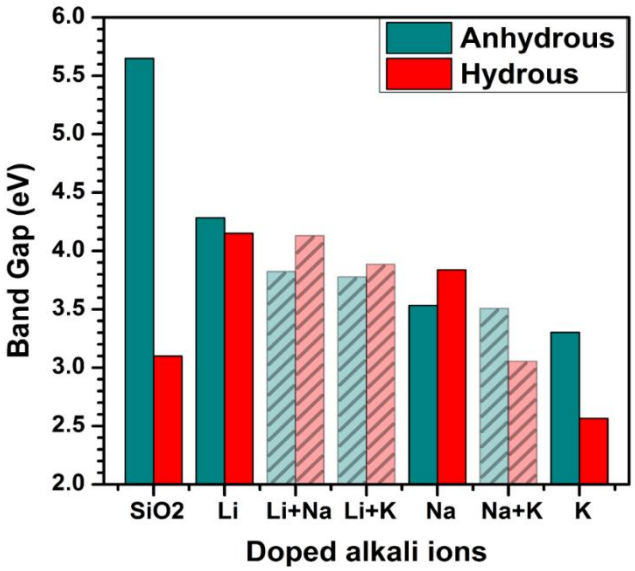

Figure 7. Comparison of band gap values between the seven anhydrous and hydrous models.

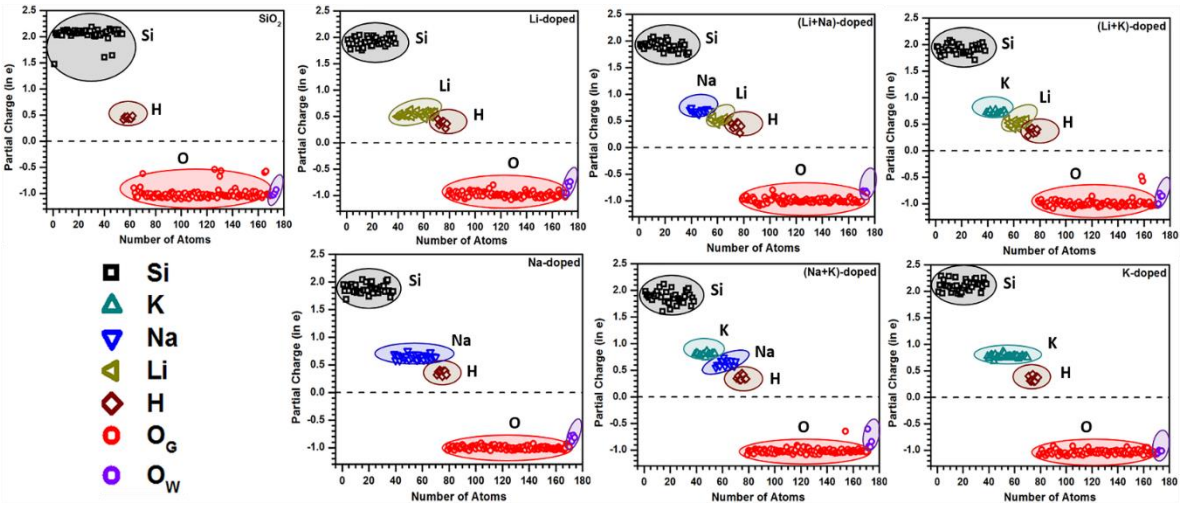

Figure 8. Calculated partial charge for different atoms in hydrated glass models. (O_G = Oxygen from glass model and O_W = Oxygen from water molecule)

3.3.3. Partial Charge Distribution

Another important quantity on the electronic structure is the calculated effective charge Q* for each atom which gives the information on charge transfer, also coined as partial charge. The partial charge for each atom is obtained according to $\Delta Q = Q^0 - Q^*$, where Q^0 is the charge on the corresponding neutral atom. The PCs for all the atoms in the seven hydrated models are displayed in **Figure 8**. The averaged PC for the atoms in the seven models is shown in **Figure 9**. It vividly shows the PC of different types of atoms. Essentially, they can be lumped into three groups: the highly positive charged Si, the smaller positively charged alkali ions and H, and negative charged O. It also shows that the PC for the second group is in the order of K > Na > Li > H. There are few O atoms with smaller PC than the average which can be traced to be the ones associated with water or hydroxyl groups. Such detailed information on PC distribution can only be obtained from first-principles calculations but not from classical MD simulations. On average, we may surmise that O atoms gain charge, whereas all other atoms

lose charges. Si is the most positive charged atom, followed by K, Na, Li, and H in that order. It is noted that the alkali ions have PC much less than the formal charge of +1 in many classical descriptions. In particular, the PC of Li is only about 0.5 electron charge, less than Na or K. This is consistent with the fact the Li-O bonds are much stronger than Na-O and K-O bonds that will be discussed in the next section. **Table 4** and **Table 6** summarize the electronic structure results and other properties, including the refractive index and total and partial BODs to be described below.

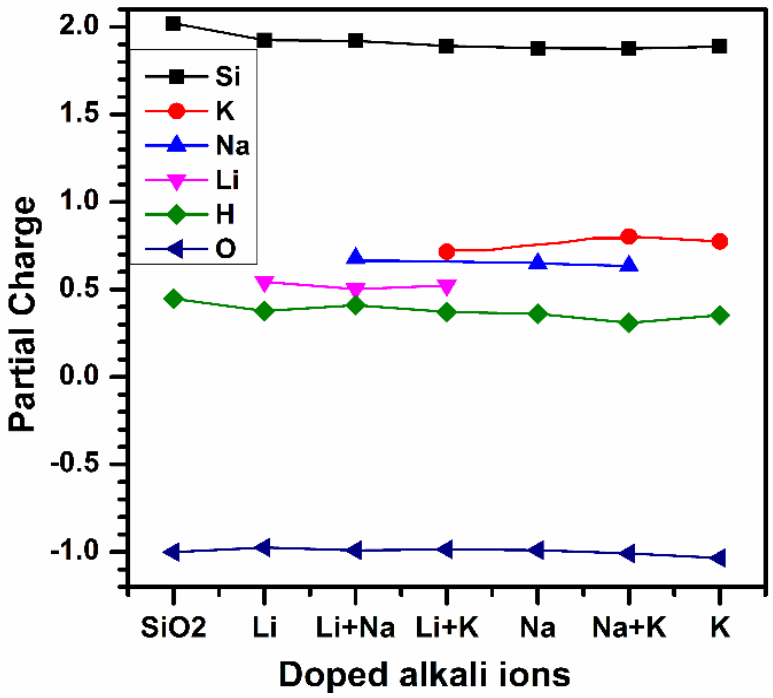

Figure 9. Calculated averaged partial charge of atoms in the hydrated glass models.

Table 6. Calculated TBOD and bonded pairwise PBOD for hydrated alkali silicate glasses.

Glass Models	TBOD	PBOD						
		Si-O	Li-O	Na-O	K-O	O-H	Si-H	Si-Si
a-SiO_2	0.0240	0.0227	-	-	-	0.0010	-	0.0003
Li-Doped	0.0275	0.0204	0.0059	-	-	0.0013	-	-
(Li+Na)-doped	0.0239	0.0183	0.0029	0.0018	-	0.0011	-	-
(Li+K)-doped	0.0211	0.0164	0.0026	-	0.0010	0.0010	-	-
Na-doped	0.0240	0.0185	-	0.0043	-	0.0012	-	-
(Na+K)-doped	0.0199	0.0159	-	0.0019	0.0011	0.0009	0.0002	-
K-doped	0.0188	0.0153	-	-	0.0024	0.0008	0.0002	-

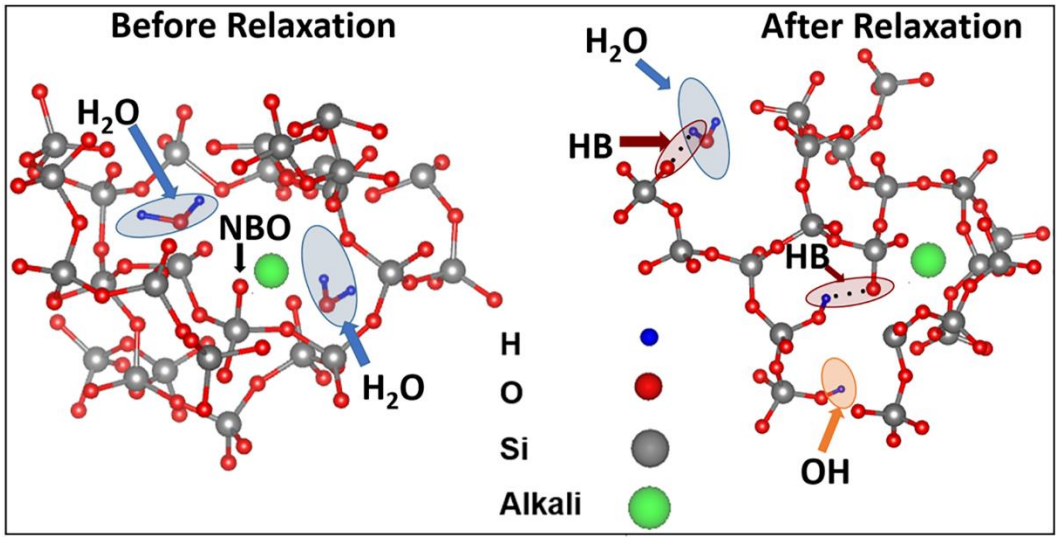

Figure 10. Sketch representing the ionization of water inside the silica network.

3.3.4. Interatomic Bonding and TBOD

We now focus on the most important part of the electronic structure, the interatomic bonding. It is obvious that the ionization of water molecules in alkali silicate glasses results in a far more complex bonding pattern and variation in the different BO values. **Figure 10** shows

an illustrative sketch of the possible internal bonding of water with the surrounding atoms before and after structural relaxation. Water can remain as H_2O molecule or ionize to form the silanol group with an O-H bond after breaking the silica network. The various alkali ions form ionic bonds with O. The non-ionized water molecule fills the interstitial void of the network and contributes to the formation of hydrogen bonds (HBs) with other nearby O atoms. It should be pointed out that the intramolecular O-H covalent bonding in a water molecule (O_w-H) is of the same strength as the O-H bond in the silanol group (O_{Si}-H) and does not affect the network structure and internal cohesion other than expansion of the volume. Weak bondings, including the O···H bonds between different pairs of atoms at a larger distance of separation, are possible. The nature of ionization of water in complex alkali silicate glasses is affected by many factors and is a topic of continuous debate. More discussion will be presented in **Section 3.4**.

The complex interatomic bonding picture in the multi-component hydrated alkali glasses can be quantitatively displayed in the BO versus BL distribution plots involving all bond pairs in the seven models shown in **Figure 11(a)**. It shows that the covalent Si-O bond is the main contributor with high BO values over a very narrow range of the BL. O-H bonds with BL of about ~1Å are also a major contributor with large BO values. There are two types of O-H bonding, the internal covalent bonding within H_2O molecules and the covalent bonding with O attached to Si. A very distinguishing feature is found in the pure a-SiO_2 with water but no alkali ions. First, all four water molecules are ionized in the absence of the alkali ions, so the O-H bonds are all from the silanol groups, Si-O-H. Second, there are two Si-Si bonds and three O-O bonds. The occurrence of Si-Si bonds does not happen in any of the alkali doped models.

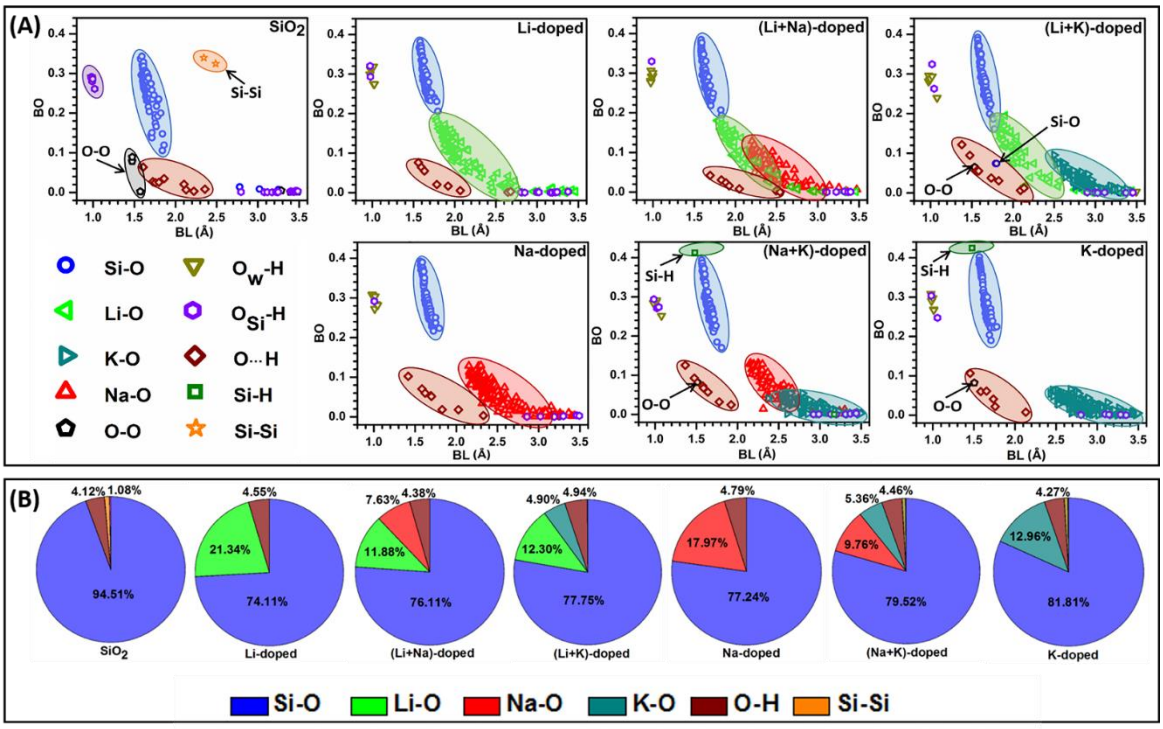

Figure 11. (A) Bond order versus bond length plot for the seven hydrated glass models. (B) Pie diagram showing the contribution on bonding due to different pairs of atoms.

Instead, strong isolated Si-H bonds are formed in (Na+K)-doped and K-doped glasses. Isolated O-O bond also occur in (Li+K)-doped, (Na+K)-doped and K-doped glasses signifying a different role played by the much larger K ion. The weaker HBs having BLs ranging from about ~1.5 Å to 2.5 Å is a common feature but has not been discussed in detail in most literature. They arise from bonding between water molecules, hydroxyl groups, or bridging O from the network. The ionic bonding between alkali ions and NBO is important in the solvated alkali-silicates, which are affected by the presence of water. They are usually stronger than the HBs. The ionic BO values follow the order of Li-O > Na-O > K-O or are inversely proportional to the size of the alkali ions. These are vividly illustrated in **Figure 11(a)**. The pie charts in **Figure 11(b)** show the percentage contribution to the total bonding from different pairs of

bonded atoms, which is dominated by Si-O bonds. When alkali ions are present, the contribution from the ionic bonding with O can account for 21.34% in Li-doped glass down to 12.96% in K-doped glasses. This shows that the Li ions form much stronger ionic bonds than Na and K, which is also evident in **Figure 11(a)**.

Detailed description on interatomic boding in a complex system such as the hydrated alkali-doped silicate glasses is always a daunting task and with conclusions from many different angles and perspectives. There has been accumulated evidence of the effectiveness of using the concept of TBOD as a single quantum mechanically derived parameter to describe the overall internal cohesion and strength in a variety of materials regardless of their structure, complexity, and composition.[122, 145, 157-162] The TBOD is the sum of individual BO values of all atomic pairs within the system normalized by the volume of the system. The BO value represents the strength of the bond between a pair of atoms and generally scales with their distances of separation or the BL. BL is a simple geometric parameter used to characterize the structure of glass by almost all the simulations using MD. In the realistic quantum calculation, the BO value depends not just on the BL but also on the local environment of atomic pairs, including the bond angles, the location of the next nearest neighbor atoms, and most importantly, the types of atoms involved in the bonding. This is clearly illustrated in **Figure 11**. **Figure 12** compares the calculated TBOD values for the seven hydrous and anhydrous alkali silicate glasses. A slight decrease in TBOD value is observed when the glass models are hydrated. The de-polymerization of the network due to ionized water and the concomitant increase in the cell volume is responsible for its reduction. In the mono-alkali doped hydrous and anhydrous glasses, the TBOD decreases with the increasing size of the

alkali ion in the order of Li-silicate > Na-silicate > K-silicate. In the mixed ion glasses, which account for the effect due to both ions, it follows the order of (Li+Na)-silicate > (Li+K)-silicate > (Na+K)-silicate. However, there is a marked decrease in the trend of TBOD for (Li+Na)-silicate and (Li+K)-silicate between Li-silicate and K-silicate with similar observation for (Na+K)-silicate between Na-silicate and K-silicate (see the vertical arrows in **Figure 12**). This is strong evidence that the so-called MAE is observed in the calculated TBOD for the hydrated alkali silicates.

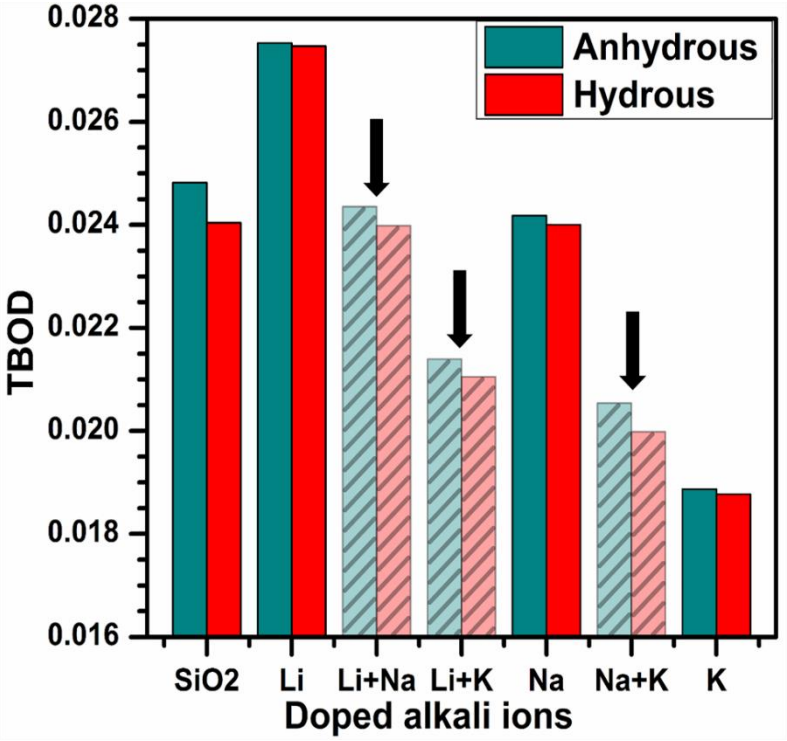

Figure 12. Calculated TBOD for the seven anhydrous and hydrous models.

Table 7. Calculated elastic constants and elastic moduli (in GPa) for the hydrous alkali silicate glasses.

Glass Models	C_{11}	C_{22}	C_{33}	C_{44}	C_{55}	C_{66}	E	K	G	η	G/K
a-SiO_2	93.12	76.61	91.82	28.54	34.97	32.38	76.86	44.22	31.75	0.210	0.720
Li-doped	78.44	86.76	97.95	32.62	32.18	37.00	78.16	46.68	32.01	0.221	0.686
(Li+Na)-doped	72.63	76.86	73.14	28.50	23.44	24.83	63.35	38.41	25.86	0.225	0.673
(Li+K)-doped	66.79	74.36	71.62	25.25	21.71	26.04	59.98	38.20	24.22	0.238	0.634
Na-doped	76.56	81.08	81.23	27.86	27.26	31.46	68.80	43.84	27.78	0.238	0.634
(Na+K)-doped	61.14	69.09	69.22	20.91	21.44	23.06	54.66	35.74	21.95	0.245	0.614
K-doped	77.60	72.60	73.35	25.84	23.31	26.97	61.79	42.02	24.62	0.255	0.586

3.3.5. Elastic and Mechanical Properties

The durability of glass generally depends on the strength of a material but also is affected by many other factors related to its environment, especially the local geometry. So the durability of glass at the surface is fundamentally different from the durability of bulk materials. Thus one would like to ask the question to what extent the durability of glass can be influenced by the intrinsic elastic and mechanical properties of the bulk glass models? This is a very meaningful and practical issue worth a detailed investigation. The calculated elastic constants and bulk mechanical parameters of the seven solvated alkali silicate glasses are listed in **Table 7**. The elastic moduli for hydrous models are compared with those of anhydrous models, including the pure SiO_2 glass in **Figure 13.** It shows that the shear modulus (G), bulk modulus (K), and Young's modulus (E) are all significantly increased when alkali silicate glasses are hydrated in these bulk models. This appears to indicate that the solvation of water in alkali silicate may increase mechanical strength in real bulk glasses and favor chemical durability.

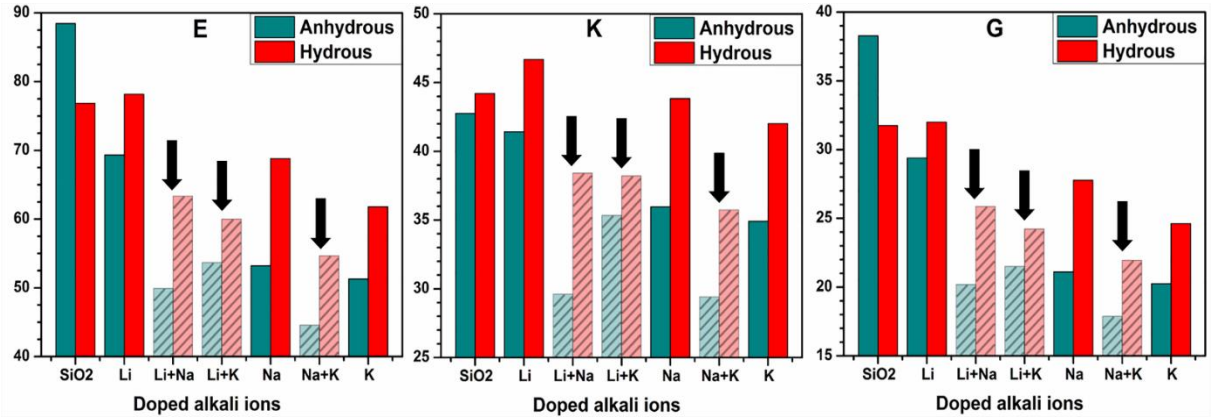

Figure 13. Calculated elastic moduli [Young's modulus (E), Bulk modulus (K) and Shear modulus (G) in unit of GPa] for the simulated glass models.

This enhancement of the mechanical properties could be explained by the fact that the presence of water molecules in the interstitial position increases the cohesion of the network, which was depolymerized in the presence of alkali ions and the OH group. In the single alkali ion-doped glasses for both hydrated and un-hydrated models, the elastic moduli follow the trend of Li-doped > Na-doped > K-doped glass. In the mixed ions glasses, the trend is similar, which are all related to the fundamental issue of a stronger interatomic bond discussed in **Section 3.3.4** above. We can also claim that an undisputable MAE is observed in the sense that the mixed models do not fit into the trend of the single ion case. The moduli values are markedly lower than expected from the average of the respective mono-alkali silicate glasses (see broad arrows in **Figure 13**). The observation of MAE in the mechanical properties fully consistent with those observed in the TBOD of **Figure 12** further strengthens the argument for using TBOD as a useful metric for materials characterization. We thus reached one of the most important conclusions that mixing of alkali ions in hydrated silicate glasses will decrease its mechanical strength, which has been enhanced by adding water molecules. We are unable to find any experimental evidence related to the mechanical properties of hydrated alkali silicate glasses for composition close to the present work.

Figure 14 shows the calculated Poisson's ratio η and Pugh's modulus ratio (G/K) for the seven simulated glass models. The Poisson's ratio increases when the glass models are hydrated. It is noted that in pure a-SiO_2 glass, a large increase of Poisson's ratio and a large decrease in G/K is noted when hydrated. In a single alkali ion-doped hydrated models, its value increases with the increasing size of the ion; that is, it follows the order of Li-silicate < Na-silicate < K-silicate. In the mixed glasses, it follows the order of (Li+Na)-silicate < (Li+K)-

silicate < (Na+K)-silicate. The alkali silicate glasses generally have a higher Poisson's ratio than pure a-SiO_2 glass. The Pugh's modulus ratio (G/K) is an inverse to Poisson's ratio and decreases in the series from Li to Na to K doped glasses. The increase in Poisson's ratio or decrease in G/K is an important finding since it indicates that the bulk glasses change from brittle to more ductile phase, which is generally considered more desirable and possibly more durable. However, we must point out again that the correlation between chemical durability and mechanical parameters can be very complicated. It has to be stressed again that the present results on mechanical properties are for specific bulk samples with a fixed alkali composition and water content as described in **Section 3.2.1**.

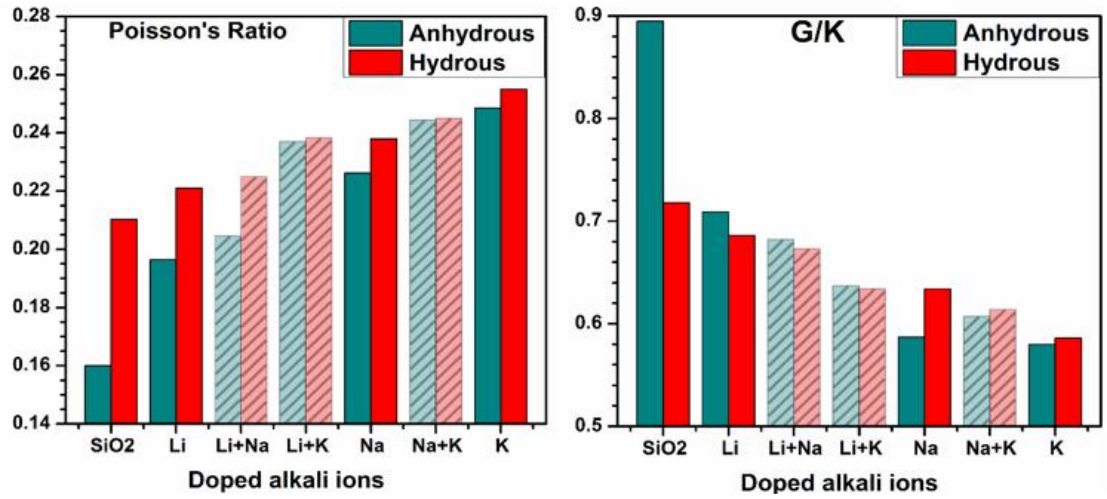

Figure 14. Comparison of Poisson ratio and G/K between hydrated and un-hydrated models.

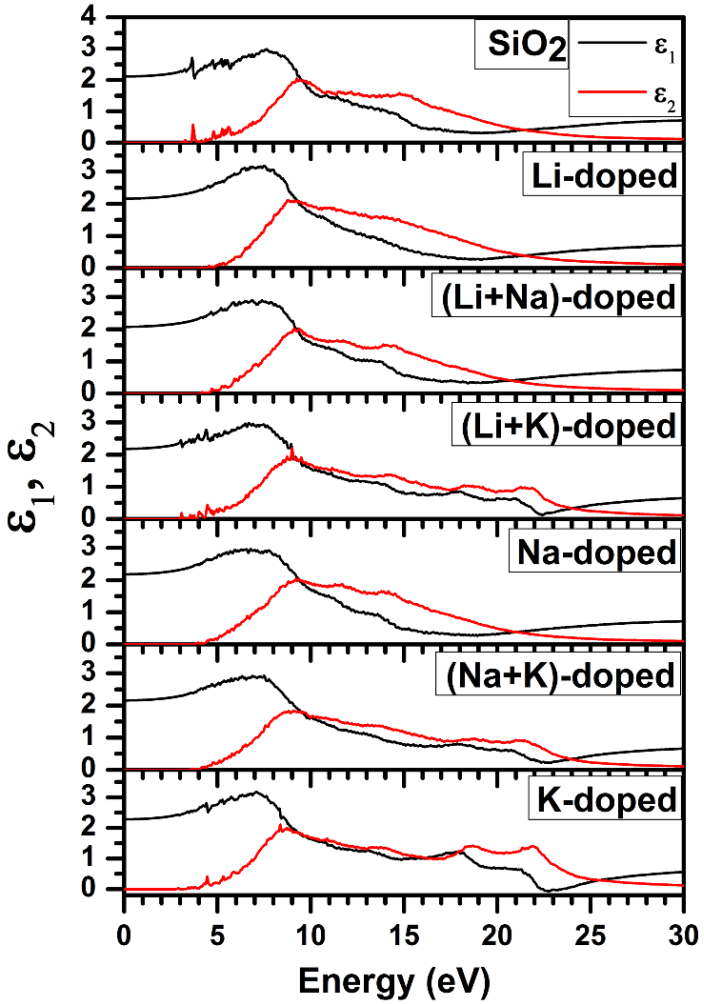

Figure 15.Calculated dielectric functions for the seven hydrated glass models.

3.3.6. Optical Properties

The calculated optical properties for the seven simulated glasses in the form of frequency-dependent complex dielectric functions as outlined in the method **Section 3.2.2** are shown in **Figure 15.** The general feature of the optical absorption curves represented by the imaginary part ε_2 are similar for all models, but the numbers of absorption peaks vary slightly. Li-silicate has only one prominent peak, pure silica has two peaks, Na-silicate and (Li+Na)-silicates have three peaks, while K-containing glass models have more than three peaks which is consistent

with the increased number of peaks in the VB and CB DOS of K containing glasses shown in **Figure 5**. When we move down the series from pure silica through Li→Na→K doped models in **Figure 15**, the absorption edge shifts to lower energy, consistent with a decreased band gap. In the mixed alkali glasses, (Li+K)-doped model has an absorption edge at the lowest energy end, and the other two mixed models follow the order of (Na+K)-doped < (Li+Na)-doped with increasing energy. The real part ε_1 calculated from the imaginary part using Kramer-Kronig conversion [163] follows a similar trend as ε_2. However, much of its value depends on the complex interplay of absorption edge, features on absorption curve, and band gap of the material. The comparison of the calculated refractive indices *n* for all glass models approximated by $\sqrt{\varepsilon_1(0)}$ is presented in **Figure 16** in the form of histograms and listed in **Table 6**. It shows that when the alkali silicate glasses are hydrated, *n* is slightly decreased for Li-silicate while it is slightly increased for Na- and K-silicate models. A MAE is observed to some extent for the mixed ions glasses. However, this is not conclusive and may depends on the specific compositions of alkali ions and water content. Hydrated SiO_2 glass has higher refractive index than anhydrous one. The refractive indices for both, anhydrous and hydrous, alkali silicates are higher than that of pure silica. This fact could be useful in the design of specific optical applications of glass where refractive is an important parameter.

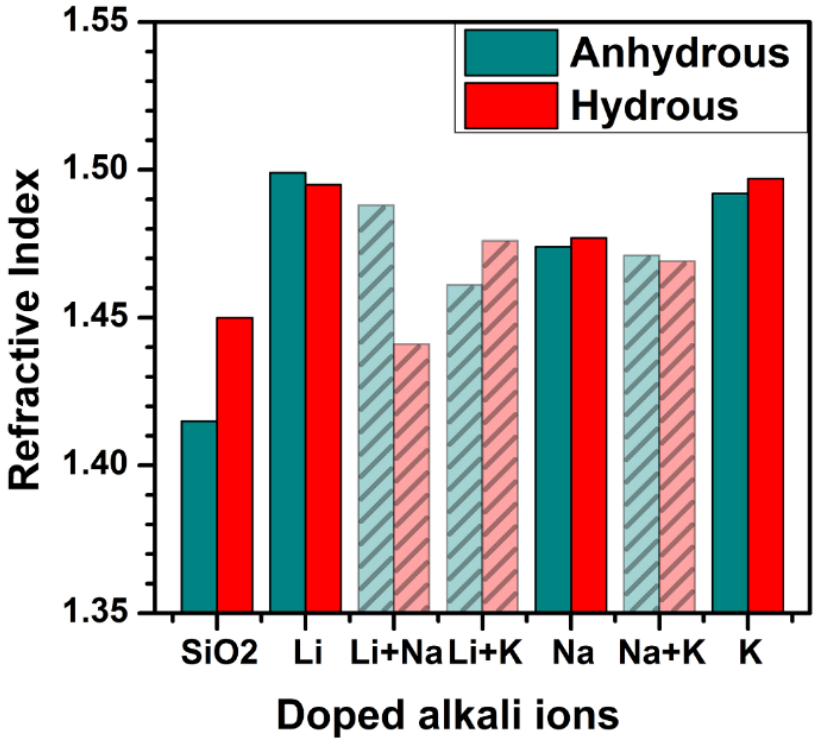

Figure 16. Comparison of refractive index between the seven anhydrous and hydrous models.

3.4. Discussion

In this section, we focus on the discussions of the results presented above on various aspects of properties in comparison with a few experiments or from other simulations. It should be stressed that such comparisons should be interpreted with caution since, in most cases, the samples or models are not exactly the same in compositions or the way samples were prepared. Within this context, we emphasize in specific perspectives this first-principles study brings the additional insights and meaningful conclusions that are currently absent.

Classical characterization of CN from structural geometry may not have much meaning in the case of complex multi-component glasses. The use of BO distribution is much more insightful. In the simulated models, CN for alkali ions mainly depends on their relative size.

Two things then become clear from calculated CN values: First, CN-2 gives a much larger CN compared to CN-1 because of the larger cut-off distances. Second, in single alkali doped glasses, CN value increases in the order of Li-ion < Na-ion < K-ion, but the trend is not clear in the mixed alkali cases when the CN-1 scheme is used. On the other hand, the trend is consistent for single and mixed alkali models when the CN-2 scheme is used. This clearly shows that CN-2 is a better criterion in defining the coordination number of alkali ions in hydrated alkali silicates.

The partial charge is another very useful quantitative information from *ab initio* calculations that are usually missing from MD simulations. It gives information of the specific charge transfer on each atom in relation to their local environment. **Figure 8** shows some of the intimate details that are part of the interatomic interactions in these seven models: (1) In the hydrated a-SiO_2 model with no alkali atoms, there are 3 Si atoms, and 6 O atoms with their PC deviates from the main group (shaded). This is consistent with the Si-Si and O-O bonds as shown in **Figure 11(b)**; (2) It clearly shows that the PC on the positively charged alkali ions and H atoms are in decreasing order of their size; and (3) The PC of H from water molecules or OH are slightly larger with associated O atom less negative O than those from the main O in the Si-O network. This is also the case with a few isolated O in (Li+K)-doped and (N+K)-doped glasses. These observations are obviously related to their special local bonding environments due to the complex ionization process in these models, as sketched in **Figure 9**.

Together with bond order values, the partial charge on each atom provides much more information on the electrostatic interactions and long-range interactions, especially when the total PC on each group of atoms can be summarized. In the present case, it is possible for us to

divide the total PC into three groups: alkali ions, Si-O network, and the water molecules, including the hydroxyl water. (See **Table 8**). It shows that in hydrated pure silica, the Si-O network has a positive PC which is balanced by water and hydroxyl group. In the case of hydrated alkali silicate glasses, both Si-O and (H_2O + OH) groups have negative PC, and total charge transfer is neutralized by positively charged alkali ions group. The total PC for alkali ion groups increases following the order of alkali ion sizes such that Li-group < Na-group < K-group.

Table 8. Calculated total PC for each group in the seven hydrated alkali-doped silicate glasses.

Groups	SiO_2	Li -doped	(Li+Na) -doped	(Li+K) -doped	Na -doped	(Na+K) -doped	K -doped
Si-O Network	4.24	-16.22	-18.19	-17.40	-19.41	-19.73	-21.62
Alkali Ions	-	17.40	19.20	19.80	20.77	22.99	24.79
H_2O and OH	-4.24	-1.19	-1.02	-2.40	-1.36	-3.27	-3.17

As already argued in the previous section, the TBOD and its partial components or PDOB is the most useful and simple quantum mechanical metric to describe each type of glasses and their internal cohesion as a complement to the total ground state energy. However, there is an important difference. Comparison of the total energy of different glass models must have the same atomic composition and number of atoms, whereas TBOD does not have this restriction and can be applied to different glass systems and compositions as long as they are calculated within the same method and same specifications. As already shown in **Section 3.3.4**, TBOD between slightly different glass structures or compositions provides the quantitative assessment of each glass. The importance of the quantitative determination of BO between every pair of atoms and the TBOD is the central theme of this paper. It can be applied to

systems with unconventional bonding such as the formation of a few isolated Si-Si and O-O bonding in the hydrated pure a-SiO_2 model, that cannot revealed by experimental probes. In classical MD simulations where the simulated results depends on the potential functions with predetermined parameters which prevents their formation. This is another vivid example of the power of the present method and approach that can yield additional insights previously not realized.

Chemical durability of glass, in general, is defined as the resistance offered by the glass surface against corrosion due to attacks by water, aqueous solution, and atmospheric agents.[164, 165] Based on a hydration effect, the glass-water reaction mechanism occurring at the glass surface is claimed to be crucial for the chemical durability of glasses. [166, 167] However, the hydration effect occurring in the bulk glass may also play a role in its mechanical strength and hence indirectly to its durability. In the present work, we show the hydration of bulk alkali silicate glasses increases their Young's modulus, bulk modulus, and shear modulus. This increase in mechanical strength with doping of water supports the durability of glass products. But to what extent the internal mechanical strength contributes to its durability and surface properties is an important research topic in glass science and that remains to be solved.

The knowledge of the refractive index is extremely important for the use of inorganic glass as an optical component. We show that doping of alkali elements in silica glass increases its refractive index in the case of Li and K but to a lesser extent with Na doping. When the alkali silicate glasses are hydrated, the refractive index varies only marginally with no clear strand except in the pure a-SiO_2. Some evidence of MAE seems present but cannot be viewed as conclusive. All this indicates that for optical properties and refractive index, in particular,

different roles of the structure, composition, hydration, and electronic properties, of these complex multi-component glasses are at play, and a firm conclusion will require more detailed experimental data and more comprehensive modeling efforts.

With regards to the mixed alkali effect, our results show that in the cases of TBOD, mechanical properties, and to a certain extent in the optical properties, MAE is observed in both hydrated and un-hydrated glasses showing an obvious deviation from the anticipated values with mono alkali doped glasses. In un-hydrated models, a similar conclusion was reported by R. Jagdt [168] on Young's modulus in (Na+K)-silicate and by K. Matusita [169] on bulk modulus in (Na+Cs)-silicate using ultrasonic interferometry more than half-century ago. We are not aware of more recent data on mixed alkali effects on bulk silicate glasses. Hence, one of the important conclusions from our study is that TBOD and elastic moduli exhibit MAE for both hydrated and un-hydrated cases in bulk silicate glasses.

3.5. Conclusions

In this paper, we report the results of detailed *ab initio* calculations of the structural, electronic, and physical properties on seven models for bulk hydrated alkali silicates and compare with the results of the corresponding un-hydrated models and pure SiO_2 glass. The main finding is the detailed description of the ionization process of water in the hydrated samples with different single and mixed alkali contents. Both molecular water and hydroxyl group OH exist in hydrated alkali silicate glasses. The complex nature of the interatomic bonding in these highly complex glassy systems is revealed. Such information is missing in most of the existing simulations based on classical molecular dynamics. The novel concept of TBOD is effectively used to characterize the internal cohesion and strength in the simulated

glasses. Hydrated Li-doped silicate is a stronger bulk glass than Na and K- doped silicates with a higher TBOD value. The band gap decreases with the increasing size of the alkali ions. A mixed alkali effect is clearly observed in TBOD and also in their mechanical property, and to some extent, in optical properties. A key finding of our study is in contrast to the notion that alkali ions and ionized water have an adverse effect on the glass network as they depolymerize it. What our simulations show that the presence of molecular water is not detrimental to the mechanical property; rather, it enhances this property in bulk samples.

It is quite obvious that the next step is to extend the present *ab initio* modeling to surface models, which could be very different from the present study restricted to bulk samples and are more important in real applications in glass technology. Along with the bulk properties, the study of surface-related properties in larger models with different water contents may reveal a more close connection to the concepts of chemical durability of glass products. Studies on such models are currently in progress, and we will report them in the near future.

CHAPTER 4

AB INITIO STUDY OF HYDROLYSIS EFFECTS IN SINGLE AND ION-EXCHANGED ALKALI ALUMINOSILICATE GLASSES

4.1. Introduction

Alkali aluminosilicates have a wide range of industrial, technological, and commercial applications.[170, 171] For example, sodium aluminosilicate glasses, after chemical strengthening, are widely used as protective display covers in modern electronic devices.[172, 173] Corning Gorilla® glass is one well-known example of such glass.[174, 175] Some specific compositions of alkali aluminosilicate are suitable for nuclear waste immobilization [50, 176]. Understanding the structural details and properties of these glasses is also important in Earth science since they are found in many rock-forming minerals.[177-179] Owing to the importance in geological phenomena and diverse applications in glass and material science, these glasses have been extensively studied in the past and continue to be the center of glass research.[180-183]

Alumina in aluminosilicate glass adjusts in the network mostly with $[AlO_4]^-$ tetrahedrons.[17, 18] However, these tetrahedrons carry a unit negative charge and differ from neutral $[SiO_4]$ tetrahedrons. As a result, alkali ions doped in an aluminosilicate network act as a charge compensator in $[AlO_4]^-$ tetrahedrons. If an excess of alkali ions than aluminum is present, those alkali ions modify the network. Thus, the alkali ions in an aluminosilicate network play two roles: a network modifier or a charge compensator in $[AlO_4]^-$ tetrahedrons, and the structure of this glass is strongly determined by the alkali to aluminum ratio R of constituent ions. For $R < 1$, alkali ions are not enough to balance the charge in some Al to be

in tetrahedral configuration, so those Al are forced into higher coordination state (5 or 6), which modify the network. For R > 1, a fraction of alkali ions compensate charge deficit in $[AlO_4]^-$ tetrahedrons, and the remaining ions modify the network. The most controversial case is for R = 1 when the numbers of alkali ions are just equal to balance the charge in $[AlO_4]^-$. At this composition, whether all Al will be in tetrahedral configuration or not is hotly debated. Some studies have suggested a fully polymerized glass structure with Si and Al tetrahedrons for R = 1.[21, 25, 26] However, some other studies have criticized the convention of such polymerization and shown the presence of non-bridging oxygen (NBO).[28, 184] There are many contradictory explanations regarding the polymerization of the alkali aluminosilicate network in relation to the ratio R. Even after numerous studies for many decades, this issue is not completely resolved. As the distribution and connectivity of Al in these glasses greatly affects the glass properties like density, viscosity, diffusivity, thermodynamic and transport properties, etc., a clear understanding of the role of alkali is extremely necessary.[185, 186] Hence, a comprehensive understanding of the structure and fundamental properties of this complex glass is essential for the design and development of the alkali aluminosilicate glasses as new functional materials.[187]

The water solubility and dissociation mechanism in silicate and aluminosilicate glasses have drawn great attention as water vapor is pervasive and has a profound effect on corrosion in these glasses. Water in almost all kinds of silicate glasses exists as molecular water H_2O and dissolved water in the form of the OH group.[43, 134, 188-190] It mostly ionizes to OH groups at small water content while remains as a molecule at large content.[42, 191, 192] Dissolved water in silica melt results in drastic changes in glass physicochemical properties like density,

viscosity, heat capacity, glass transition temperature, refractive index, etc.[188, 193-196] Hydrolysis in pure silica as well as in alkali silicate glasses is well studied by various experimental techniques and confirmed that water can break the Si-O-Si network into Si-OH following the reaction Si-O-Si + H_2O → 2 Si-OH.[72, 197, 198] However, this mechanism in more complicated multi-component alkali aluminosilicate glasses is comparatively less studied, and still many things left to understand in detail. Unlike silica, whether the water in alkali aluminosilicate glass depolymerizes the network or not is the subject of contention among glass researchers. Many arguments are made in support of and against the de-polymerization of the glass network, which makes the hydrolysis in alkali aluminosilicate glasses even more controversial and intriguing. Some studies have shown that due to hydrolysis, OH groups are present as bridging hydroxyls in the form of Si-OH-Al linkage and free hydroxyls as M-OH, leaving the degree of network polymerization unchanged.[199-203] However, this mechanism is severely criticized by other studies, and they support the de-polymerization of aluminosilicate framework by water along with the formation of Si-OH and Al-OH species.[196, 204-209] Despite numerous studies, the structural role of water in alkali aluminosilicate glasses remains unclear. A definitive conclusion regarding the hydrolysis of these glasses at the atomistic level is still lacking.

Another hotly debated issue in alkali-doped glasses is the so-called mixed alkali effect (MAE). It is an observation of the non-additive variation in some glass properties when one type of alkali ion is partially substituted by another, forming the mixed ions glass. The MAE has been the subject of intensive study for many years.[30, 32, 210, 211] Many studies are focused on MAE manifested in transport properties like diffusion, conductivity, viscosity,

etc.,[38, 212-214] while it is less studied in static properties like molar volume, mass density, optical and mechanical properties. Herein, we carry out a systematic study on the MAE for static properties based on precisely created glass structures from a more accurate AIMD technique. Because of the complexity in the underlying mechanism and many contradictory theories related to MAE, this phenomenon remains a puzzling and unresolved topic. Accurate and carefully designed simulations can facilitate the understanding of this phenomenon.

In the present work, we aim to clarify some of the important issues raised above. Our main goal is to understand the alkali ion size effect and hydrolysis process in alkali aluminosilicate glasses to provide new insights into their physicochemical properties. To this end, we carry out a comprehensive study on the structure and properties of both anhydrate and hydrated glasses. Detailed information on the electronic structure and interatomic bonding is revealed, which is difficult to access by experimental means and missing in computational studies of these glasses. We show that theoretical simulation can be a powerful alternative to explore the properties of complex glasses using the state-of-the-art AIMD method and large-scale quantum mechanical calculations. This paper is structured as follows: **Section 4.2** outlines the model construction and the simulation strategy used. The comprehensive results and their discussions are presented in **Section 4.3**. In the last **Section 4.4**, we provide a summary and major conclusion together with the prospect for future directions.

4.2. Simulation Strategy

Computer modeling and simulation are an alternative to experimental techniques to provide insight into issues that cannot be addressed directly by experiment. It helps in a comprehensive exploration of local atomic structures and can guide the experiment in many

cases. Molecular dynamics (MD) is one of such modeling tools widely used in glass studies and has successfully applied for silicate glasses.[215] In such studies, the quality of simulation is strongly determined by the functional form of interatomic potential and the parameters used to define it. Classical MD has been used to some extent to study sodium aluminosilicate glasses [216-223] and in a limited amount for potassium and mixed alkali aluminosilicate glasses.[214, 224] The lack of accurate potential in the case of complex multi-component glasses with mixed alkali ions and their hydrated structures imposes an unsurmountable obstacle for classical MD. Especially in the case of a glass-water reaction with mixed ionic, covalent, and hydrogen bonding, developing a potential that can describe the hydrolysis of the glass network and the chemical reaction occurring thereby is the most challenging task. For such a system, density functional theory (DFT)-based AIMD is the only alternative where the ionic forces are calculated on the fly during simulation from an accurate treatment of electronic structure. Thus, we choose AIMD to simulate the single and mixed alkali aluminosilicate models, including glass-water reaction and the related properties.

We construct three anhydrate alkali aluminosilicate glasses: Na-doped (NAS), (Na + K)-doped (NKAS), and K-doped (KAS) using the melt and quench technique. This allows us to get an overview of the nature of cation effects on the single and mixed alkali aluminosilicate glass properties. The hydrated models are constructed by doping 12 water molecules in each anhydrate model and are correspondingly named as NAS-W, NKAS-W, and KAS-W. So, we simulate and study 6 models in this work. **Table 9** lists the glass composition in mol % and the number of atoms in each model. The anhydrate (hydrated) model has 680 (716) atoms each.

The same names listed in Table 9 are used throughout the text, in other tables, and in the figures to facilitate the presentation and discussion.

Table 9. Representation of simulated glass models, their composition in mol %, and the corresponding number of atoms.

Glass Models	Si	Al	Na	K	H	O	Total	H_2O
NAS $(Na_2O)_{0.2}(Al_2O_3)_{0.2}(SiO_2)_{0.6}$	120	80	80	-	-	400	680	-
NKAS $(Na_2O)_{0.1}(K_2O)_{0.1}(Al_2O_3)_{0.2}(SiO_2)_{0.6}$	120	80	40	40	-	400	680	-
KAS $(K_2O)_{0.2}(Al_2O_3)_{0.2}(SiO_2)_{0.6}$	120	80	-	80	-	400	680	-
NAS-W → NAS + 12 H_2O	120	80	80	-	24	412	716	6
NKAS-W NKAS + 12 H_2O	120	80	40	40	24	412	716	6
KAS-W KAS + 12 H_2O	120	80	-	80	24	412	716	5

Similar to our previous studies [85, 87, 122], we used AIMD as implemented in the Vienna *ab initio* simulation package (VASP) [225] to construct our dry glass models. The initial models are created by randomly enclosing the atoms in a cubic box with periodic boundary conditions and cell parameters determined based on available experimental density.[226] The initial configuration of each system was heated to 4000 K, well above the melting temperature of alkali aluminosilicate glass within two ps. The melt was then well equilibrated at this elevated temperature for ten ps to reach the steady liquid state independent of the initial random distribution of atoms. The melt was then quenched to room temperature, 300 K adopting two different quenching rates. From 4000 to 2000 K a slightly higher cooling rate (~50 K/ps) was used but in the glass forming region below 2000 K, a nominal quenching rate of ~25 K/ps was

used. The structures in the glassy state at room temperature were further equilibrated for 10 ps, resulting in the total simulation time for each model to be 130 ps. This is a reasonable time duration for model construction considering the size as the models are among the largest attempts for AIMD simulations. After reaching the last configuration of the trajectory for each model at room temperature, we switch back to general relaxation to optimize the structure with no constrain on the cell size or shape until the total energy is fully converged to the specified criterion of less than 10^{-5} eV for each model. The structures of the fully relaxed models at room temperature are used as input in the orthogonalized linear combination of atomic orbitals (OLCAO) method for electronic structure, bonding, and optical properties evaluation.[93]

Each of the three hydrated models, NAS-W, NKAS-W, and KAS-W, contains 12 water molecules. This number of water molecules is determined by a series of test calculations by doping of 6, 8, 10, 12, 15, and 20 water molecules dispersed at the interstices of the NAS glass model so that they do not overlap with the host atoms. Each model with a different number of water molecules is then fully relaxed and used in the OLCAO calculation to obtain the TBOD and highest internal cohesion. We found that the model containing 12 water molecules exhibits the highest TBOD. Based on these extensive tests, we decided to adopt 12 water molecules in all three models in the current work. As our glass models are fairly large and *ab initio* DFT calculation for such a large and complex system is very expensive, testing for the optimal number of water molecules for each of them will be a daunting task and not cost-effective. Details about hydrated model creation and corresponding TBOD values for tested models are reported in our previous work.[87]

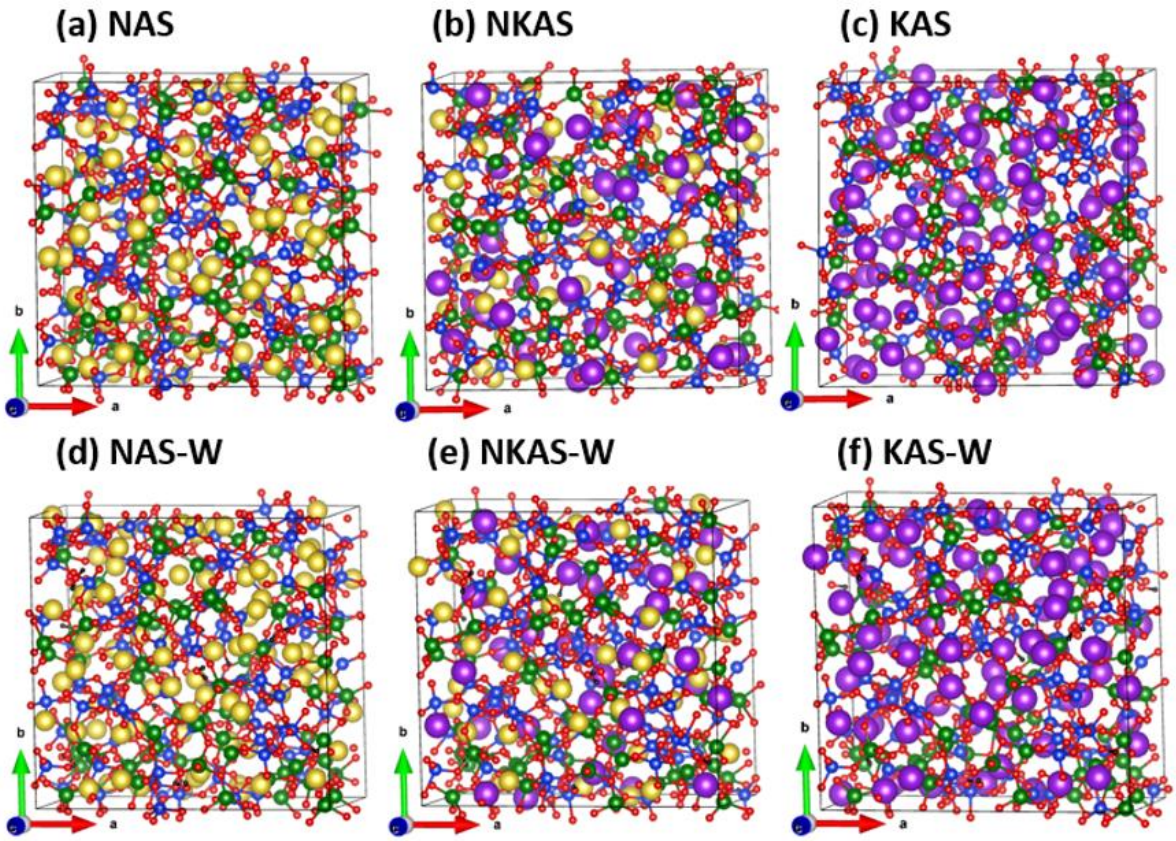

Figure 17. Ball and stick representation of relaxed glass structures (a) NAS, (b) NKAS, (c) KAS, (d) NAS-W, (e) NKAS-W, (f) KAS-W. Si (Blue), Al (Olive), Na (Golden), K (Purple), O (Red) and H (Black).

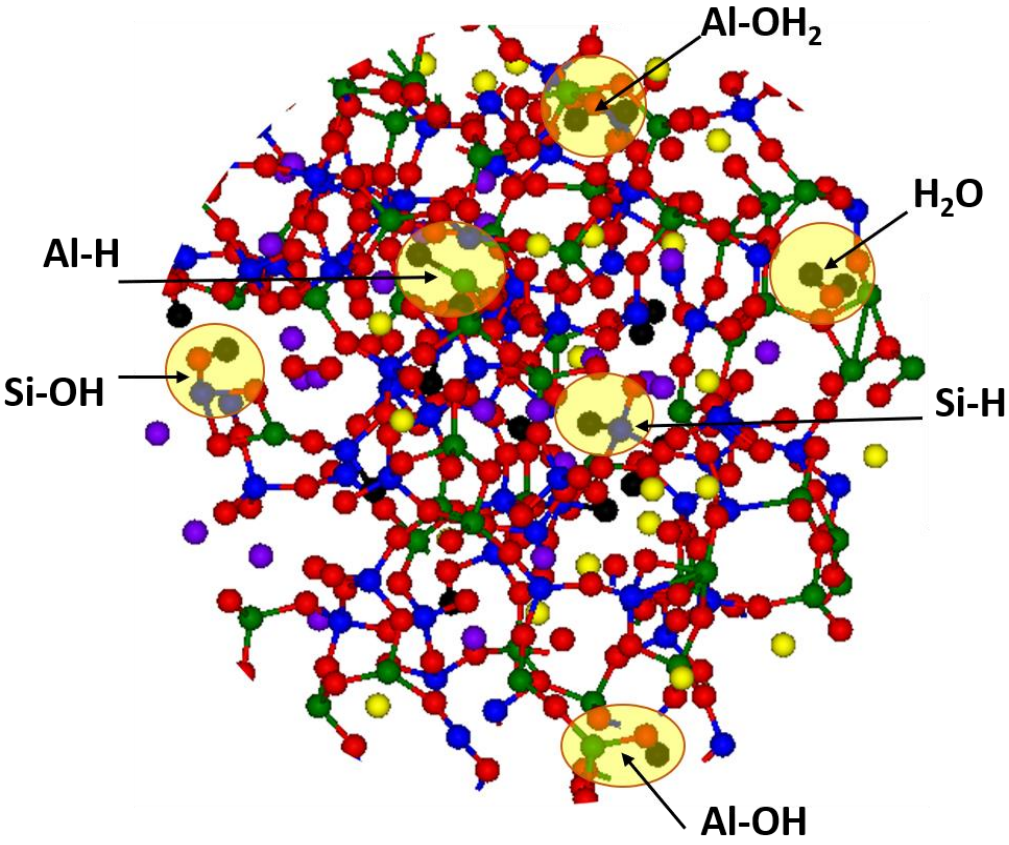

Figure 18. Sketch of simulated glass model showing the molecule H_2O and ionized water OH present in the glass.

Table 10. Structural parameters of simulated glass models (Volumes are expressed in $Å^3$ and density in gm/cm^3). * Ref. [226]

Glasses	a(Å)	b(Å)	c (Å)	α^0	β^0	γ^0	Volume	Density
NAS	21.32	21.07	21.16	88.83	91.24	90.82	9500.51	2.41, 2.43*
NKAS	21.33	21.34	21.36	88.39	88.85	89.66	9720.91	2.46
KAS	21.60	21.59	21.59	89.25	90.93	89.46	10065.92	2.49
NAS-W	21.44	21.12	21.42	89.28	90.50	91.09	9699.99	2.39
NKAS-W	21.68	21.32	21.82	88.69	90.23	91.13	10077.95	2.41
KAS-W	22.02	21.51	22.05	89.17	90.09	91.73	10436.89	2.43

4.3. Results and Discussions

4.3.1. Structural Analysis

4.3.1.1. Simulated Dry and Hydrated Structures

The snapshots of six fully relaxed glass models are displayed in **Figure 17,** which shows that the backbone of the network is formed with Si and Al tetrahedrons connected by bridging O. Detailed inspection of these figures shows that some water molecules remain intact as molecular water H_2O while remaining are dissociated producing hydroxyl group OH bonded with Si or Al as shown in **Figure 18**. The number of undissociated water molecules in the hydrated models is listed in **Table 9**. It is observed that the Na and K containing glass has different abilities to dissolve water. The corner-sharing Si-O and Al-O bonds afford the geometric freedom to form the random network structure and hence avoid crystallization. As these balls and stick sketches of the simulated glasses are merely the geometrical representation, details about the bonding structure and their electronic property will be discussed in the next sections. **Table 10** lists the structural parameters of simulated glasses. It shows that the density of the hydrated models decreases due to the volume expansion with the presence of water molecules.

4.3.1.2. Pair Distribution Function Analysis

In a non-crystalline amorphous material, the pair distribution function (PDF) provides the short-range local structural information of ions in the environment of neighboring ions. **Figure 19** shows the calculated PDFs for cations-oxygen (Si-O, Al-O, Na-O, K-O, and H-O) and O-O pairs in six glass models. In the double paneled figure, the top panel is the PDF for dry models, while the bottom panel is for hydrated models. The primary peak for Si-O PDF is at

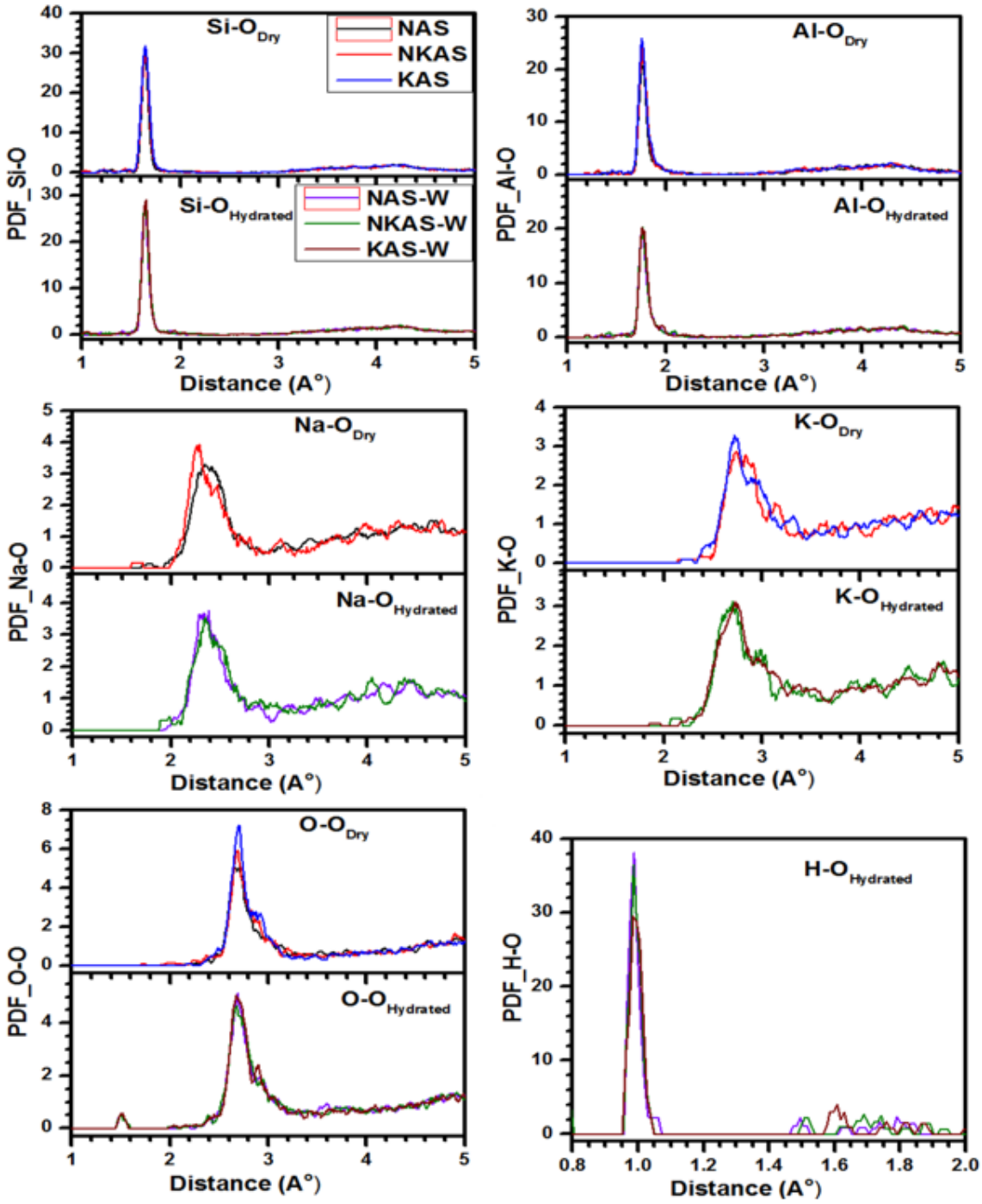

Figure 19. (a) Si-O, (b) Al-O, (c) Na-O, (d) K-O, (e) O-O and (f) H-O pair distribution function (PDF) in simulated dry and hydrated glass models. The top panel of figure (a-e) represents PDF in dry model while bottom panel is for hydrated models.

1.64 Å in dry models and at 1.65 Å in the hydrated models. This peak position is insensitive to the type of alkali ions and does not change in the series, but the peak intensity increases with increasing alkali ion size in both dry and hydrated glasses. Due to hydrolysis, the Si-O peak changes by 0.01 Å, and the peak intensity decreases slightly. The peak of the Al-O pair lies at 1.75 Å in both dry and hydrated models implying that this peak is insensitive for both, size of alkali ions and the hydrolysis effect. However, like Si-O, the peak intensity increases with increasing alkali ion size and decreases due to hydrolysis. The Al-O PDF is broad with less intensity than Si-O due to the weaker covalent feature of the Al-O bond than Si-O. The sharply peaked PDFs for Si-O and Al-O pairs imply a clearly defined short-range order (SRO) in these glasses. These pairs do not show any noticeable peaks beyond 2 Å, indicating the lack of long-range order (LRO) beyond this distance. Atila et al. found the first peak for Si-O, and Al-O pairs in NAS and KAS does not depend on the type of alkali ion and noted the peaks at around 1.61 Å and 1.73 Å respectively in both glasses with 50 mol % SiO_2 and R =1.[222]

The PDFs for M-O (M=Na, K) and O-O pairs are quite broad compared to Si-O and Al-O, and the peak lies beyond 2 Å. The primary peak positions for Na-O, O-O and K-O pairs are at ~2.30 Å, ~2.68 Å, and ~2.72 Å, respectively. The peaks for Na-O and K-O pairs are sensitive to the presence of other alkali and to hydrolysis. Due to hydrolysis, the averaged bond length for these pairs increases slightly by 0.01 Å (K-O) - 0.04 Å (Na-O). Like Si-O and Al-O, the peak intensity in these pairs slightly decreases due to hydrolysis. In O-O pairs, the peak position appears to be less sensitive to alkali ion size; however, its intensity increases with increasing alkali ion size. A quite interesting result is observed in O-O PDFs for hydrated models in which a secondary peak of small intensity appears at 1.48 Å. Due to hydrolysis, the

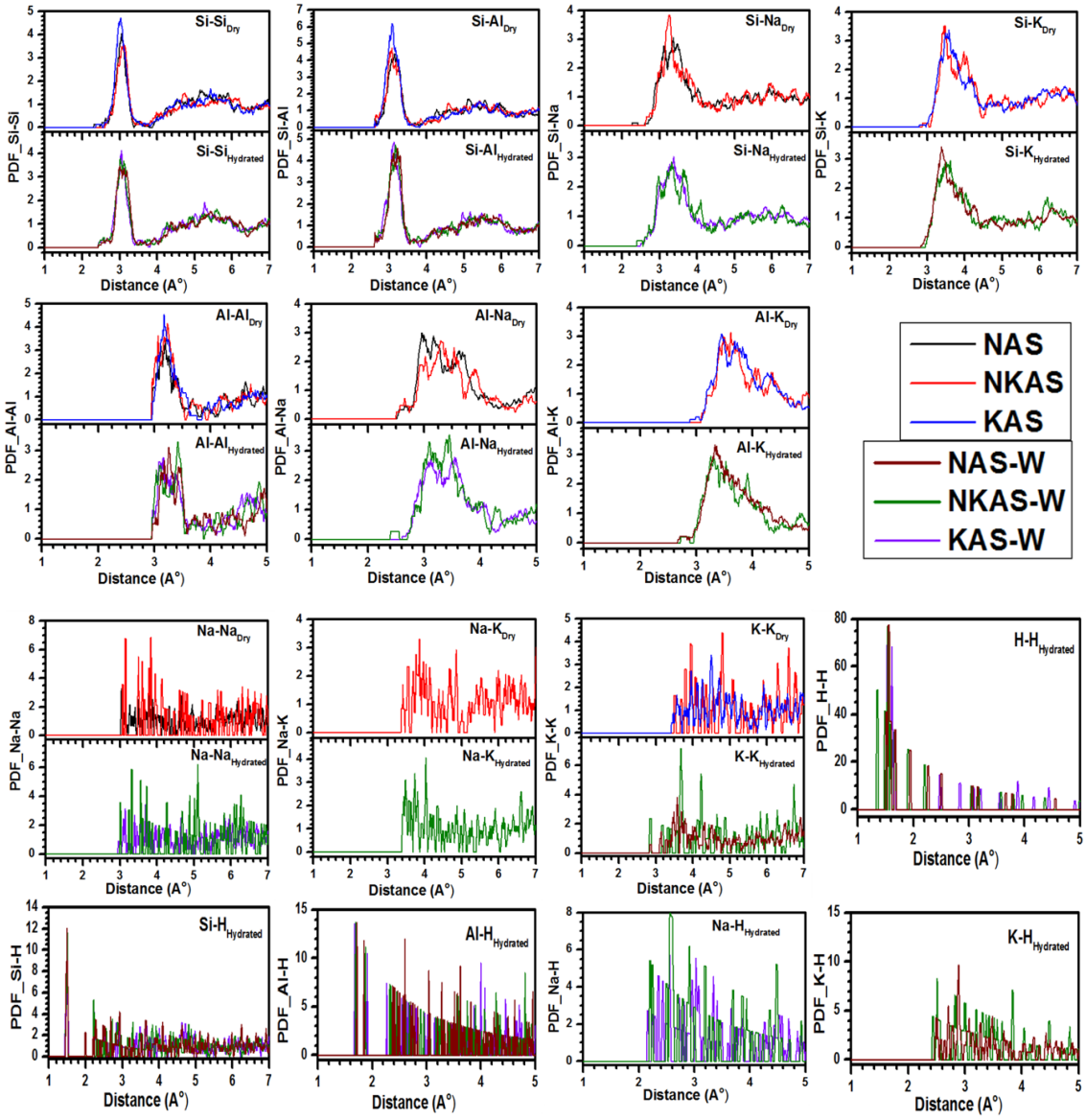

Figure 20. Calculated pair distribution function (PDF) among the cations in the simulated glass models. In the two-panel figure, top panel represents the PDF for dry models while bottom panel represents that for hydrated models.

intensity of O-O pairs decreases. In the hydrated models, the H-O pair is sharply centered at ~0.98 Å, reflecting the rigid covalent O-H bonds. Minor peaks of small intensity are observed beyond 1.5 Å resulting from the weak hydrogen bonding in the network. Based on the averaged distance of the peak position, the bond length follows the order of H-O<Si-O<Al-O<Na-O<O-O<K-O. The PDFs for cation-cation pairs are shown in **Figure 20**. It shows that the PDFs for some pairs like Si-Si, Si-Al have well-defined primary peaks while the PDFs for other pairs have the primary peak merged with secondary peaks implying the change in nature of bonding between those ions. Especially the alkali-alkali and (Si, Al, Na, and K)-H PDFs have sharp distributions.

4.3.1.3. Bond Angle Distribution Analysis

The bond angle distribution (BAD) provides information on the medium-range order property in the simulated glasses. The inter-tetrahedral angles O-Si-O and O-Al-O for Si- and Al-tetrahedral units are presented in **Figure 21**. The O-Si-O angles in both dry and hydrated models are sharply distributed with the primary peak centered at ~109^0, close to the value in perfect tetrahedral geometry (109.5^0), which implies regularity of SiO_4 tetrahedrons in the simulated glasses. The peak position of this angle is not much sensitive to alkali ions size and hydrolysis effect; however, the intensity changes slightly with alkali ions size. The distribution for O-Al-O angles in dry models is centered in the range of 109^0-112^0. In the hydrated models, the peaks for this angle are broader and spread in a wider range, 106^0-112^0, than in dry models. The peak position for this angle depends on the alkali ion size, and the deviation is higher in hydrated models. The intensity of this peak increases in dry models and decreases in hydrated models when alkali ion size increases. The O-Al-O angle distribution in both dry and hydrated

models is broader and has less intensity than O-Si-O, indicating the irregularity of [AlO_n] polyhedrons.

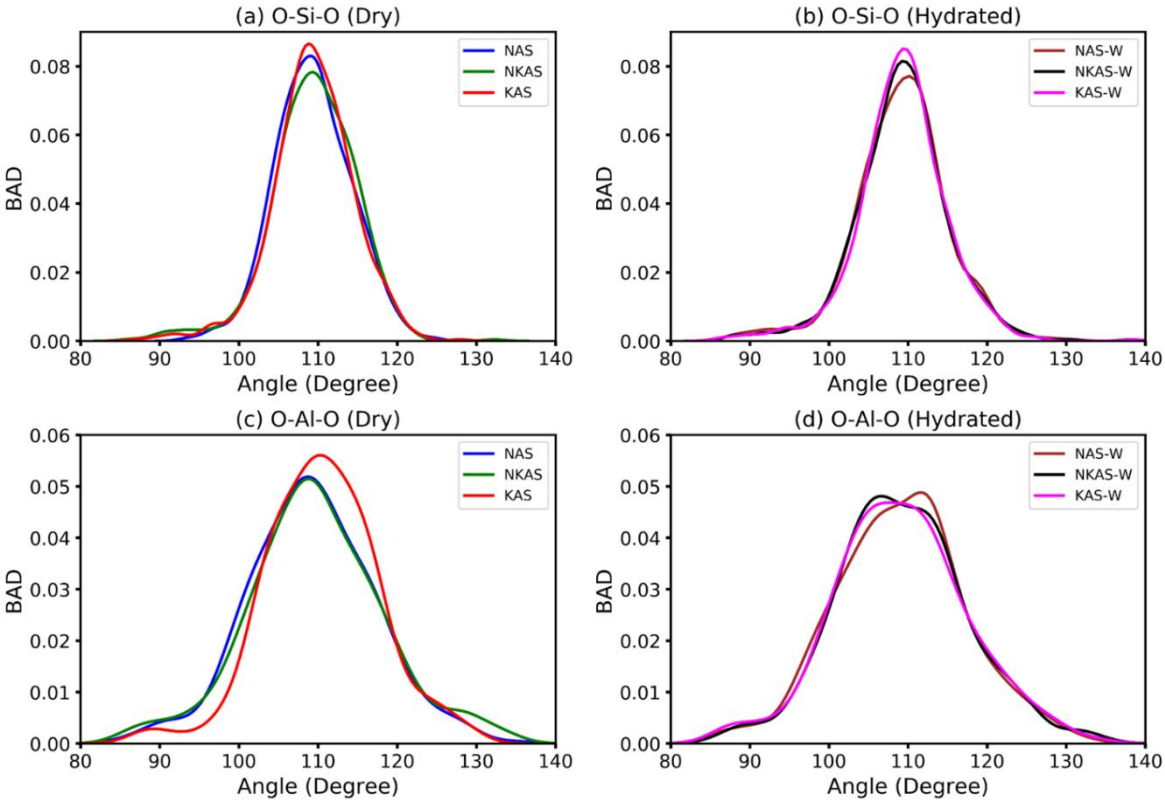

Figure 21. Bond angle distribution for (a-b) O-Si-O, and (c-d) O-Al-O in simulated dry and hydrated glass models, respectively.

The distribution of bond angles Si-O-Si, Si-O-Al, and Al-O-Al, for inter-glass network former tetrahedral units in simulated glasses are shown in **Figure 22**. The framework geometry of these bridging angles, which is governed largely by constraints on Si-O and Al-O bonds, determines the major structural feature of the simulated glasses. The Si-O-Si angle in dry models is centered in the range of 130^0-$140^{0,}$ and it shows the distribution strongly depends on

the size of alkali ions. In the hydrated glass, the central peak is around $130^{0,}$ and it is less sensitive to alkali ions size. This angle spreads over a wider range in the (Na+K)- and K-doped glasses than Na-doped glass in the dry models, while it spreads in the same range in the hydrated models. The Si-O-Al angle is centered in the range of 125^0-135^0 in dry models while around 130^o in hydrated models. The Si-O-Al distribution has less intensity than Si-O-Si, and peaks are centered at a lower value in dry models. The difference in the distribution value of Si-O-Si and Si-O-Al angles is due to the difference in charge distribution of Si and Al. The bond angle calculated for Al-O-Al in dry models is centered in the range 120^0-$135^{0,}$ and in the hydrated models, it is centered around 125^0. The Al-O-Al angles spread over a wider range, centered at a lower value, and have a lower intensity compared to Si-O-Si and Si-O-Al angles. The broader distribution of this angle reflects the presence of some higher coordinated Al (5 and 6) than mostly 4-coordinated Si. The presence of Al-O-Al network linkage in these glasses implies violation of the so-called Al-avoidance principle which states that in two bridged tetrahedrons, only one Al is possible as a central atom.[227] It shows that Loewenstein's Al-avoidance principle obeyed in many aluminosilicate crystalline phases is not necessarily valid in amorphous glasses. In all three types of bridging angles, the deviation of peak position in hydrated models is small compared to dry models. The distribution for some of these angles is bimodal, with a small peak centered around 90^0, which arises due to edge-sharing polyhedral units. Similar results are reported for bridging angle distributions in a study of amorphous Al_2O_3 and alkali aluminosilicate glasses.[217, 228]

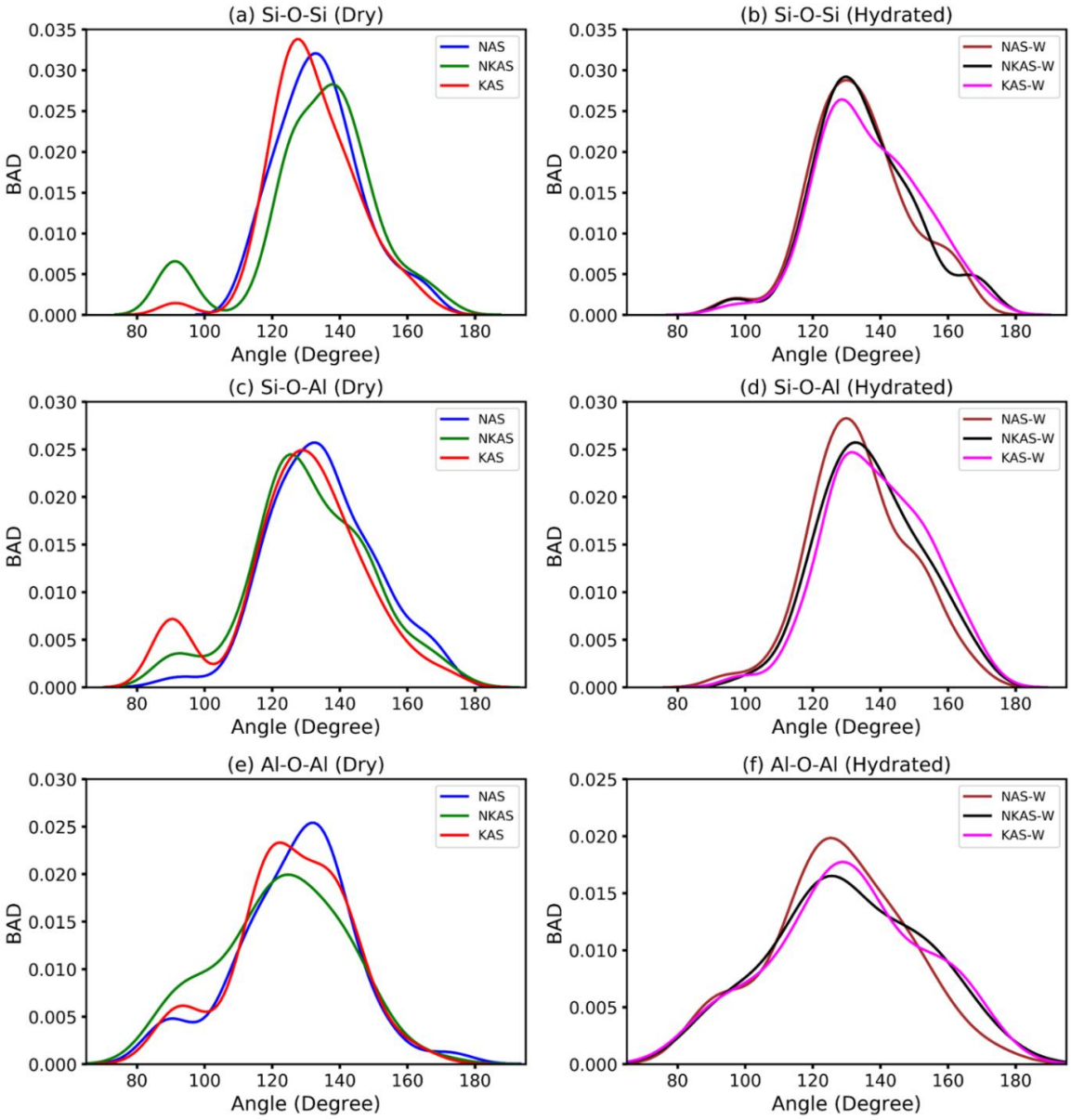

Figure 22. Inter-polyhedron bond angle distribution of (a-b) Si-O-Si, (c-d) Si-O-Al and (e-f) Al-O-Al in simulated dry and hydrated glass models, respectively.

Table 11. Calculated coordination number and partial charge (in unit of e) of atoms, band gap (eV) and refractive indices (n) in the simulated glasses (Cutoff distances for Si-O, Al-O, Na-O, K-O and H-O are 2.20, 2.40, 3.10, 3.80, and 1.40 Å respectively).

Glasses	Coordination Number					Partial Charge						Band Gap	n
	Si	Al	Na	K	H	Si	Al	Na	K	H	O		
NAS	4.00	4.08	5.40	-	-	1.90	1.56	0.69	-	-	-1.02	3.64	1.48
NKAS	4.00	4.06	4.73	6.08	-	1.91	1.58	0.69	0.72	-	-1.03	3.62	1.49
KAS	4.00	4.03	-	5.89	-	1.92	1.59	-	0.72	-	-1.04	3.26	1.51
NAS-W	3.97	4.09	5.26	-	0.79	1.85	1.57	0.69	-	0.26	-0.99	2.52	1.51
NKAS-W	3.95	4.08	4.50	6.45	1.00	1.87	1.57	0.68	0.68	0.26	-0.99	2.27	1.53
KAS-W	3.96	4.11	-	5.84	0.88	1.88	1.57	-	0.68	0.27	-1.00	2.22	1.54

4.3.1.4. Coordination Number Analysis

The coordination environments of Si and Al are important parameters in delineating the tetrahedral distribution of these ions in the network and their value depends greatly on the chemical composition as well as on thermal and pressure history of glass formation.[229, 230] The averaged coordination number (CN) of ions in the simulated models can be obtained by integrating the PDF to a specific cutoff distance equal to its first minimum for each pair. The calculated CNs of cations Si, Al, Na, K, and H with O and the cutoff distances used for each pair are listed in **Table 11.** The averaged CN of Si in dry models is 4, which implies perfect SiO_4 units in our simulated models. A similar result is reported in theoretical [222] and experimental [231] studies of alkali aluminosilicate glasses with slightly different silica compositions. In the hydrated models, the CN of Si decreases slightly, but it is still close to 4, implying that the local structure around Si is not that much sensitive to hydrolysis.

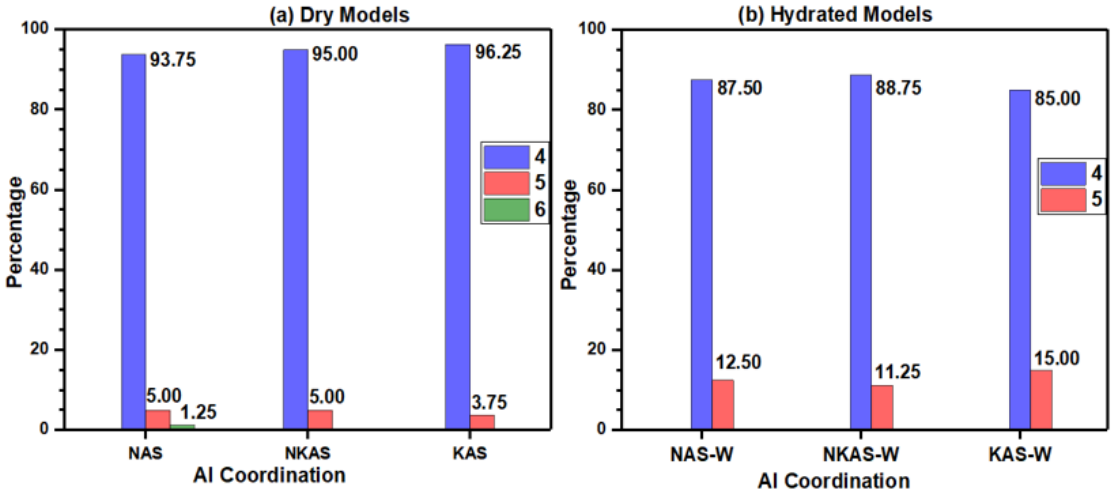

Figure 23. Distribution of Al coordination with O in aluminosilicate skeleton of simulated dry and hydrated glasses.

The distribution of Al coordination in aluminosilicate glass greatly influences the glass properties like density, viscosity, compressibility, heat of mixing, etc.[19, 232, 233] Therefore, it is important to carefully analyze the higher coordinated Al to understand glass properties with different alkali ions sizes and when the glass is hydrated. The averaged CN for Al in all models is slightly higher than 4 due to the presence of higher coordinated Al. **Figure 23** shows the distribution of Al coordination with O atom expressed in percentage. Even if enough alkali ions are present to compensate the charge in $[AlO_4]^-$ tetrahedrons, all Al do not maintain tetrahedral distribution rather, few 5-coordinated Al and a very small fraction of 6-coordinated Al (1 atom in NAS glass) exist in the simulated glasses. As Na and K have different abilities to balance the charge in Al polyhedrons, the Al coordination is different in the Na and K containing glasses. The majority of Al, i.e., more than 90%, forms tetrahedral coordination in dry models, and this value increases in moving from Na-doped to K-doped glass. Only 1 Al atom is found 6-coordinated in NAS glass; however, such Al does not exist in other glasses. In dry models, the total content of higher coordinated Al (5 and 6) decreases in the series from Na- to K-doped glass. Due to hydrolysis, the network gets depolymerized, and the amount of 4-coordinated Al decreases while 5-coordinated Al increases in each of the hydrated models. The mixed ions glass, NKAS-W, has the lowest percentage of 5 coordinated Al, and KAS-W has the highest value, followed by the NAS-W model. The Al coordination changes to a higher value to maintain the charge neutrality when the alkali ions do not compensate the charge in $[AlO_4]^-$.[234] The existence of 5-coordinated Al at ambient pressure in alkali aluminosilicate glasses is verified experimentally.[231, 235] Their content depends on the cooling rate, and they are found to increase with an increase in fictive temperature.[236] The CNs for Na and K

ions are greater than 4, and K has higher CN than Na. For H atom, CN value is 1 in NKAS-W glass while less than 1 in the other two NAS-W and KAS-W glasses. **Figure 24** shows the averaged CN of cations (Si, Al, Na, K, H)-O pair with varying cutoff distances. For Si and Al, they sharply rise after 1.6 Å and 1.7 Å respectively and maintain a constant value after that, but for Na and K, they keep increasing with increased cutoff distances. For H, the CN increases sharply at 1 Å, but after that, it increases continuously with increase in cutoff distance.

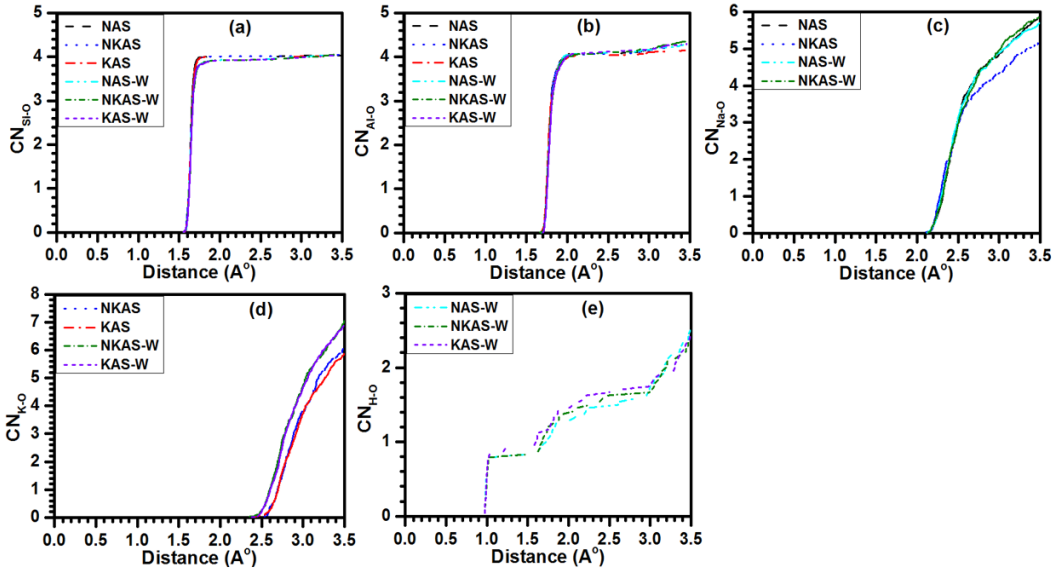

Figure 24. (a) Si-O (b) Al-O (c) Na-O (d) K-O and (e) H-O coordination number (CN) functions in the simulated glass models.

4.3.2. Electronic Structure

This section reports the details on electronic structure results, including the interatomic bonding among the atomic species in simulated glasses. Electronic structures are fundamental properties of a material at the atomistic level, which help understand the macroscopic properties emerging from microscopic characteristics. Despite several theoretical studies on

alkali aluminosilicate glasses, it is intriguing to note that electronic structure information is still missing or not widely available. We think the detailed analysis of the electronic structure carried in this work will fulfill this gap.

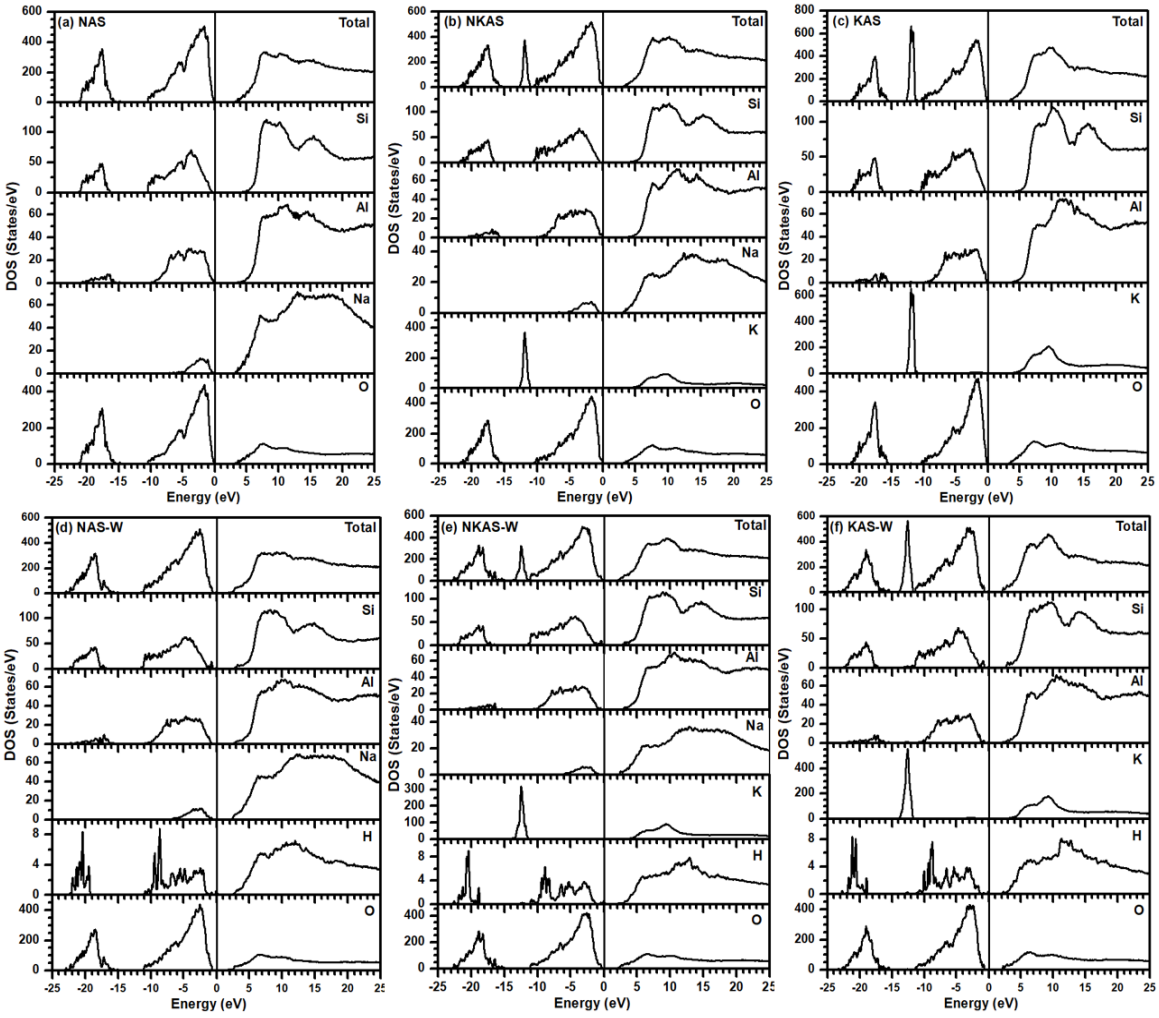

Figure 25. Calculated total and atom resolved partial density of states (DOS) for (a-c) dry and (d-f) hydrated alkali aluminosilicate glasses.

The calculated total and atom resolved partial density of states (DOS) in the simulated dry and hydrated models are presented in **Figure 25 (a)** and **(b),** respectively. The zero of the energy scales is set at the top of the occupied valance band (VB), separated from the unoccupied conduction band (CB) by the band gap E_g. The total DOS (TDOS) in VB splits into two segments, lower and upper, separated by about 5.0 eV in dry models and a slightly smaller value in the hydrated models. The partial DOS (PDOS) reveals far more information on these spectra and shows the lower segment of TDOS originates mainly from the O atom (2-s orbital). The O atom contributes to the upper segment of the VB and in the CB region TDOS also. The orbitals from Si and Al mainly contribute to the upper segment of the VB and in the CB region TDOS. The alkali ion Na predominantly contributes to the CB region, while K contributes to the CB region as well as in the VB region for a sharp peak in between lower and upper segments. In the hydrated models, the H atom has a small contribution in both VB and CB spectra. After doping K ions, a sharp peak originating from the semi-core K-3p orbitals emerges between the lower and upper VB DOS segment in both dry (NKAS and KAS) and hydrated (NKAS-W and KAS-W) models. This makes the VB spectra quite different for K- and Na-containing glasses. In dry models, this sharp spectrum is separated by about 1.0 eV from upper segment VB DOS while this separation is almost zero in the hydrated models. These differences in DOS spectra reflect the short- and intermediate-range differences due to different alkali ions size and hydrolysis. This information at atomic levels is quite useful in the electronic structure and helps to understand optical properties in the simulated glasses.

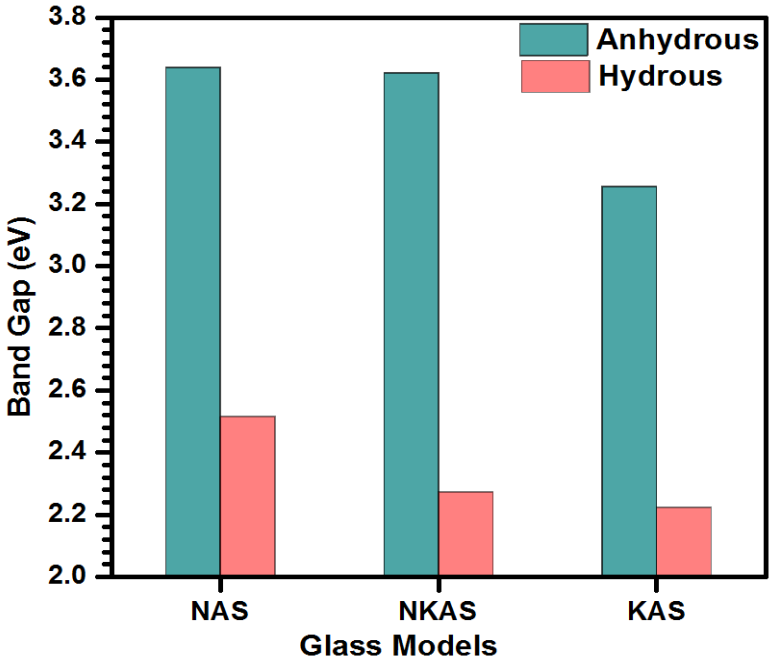

Figure 26. Variation of band gap in the simulated glasses.

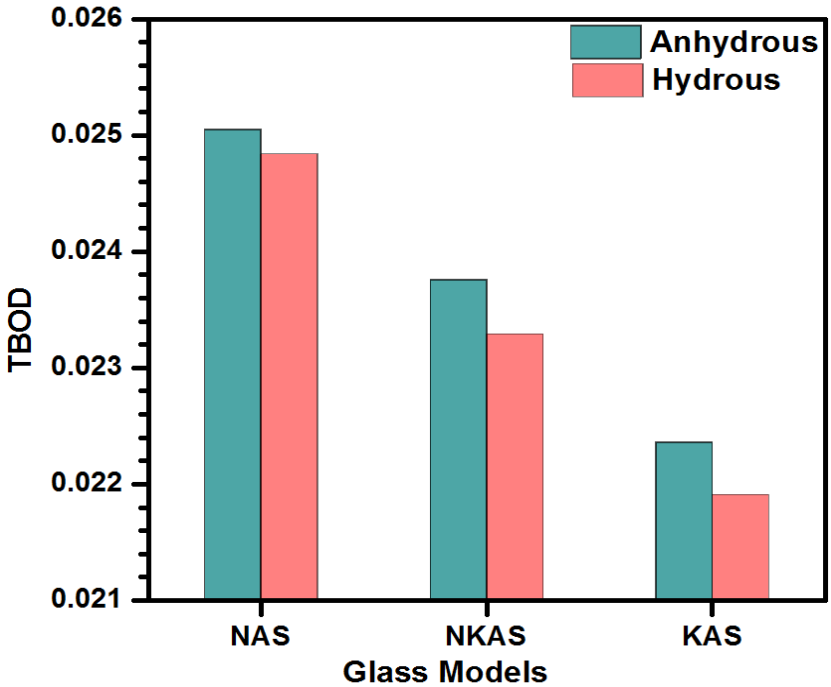

Figure 27. Variation of TBOD in the 6 simulated glass models.

The CB total spectrum is quite flat and more similar in dry and hydrated glasses. PDOS shows, each atom contributes to a certain extent to the CB spectrum. In moving from Na-doped to K-doped glasses in both dry and hydrated models, the E_g decreases as shown in **Figure 26**. The calculated E_g values for all models are listed in **Table 11**. Due to hydrolysis, the band gap decreases sharply in all three models. In the dry models, the band gap decreases faster on moving from NKAS to KAS glass, while in the hydrated models, it is from NAS-W to NKAS-W. The decrease in band gap is not linear but shows no sign of MAE. We want to inform that the calculated band gap in this study might be smaller than the experimental value as it is well known that LDA calculation generally underestimates the band gap.

We now discuss about the internal bonding topology and provide a complete interatomic bonding picture in the simulated glasses. The bond order (BO) value in a material measures the relative strength of a bond between a pair of atoms and quantifies that material's bond stiffness and internal strength.[158, 237] As BO is a quantum mechanically derived value, it is a far more accurate and concise parameter to define bonding structure than using purely geometrical parameters like PDF, CN, etc. In general, BO scales with bond length (BL), but in the realistic quantum mechanical calculation, the effect of bond angles and contributions from surrounding atoms in the local environment of bonded pairs are also included. The BO values in a system sum up to give a single quantity called total bond order (TBO) value. The TBO value normalized with the volume of the cell gives TBO density (TBOD) which depends on the number of bonds and strength of each bond pair. TBOD is a compelling indicator and a single quantum mechanical metric to characterize the overall cohesion of the material. **Figure 27** displays the calculated TBOD in the six models. It decreases in the series with increasing

size of the alkali ion in both dry and hydrated models that can be attributed to the increased volume in the series with K. For the same reason; the hydrated models have lower TBOD than the dry one. The decreased TBOD in the series implies that the increase in alkali ion size weakens the alkali aluminosilicate glass network. The lower TBOD value in the hydrated model suggests water ruptures the glass network depolymerizing it, and decreases the total internal cohesion. We did not notice any sign of MAE in TBOD.

Table 12. Calculated TBOD and PBOD in the simulated glasses (in unit of e/Å^3).

Glasses	TBOD	PBOD						
		Si-O	Al-O	Na-O	K-O	O-H	Si-H	Al-H
NAS	0.0251	0.0147	0.0081	0.0023	-	-	-	-
NKAS	0.0238	0.0141	0.0078	0.0012	0.0007	-	-	-
KAS	0.0224	0.0135	0.0074	-	0.0015	-	-	-
NAS-W	0.0248	0.0138	0.0077	0.0023	-	0.0006	0.0002	0.00004
NKAS-W	0.0233	0.0132	0.0074	0.0011	0.0007	0.0006	0.0002	0.00004
KAS-W	0.0219	0.0126	0.0071	-	0.0013	0.0006	0.0002	0.00003

To make our results more meaningful, we resolve the TBOD for each model into partial BOD (PBOD) based on different types of bonded atomic pairs or groups of atoms. The calculated TBOD and PBOD are listed in **Table 12** and plotted in **Figure 28.** The figure shows that the contribution from the Si-O pair dominates in all models ranging from 55.88% in NAS-W to 60.48% in KAS. After Si-O, the Al-O pair contributes significantly to the TBOD with values ranging from 30.95% in NAS-W to 33.04% in KAS. The M-O (M = Na, K) and H-O pairs have a small contribution in TBOD compared to Si-O and Al-O pairs. In the hydrated models, NAS-W, NKAS-W, and KAS-W, the total contribution in TBOD from Si-H, Al-H,

and O-O pairs are 1.17%, 1.17% and 1.19% respectively. In both dry and hydrated models, it is observed that with increasing alkali ion size, the PBOD for the total M-O pair decreases while it increases for Si-O, Al-O, and H-O pairs. Due to hydrolysis, the PBOD for Si-O and Al-O pairs decreases in the simulated glasses, which implies the breakdown of the network due to ionized water. Such details on bonding structure, which are generally missing in other MD studies, are important to understand the mechanical and other physical properties of glasses. The next section will extend bonding structure analysis relating to the hydrolysis effect.

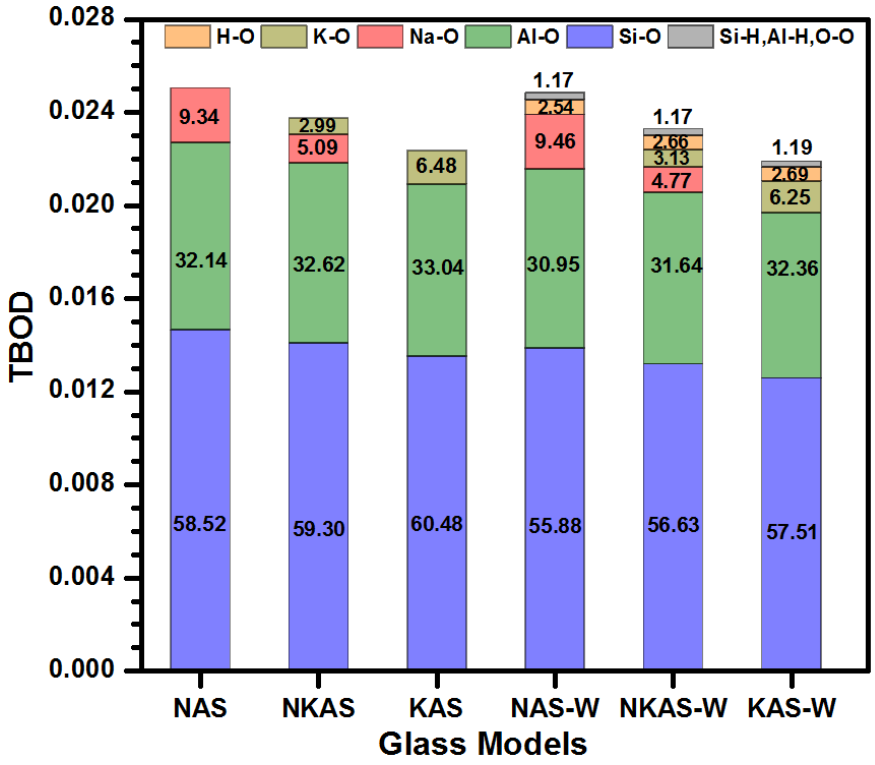

Figure 28. Distribution of TBOD along with the pair resolved PBOD from different bonding pairs in the 6 simulated glasses. The number in the bars shows percentage contribution of particular pair to the total TBOD.

4.3.3 Internal Bonding, Hydrolysis, and Charge Transfer Analysis

To dig deeper into the hydrolysis effect, we present critical analysis and quantitative results of bonding and charge transfer in the simulated glasses. MD simulation can provide statistical structural information like bond length, bond angle, CN, etc., based on geometry; however, a rigorous quantum mechanical calculation is necessary to reveal the intimate details of interatomic bonding. **Figure 29** shows a complete distribution of BO and BL in the form of a scatter plot along with the intensity in the corresponding axes for major bonding pairs Si-O, Al-O, and M-O (M = Na, K) in both dry and hydrated glasses. The Si-O and Al-O have a covalent character with a high BO value, and they are distributed in a narrow BL region shown by a sharp peak on the top of the BL axis. The alkali ions form mostly ionic bonds with lower BO values and spread over a wider BL region, shown by a broad distribution on the top of the BL axis. Among all, Si-O bonds are much stronger with higher BO values followed by Al-O, which implies Si-O are more covalent in nature than Al-O. The Si-O bonds have a shorter BL, and the BO values are clustered in a narrow region due to rigid SiO_4 tetrahedrons, while BO for Al-O bonds spreads a little wider than Si-O, which indicates the flexibility of $[AlO_n]$ (n = 4, 5, and 6) polyhedral in joining the glass network. Both bonds spread on a broader region with increased alkali ion size in both dry and hydrated models. Due to hydrolysis, the BO distribution for these bonds spreads wider than the corresponding dry model, and the intensity decreases slightly, as shown on the right BO axis. The K-O bonds are weaker than Na-O with a low BO value indicating that an increase in alkali ion size weakens the glass network. The BO values for K-O spread in a narrow region with high intensity than Na-O, as indicated by a sharp peak on the right BO axis. The averaged BO value follows the order of Si-O>Al-O>Na-

O>K-O in moving from Na-doped to K-doped glass in both dry and hydrated models. It should be made clear that the overall BO for any pair depends on the strength and number of bonds. In the hydrated models, additional bonding pairs O-O, Si-H, Al-H, and O-H exist, making the bonding structure more complex and complicated. Details about these bondings and the hydrolysis effect are discussed in the following paragraph.

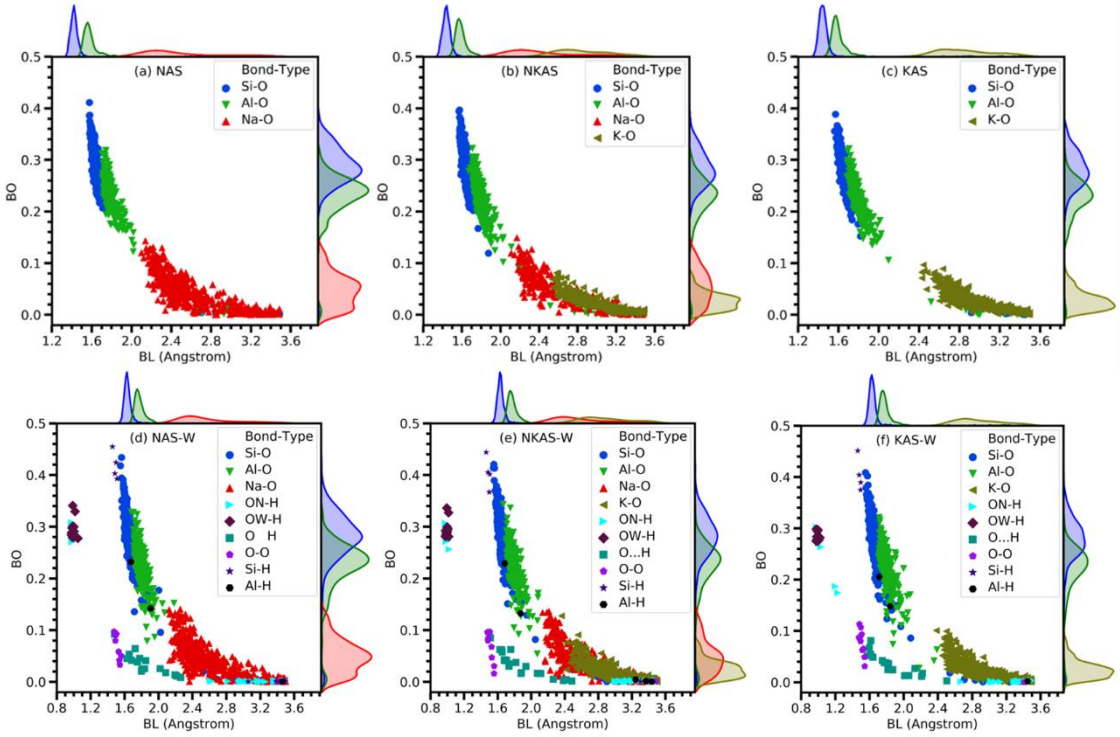

Figure 29. BO vs BL plot in the simulated (a-c) dry and (d-f) hydrated glass models. Possible bond pairs in each model are shown in the insets.

The ionization of water molecules in the hydrated models results in far more compound bonding patterns that cannot be described by simple geometry. In contrast to the dry models, O-O bond pairs with BL around 1.48 Å appear in the hydrated models, which have BO values much lower than that of Si-O and Al-O bonds but are comparable with M-O pairs. In the

hydrated models, strong Si-H and Al-H covalent bonds exist at ~1.5 Å and ~(1.7-1.9) Å with high BO values like Si-O and Al-O, respectively, but they are very few in number. A detailed analysis shows H atoms are involved in three types of bonding with O atoms: bonding with O in a water molecule (O_W-H), with O in the network (O_N-H), and hydrogen bonds (HB) (O···H). Based on the BL value, the O-H bonds in the systems are distributed roughly into three regions, O-H with BL < 1 Å (O_N-H and O_W-H), with BL between (1.5 – 2.5) Å (O···H), and with BL beyond 2.5 Å (O_N-H). The O_W-H and O_N-H pairs (with BL < 1 Å) have higher BO values since they are covalent in character. These pairs have comparable BO values, and BL lies at ~1 Å. The HBs have BL ranging from 1.5 to 2.5 Å and BO values lower than 0.1, which are not sensitively depending on the alkali ion types. The HBs are inherently weaker than covalent or ionic bonds. The discussion of HB in the solvated model is an important subject and well recognized by many but seldom discussed in a quantitative manner. In our system, the possible HBs are due to H from the water or OH group and O from the network or another water molecule. Since we have doped only 12 water molecules, and most of them (6 or 7) are dissociated, and the remaining water molecules are far apart, we did not observe HBs between two water molecules. The O-H bonds beyond 2.5 Å, namely O_N-H, have small BO values, even smaller than M-O pairs. The O_N-H bonds bonded with network former ions Si and Al form Si-OH and Al-OH pairs, breaking the network and depolymerizing it. The molecular water remained undissociated in the interstices position does not modify the network rather contributes to the internal cohesion with BO value around 0.3. We also found the existence of H_2O molecule bonded with Al in tetrahedral configuration; in such conditions, the charge balancing alkali ion turns into a network modifier and depolymerizes the network.

Another important electronic structure property from OLCAO calculation is the effective charge Q* for each atom in the system. It is a simple and effective way to describe the charge distribution of atoms in the system. From Q*, the partial charge (PC) ΔQ^* is calculated, defined as the deviation of Q* from the charge of the neutral atom Q^0, i.e., $\Delta Q^* = Q^0 - Q^*$. PC provides valuable information on charge transfer between atoms in the system related to the interatomic bonding, and they are helpful in providing the physical insight for the interpretation of experimental data. The net PC is zero in a closed and charge-neutral system, but each atom will have a different local PC value due to charge transfer. The calculated averaged PCs for each atom are listed in **Table 11**. For Si and Al, this value increases with increasing alkali ion size. The PC for Si, Al, Na, and K decrease in the hydrated models than corresponding dry models except for Al in NAS-W.

The distributions of PC for each atom in the simulated models are shown in **Figure 30**. In all models, Si, Al, and alkali ions (M = Na and K) lose charge while O gains. In the hydrated models, we split the PC for O into O_N, oxygen from the network, and O_W oxygen from water. We observed that O atoms in O-O bonding and in undissociated water molecules have less negative PC values. The H atoms can lose and gain charge depending on their local bonding configuration in a rather complicated fashion. All H atoms bonded with O are positively charged. In the present case of hydrated models, we found that H atoms gaining charge are bonded to Si or Al atoms. In the previous study on the hydration of alkali silicate glass, H atom bonded with Si could lose charge [86]. It clearly shows that the hydrolysis in the alkali aluminosilicate system is complex and peculiar, and different from the alkali silicate system. Such information is quite useful while developing the potential in MD study of the hydrated

alkali aluminosilicate system. In an empirical or semi-empirical type of calculation, the subtle differences in the atomic charge are frequently ignored or cannot be accurately accounted for. Obviously, more details on PC and charge transfer in the complex solvated alkali-aluminosilicate glass remain to be further analyzed. Generally speaking, we could conclude that the calculated averaged PCs for each type of atom follow the order of Si > Al > M > H > O as listed in **Table 11**.

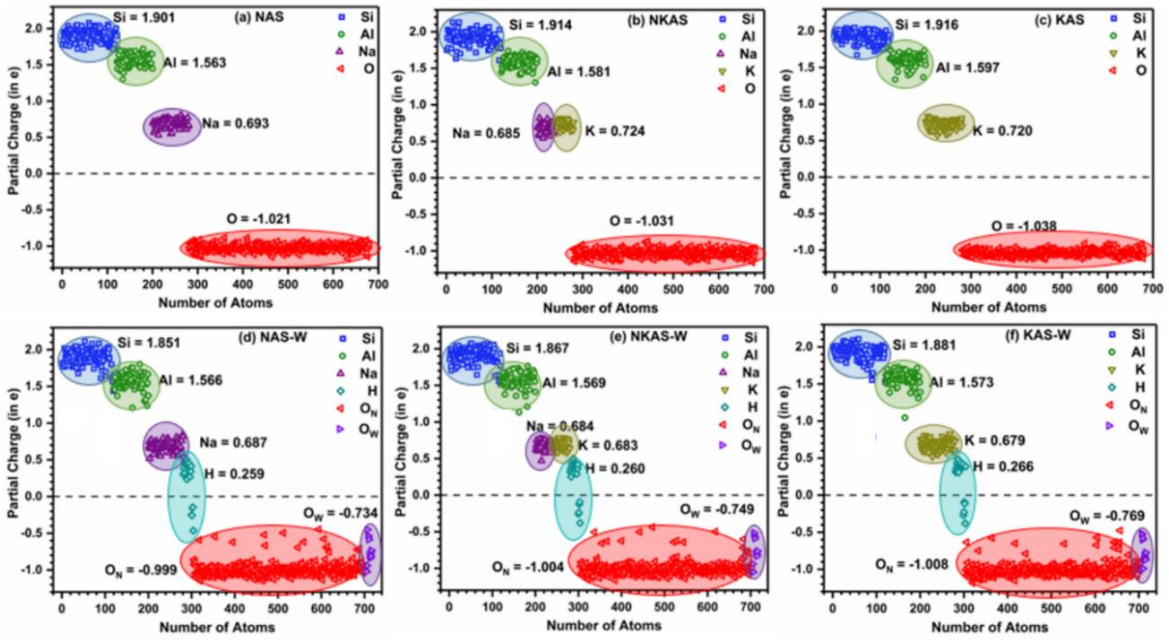

Figure 30. Calculated partial charge for each atom in the simulated (a-c) dry and (d-f) hydrated glass models. The numerical value is the averaged PC for individual atom. (O_N = Oxygen atom from glass network and O_W = Oxygen atom from doped water molecule).

4.3.4. Optical Properties

The optical properties of glass materials are always important for their optoelectronic applications. As the optical property of aluminosilicates can be tuned easily by doping of single

and mixed alkali and their migration in glass network in the phenomena like ion exchange greatly affects the refractive index [238], understanding the optical behavior in alkali aluminosilicates is very important. However, the studies on optical properties on this complex system are less reported rather than a few old calculations.[22, 239] The calculated optical properties in the six simulated glass models in the form of frequency-dependent complex dielectric functions and energy loss function (ELF) are shown in **Figure 31**. It shows the real (ε_1) and imaginary (ε_2) dielectric functions in the photon energy range up to 30 eV and the ELF in the energy range up to 50 eV. Details of formulae and methods are described in SI. Here, we mostly focus our discussion on ε_2. The general feature of the optical absorption curve ε_2 is similar in the simulated glasses; however, the observed number of absorption peaks vary when the alkali ion type changes. The number of absorption peaks in ε_2 increases in moving from Na- → (Na+K)- → K-doped glass, which is consistent with the number of broad peaks observed in the conduction band DOS shown in **Figure 25**. The first absorption peak in ε_2, which is very broad, is even broader in the hydrated models than the dry models. They can be considered to be transformed into a flat plateau by merging with the shoulder next to the first peak. The intensity of absorption curve ε_2 increases rapidly after overcoming the threshold energy. An important difference in the absorption curves of the studied glasses is the absorption edge. The absorption edge, which is related to the band gap, shifts slightly to higher energy end in moving from Na-doped to K-doped glass for both dry and hydrated models. The absorption edge in the hydrated models occurs at lower energy than the corresponding dry model. The variations in ε_2 reflect the complex interplay of slight differences in the electronic structure due to the different sizes of alkali ions and the presence of water.

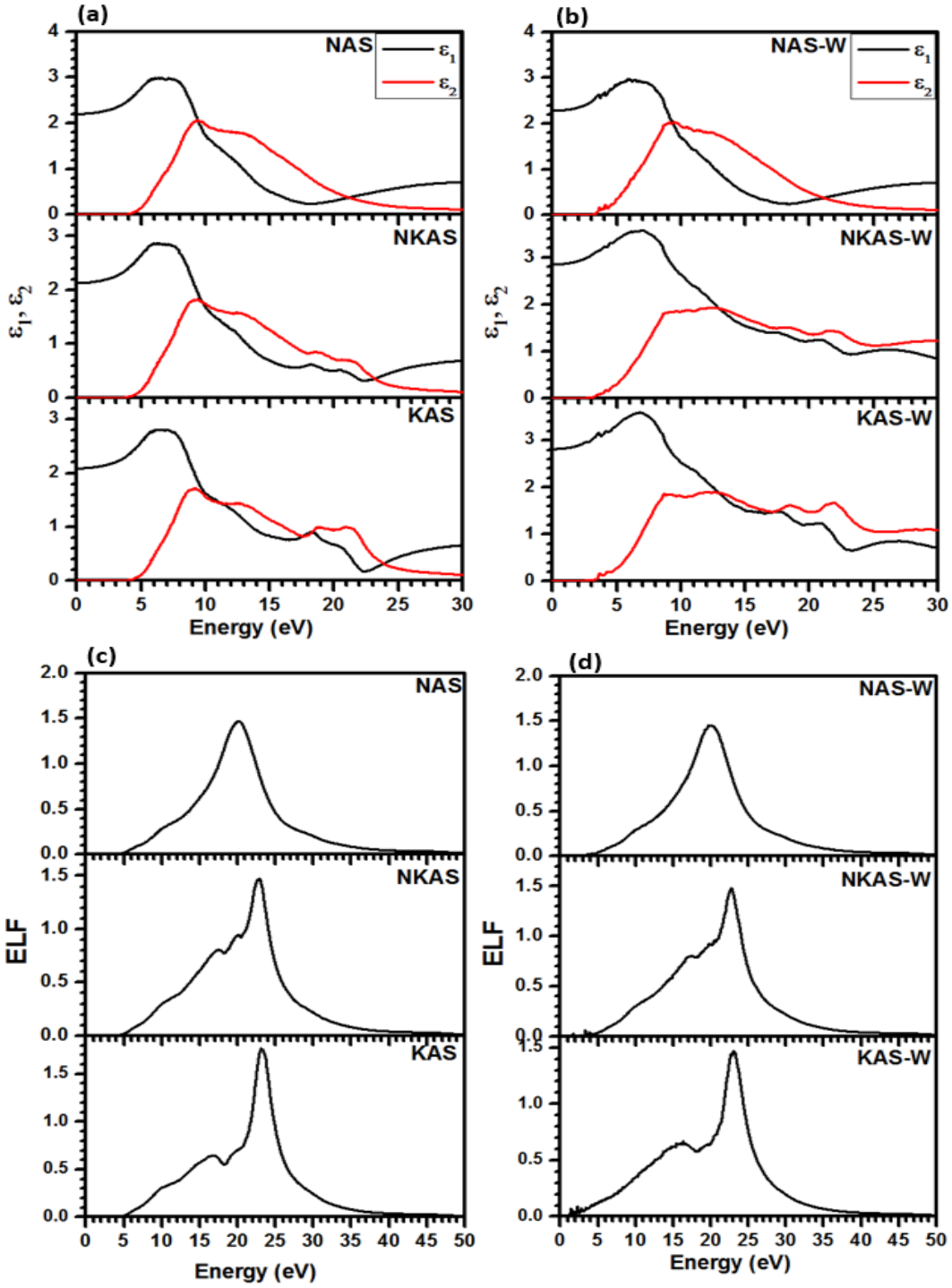

Figure 31. Calculated dielectric function ($\varepsilon = \varepsilon_1 + i\varepsilon_2$) and energy loss function (ELF) for (a) and (c) dry and (b) and (d) hydrated glass models, respectively.

The real part of the dielectric function ε_1 is calculated from ε_2 via Kramers-Kronig conversion, and its spectrum follows a similar feature as ε_2. The value of ε_1 at zero frequency limit, ε_1 (0), represents the electronic part of the optical dielectric constant and is related to the refractive index of glass by $n = \sqrt{\varepsilon_1}$ (0). **Figure 32** shows the calculated refractive index in the simulated glasses. Its value depends on the interplay of band gap, absorption edge, and the specific feature of the absorption curve. It increases linearly in the series with increasing size of alkali ions in both dry and hydrated models. The hydrated models have larger refractive indices, but the rate of increase in the series is almost the same. These data clearly show that as far as the refractive index is concerned, there is no evidence of MAE.

The ELF shown in **Figure 31** (c-d) is determined from both the real and imaginary parts of the dielectric function. The ELF of material is easier to measure in some experiments, and they are usually dominated by a peak at the Plasmon frequency ω_p, which is the frequency for the collective excitation of valance electrons in the solid. The figure shows that the Plasmon peak moves to a higher energy side in moving down from Na- to K-doped glass and becomes sharper and more asymmetric with the development of a shoulder on the lower energy side. This feature is almost similar in both dry and hydrated models. The ω_p lies at 20.07 eV, 22.92 eV, and 23.12 eV in dry models, NAS, NKAS, and KAS, respectively, while this value in the corresponding hydrated models, NAS-W, NKAS-W and KAS-W is at 20.02 eV, 23.14 eV, 23.97 eV. An important observation is that the observed difference between NAS and the K-containing models (NKAS and KAS), and the similar features between NKAS and KAS demonstrating the critical role played by K ions in the ELF, and the lack of any evidence regarding the MAE.

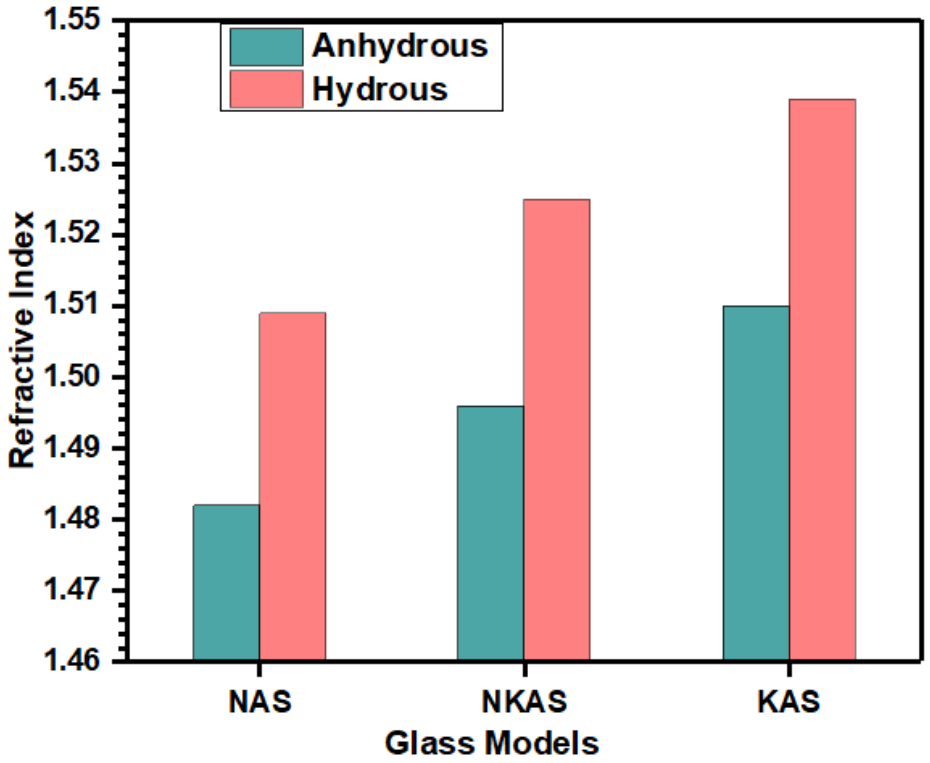

Figure 32. Variation of refractive index in the dry and hydrous alkali aluminosilicate glasses.

4.3.5. Mechanical Properties

With the increasing technological and commercial applications of all types of silicate glasses, its mechanical property is of crucial importance in controlling the quality and suitability of the glass products for some target and novel applications. Mechanical properties in glass are the compound effects of its fundamental properties such as network polymerization, ring structure, coordination state of atoms, atomic packing density, internal bonding, nature of doping element, solvation effect, etc.[240, 241] The network former and modifying cations greatly influence such properties. Hence, a deep understanding of composition-structure relation and properties is necessary to improve the mechanical

Table 13. Elastic constants and elastic moduli (in GPa) of the simulated glasses.

Glasses	C_{11}	C_{22}	C_{33}	C_{44}	C_{55}	C_{66}	E	K	G	η	G/K
NAS	91.019	89.407	90.716	30.575	32.264	31.069	76.940	48.975	31.070	0.2382	0.6344
NKAS	84.763	83.035	81.417	29.559	29.723	29.887	71.574	45.877	28.861	0.2400	0.6291
KAS	70.470	85.317	77.648	27.814	28.112	24.392	66.225	41.047	26.897	0.2311	0.6553
NAS-W	90.716	86.834	82.539	29.737	29.617	29.740	73.386	47.178	29.573	0.2407	0.6268
NKAS-W	76.894	74.700	77.648	28.198	29.425	28.477	67.372	42.748	27.225	0.2373	0.6369
KAS-W	74.515	70.365	73.825	25.011	26.281	26.230	62.079	41.649	24.800	0.2516	0.5954

properties in glass. We have calculated the mechanical properties of the six dry and solvated alkali aluminosilicate glasses. **Table 13** lists their calculated elastic constants and bulk mechanical parameters. **Figure 33** shows the variation of elastic constants in the dry and hydrated glass models. From the material science perspective, the elastic constants contain some important information. They determine the material's response to external forces characterized by elastic moduli and help determine the strength of the material. It is well-known that the elastic constants in amorphous solids are close to satisfy isotropic nature.[242] However, a slight difference in C_{11}, C_{22}, and C_{33} reflects a small degree of anisotropy in the simulated models. Similarly, the shear stiffness constants $C_{44,}$ $C_{55,}$ and C_{66} also show only a small difference except in the NKAS and NAS-W models. The elastic constants decrease in moving from Na-doped to K-doped glasses in a nonlinear fashion in both dry and hydrated glasses.

The elastic moduli, Young's modulus (E), bulk modulus (K), shear modulus (G) and Poisson's ratio (η) are presented in **Figure 34** in the form of a vertical bar diagram. E, K, and G decrease in the series from Na- to K-doped glasses in both dry and hydrated models. The increase in alkali ion size produces a more depolymerized network and diminishes the internal strength, which results in a decrease in elastic moduli. C. Weigel et al. [243] studied the elastic moduli in NAS and KAS glass containing 50 mol% silica with Na/Al = 1 and observed the similar result that the latter has smaller E, K, and G values. For NAS glass, our calculated values of E and G are in good agreement with experimental values reported by Eagan and Swearekgen [226], which we have discussed in our previous work.[87] On moving from Na- to K-doped glass through (Na+K)-doped mixed ions glass in the series, the elastic moduli

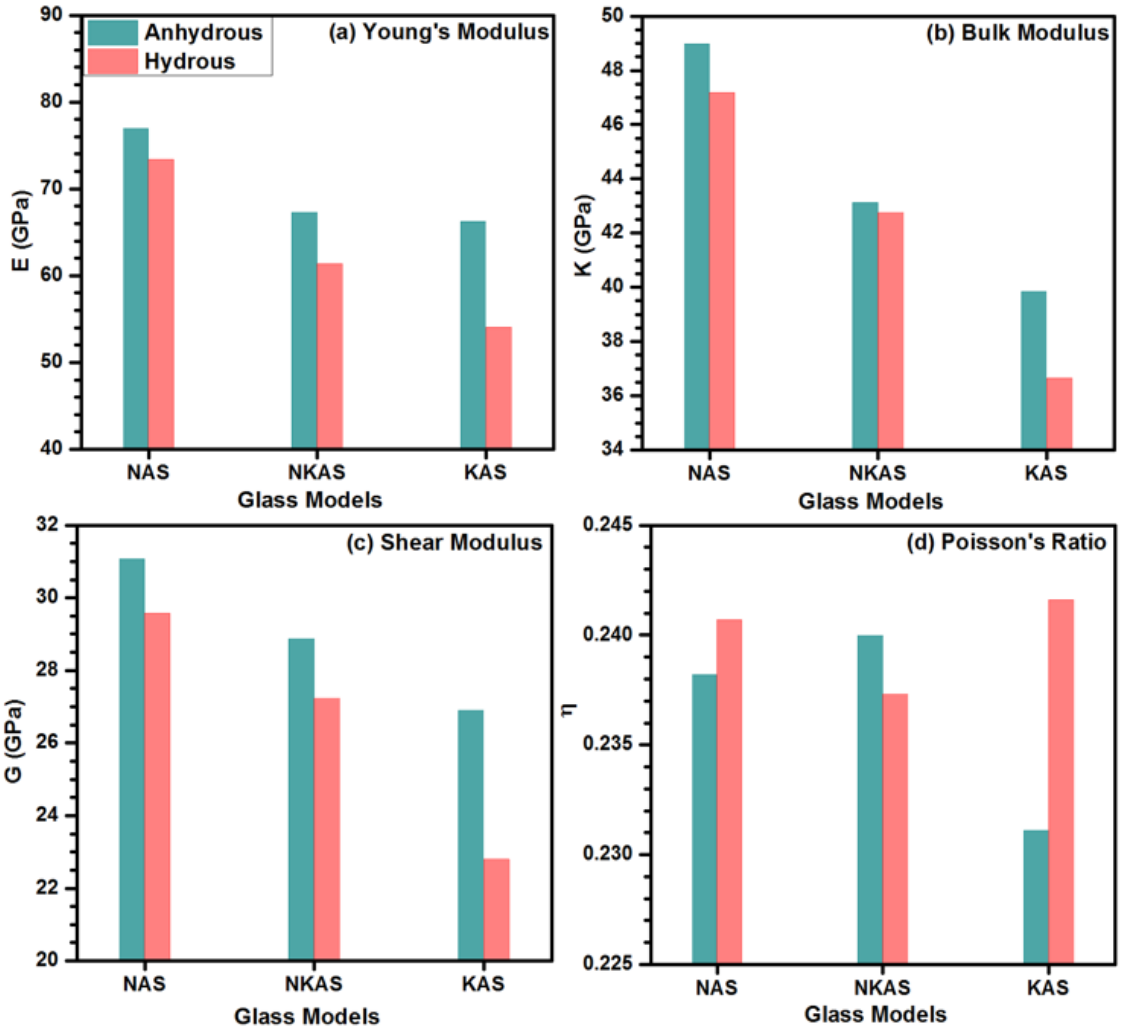

Figure 33. Calculated elastic moduli and Poisson's ratio in the simulated glasses: (a) Young's modulus E, (b) Bulk modulus K, (c) Shear modulus G, (d) Poisson's ratio η. The opposite direction of point of inflection in the curve drawn in figure (d) shows the opposite direction of the mixed alkali effect in η between the dry and hydrated models.

decrease in an approximately linear fashion, thus suggesting that the MAE cannot be observed in the individual mechanical modulus of either dry or hydrated alkali aluminosilicate glasses. However, the Poisson's ratio η in the series shows a very different scenario. The mixed (Na + K)-doped glass has a larger Poisson's ratio η than either Na-doped or K-doped glasses in dry

models or the observation of the MAE. This MAE is in the opposite direction in the hydrated models, as shown in **Figure 34 (d)** by a curve with the inflection point in the opposite direction. This may be the first time to reveal the effect of solvation on the MAE in the mechanical properties of alkali aluminosilicates. Our results clearly show that mixed alkali metals in solvated models lower the Poisson's ratio, thus making the glass more brittle. Such insights could be helpful in the search for stronger glass. The calculated Poisson's ratio comprehensively assesses average bulk mechanical properties as it depends on both K and G. **Table 13** lists the Pugh's modulus ratio G/K, which is just an inverse of η.

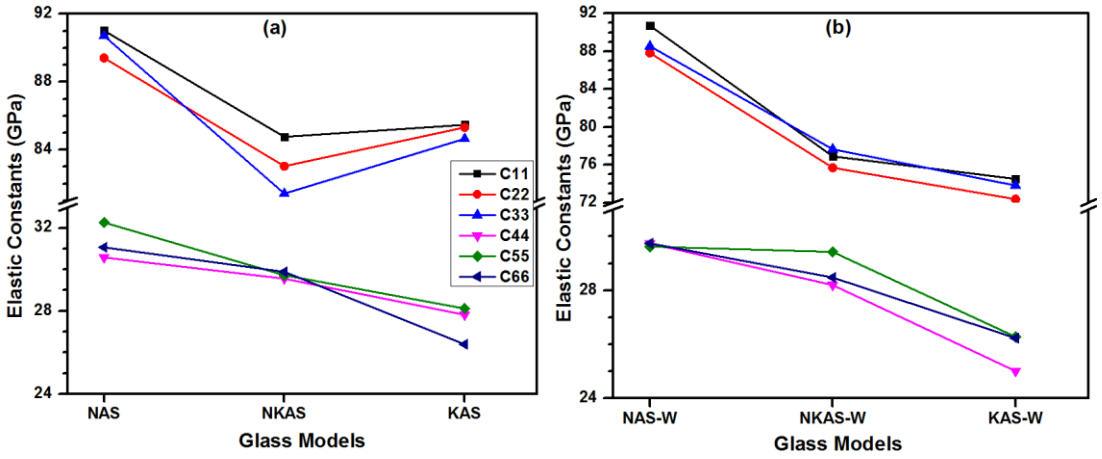

Figure 34. Calculated elastic constants in the (a) dry and (b) hydrated glasses.

4.4. Summary and Conclusion

Single and mixed alkali doped three dry and three solvated models of alkali aluminosilicate glasses with Na/Al = 1 are constructed from AIMD, and the electronic structure, mechanical, and optical properties are evaluated using *ab initio* methods. The comportment of network-forming Al ions in the environment of alkali ions is analyzed. One

of our findings is that Al forms mostly the tetrahedral coordination in both dry and hydrated glass, and the presence of five coordinated Al is higher in the hydrated glass. Our results refute the long-established Al-avoidance principle in both dry and hydrated models. A novel concept of TBOD is used to define the internal cohesion and hydrolysis effect in the simulated glasses. The band gap and TBOD decrease in the series while the refractive index increases due to an increase in alkali ion size and hydrolysis in the studied glasses. The band gap decreases sharply due to hydrolysis. The potassium doped aluminosilicate glass is weaker than the sodium doped in both dry and hydrated cases with a low TBOD value. The in-depth bonding analysis in hydrated models and its comparison with dry models reveals the change in bonding structure due to hydrolysis and provides new insights to understand hydrolysis in glass at an atomistic level. Another finding is hydrolysis depolymerizes the alkali aluminosilicate framework and decreases its internal strength. The network depolymerization increases with an increase in alkali ion size. Water remains as ionized water in the form of OH group and intact as molecular water H_2O inside the alkali aluminosilicate network. The elastic moduli decrease in the series when the alkali ion size increases in the studied glasses. The most important discovery is that we find the mixed alkali effect in the Poisson's ratio for both the dry and solvated models, and they are in the opposite direction. Thus, adding K to the Na-doped aluminosilicates glass with water could make the glass more durable and gives an insight with serious implications on the processing for commercial glasses.

The hydrolysis on glass surfaces, including the corrosion and leaching effect, is an important and challenging problem in glass science and is not entirely understood even the studies are being carried for many decades. The simulation method and approach developed in

this paper will be extended and applied to such problems in even more complex aluminosilicate systems to make the results more aligned with real commercial products. Such results will be reported in the near future.

CHAPTER 5

AQUEOUS CORROSION EFFECTS OF Na/K-Cl SALTS ON ALUMINOSILICATE GLASS USING *AB INITIO* MOLECULAR DYNAMICS

5.1. Introduction

The increased applications of aluminosilicate (AS) glasses in many fundamental and technological fields with possible exposure to aqueous and humid environments have sparked significant interest in a comprehensive understanding of the AS glass-water interaction, corrosion of the surface, and its strengthening. The chemical corrosion of AS glass by water is a serious problem with implications in many fields like geochemistry, biomineralization, the management of radioactive nuclear wastes, the bioactive glass for the growth and repair of tissues, etc.[244-246] As the glass corrosion starts on the surface and spreads into the bulk, the investigations need to focus on the surface properties. To this end, many researchers have invested in exploring the aqueous corrosion of simple and multicomponent silicate glass surfaces like alkali silicate, AS, boro-AS, etc., and increasing their wear resistance to ensure the long-term durability against chemical attacks.[247-256] However, the atomic-scale information on hydrolysis and corrosion in the case of complex glasses is still lacking despite these extensive efforts. Hence, it is essential to unravel atomistic details of the glass-water interface, the behavior of ions, and the degradation mechanism of AS glass surfaces in an aqueous solution to advance them as mechanically strong and durable functional glasses.

Water corrodes the AS glass by diffusion and exchange of ions resulting in a chemical modification of the surface. Due to corrosion, the static fatigue life of glass reduces, and its physical and chemical properties modify significantly.[62, 135, 257, 258] The hydrolysis in

silica and alkali silicate glass has been well-studied in the past, and it has been confirmed that water depolymerizes the silicate network and deteriorates its mechanical strength.[40, 55, 62, 259] However, the hydrolysis of AS glass remains poorly understood due to the complex glass-water interface and reaction mechanism. In addition, unlike silicate glass, whether or not water depolymerizes the AS network is a subject of contention. Existing studies are in support of and against the depolymerization of AS network due to hydrolysis.[201, 203, 205, 208] The possible unlimited configurations of a surface make the hydrolysis and rearrangement of the network even more intricate in these glasses. Furthermore, the alkali ions in AS glass act as a charge compensator for $[AlO_4]^-$ tetrahedra or the network modifier and show a different hydrolysis behavior. Alkali ions acting as network modifiers are more prone to water attack and accelerate corrosion than charge-balanced conditions. Hence, it is extremely important to provide a definitive conclusion on the hydrolysis of AS network and understand the role of alkali ions in its aqueous corrosion.

The presence of NaCl and KCl salts significantly affects glass corrosion. However, the aqueous corrosion effects of these salts on AS glasses are not explored yet. The complex reaction mechanism of these salts with AS glass network in the aqueous medium makes understanding the microscopic origin of the glass-water interaction challenging for theoretical and experimental studies. Furthermore, the dissolution of these salts is a primary concern in the field of nuclear waste glasses. For example, due to the less solubility of Cl in silicate glasses, the vitrification of some hazardous nuclear wastes containing a large amount of Cl becomes problematic.[260, 261] Especially, the stability of the glass network after the incorporation of salts is the primary concern. In addition, doping of mixed NaCl-KCl salt

makes the hydrolysis and dissolution of glass intricate due to the different alkali ions sizes and mixed alkali effect (MAE). MAE is a non-linear variation in glass properties when two or more alkali ions are mixed.[30] Hence, it is crucial to investigate the detailed effect of Na/K-Cl salts on hydrolysis and the stability of AS glass network.

Many endeavors have been made to probe the glass-water interface experimentally using different instrumental techniques. The surface analytic methods like X-ray photoelectron spectroscopy (XPS), nuclear magnetic resonance (NMR) spectroscopy, scanning/transmission electron microscopy, Neutron diffraction, infrared (IR) and Raman spectroscopy, atom probe tomography, etc., are widely used to investigate the changes in the chemical composition of glass surface aftermath of glass-water interaction.[42, 68-75, 262] Vibrational spectroscopy like sum-frequency generation and second harmonic generations are used to characterize the water absorbed layer and polarization of water molecules on the surface.[76, 263] Although the experimental studies explore the characteristics of the glass surface and consequent changes due to water contact, they cannot provide critical information and microscopic details regarding the chemical reaction mechanism and surface properties at the atomic level. As an alternative, the simulation methods like ab initio molecular dynamics (AIMD), classical MD, Monte Carlo (MC), etc., have demonstrated their success in providing the atomistic information of glass-water interface reactions in silicate and AS glasses.[77-84, 256, 264] It is of utmost importance in MD simulations that the empirical force field should be sufficiently accurate. Especially in the case of multicomponent glass with water on its interface, developing such a force field that accurately treats the glass-water reaction mechanism is exceptionally challenging. Hence, the complex glass surface-water interface study has been limited in MD

due to the lack of potential to reproduce the accurate surface chemistry with hydroxylated groups. In contrast, the AIMD, in which the interatomic forces are calculated quantum mechanically, can effectively investigate the hydrolysis and corrosion of complex glasses providing more precise results. Hence, AIMD is inevitable to explore the aqueous corrosion of complex glasses like AS in this study.

This work addresses the issues raised above and provides detailed insights into the aqueous corrosion of AS glass surfaces. Our study is divided into two parts. In the first part, we simulate pure AS and sodium AS (NAS) glass-water interface models and investigate the effects of water on the glass surface with and without leachable alkali ion Na. In the second part, we simulate the 6, 10, and 14 molecules of NaCl, (Na+K)Cl, and KCl salts doped AS glass-water interface and analyze the aqueous corrosion effects of these salts on the glass surface. In the case of (Na+K)Cl, the NaCl and KCl salts are mixed in equal proportion. The key question of investigation is how the local structure, properties, and internal bonding change due to water and the doping of salts. The simulated models are sufficiently large to include the effects of defects and other structural complexity that might occur on the glass surface. The use of a more accurate AIMD ensures the reliability and accuracy of our results. The rest of the article is organized as follows: The following section discusses the procedure of model construction and methods used. The most important part is the results and discussion section, which presents our findings and critically analyzes them compared with the existing results. Finally, a brief conclusion and plan for future direction are presented.

5.2. Methods and Model Construction

5.2.1. Computation Methods

This work used DFT-based two methods: Vienna *Ab Initio* Simulation Package (VASP) [91, 103] and the orthogonalized linear combination of atomic orbitals (OLCAO) [93] for simulation and properties evaluation. In VASP simulation, we used the projector augmented wave (PAW) method [92, 104] and defined the exchange-correlation energy by Perdew-Burke-Ernzerhoff (PBE) generalized gradient approximation (GGA) [100]. We sampled the Brillouin zone at Γ-point only as the simulated models have sufficiently large supercells. The cutoff energy was set to a reasonably high value of 500 eV for the plane-wave basis expansion. The electronic convergence criterion was chosen to be 10^{-5} eV, and the forces were converged to 10^{-3} eV/Å at zero pressure.

The VASP relaxed glass models were further treated using OLCAO to analyze the internal bonding and partial charge. We have shown in the past a combination of these two methods is most effective in studying the electronic structure results in large and complex amorphous solids [119-122], crystalline materials [265-267], liquid [123], and biological system.[268-270] The details of the OLCAO calculation are explained in Chapter 2.

5.2.2. Simulation of Bulk and Interface Glass Models

Bulk glass models were simulated using a melt-quenching technique in the AIMD framework, similar to our previous works.[85, 87, 88] The AIMD simulation was carried under the NVT ensemble with an ionic time step of 1 fs where the number of atoms (N), the volume of the simulation cell (V), and temperature (T) were held constant. A Nose thermostat was used to control the heat bath temperature.[271, 272] The initial models were designed by enclosing atoms randomly distributed in a simulation box with experimental density.[226, 273] These models were then heated to 4000 K, well above the melting point of AS and NAS

glasses, shortly for 2 ps. Next, the melts were equilibrated for 10 ps at this elevated temperature to ensure the initial atomic position memory and velocity history were entirely lost. The melted structures were then quenched to room temperature 300 K using a nominal quenching rate of ~25 K/ps in the glass forming region. The melt-quenched glasses at 300 K were equilibrated for 10 ps to minimize temperature and pressure fluctuation. Finally, the AIMD structures at 300 K were fully optimized by VASP to obtain the bulk AS and NAS glasses named AS-Bulk and NAS-Bulk, respectively. The final relaxation of systems following the AIMD ensures the high accuracy of the simulated structures. More details about bulk models creation can be found in our previous works.[87, 88]

Table 14. Summary of the simulated bulk, surface, and interface models for AS and NAS glasses.

Glass Models	Na	Al	Si	O	H	No of Atoms
AS-Bulk →$(Al_2O_3)_{0.4}(SiO_2)_{0.6}$	-	160	120	480	-	760
AS-Surf →$(Al_2O_3)_{0.4}(SiO_2)_{0.6}$	-	160	120	480	-	760
AS-Intf →AS-Surf+229H_2O	-	160	120	709	458	1447
NAS-Bulk→$(Na_2O)_{0.2}(Al_2O_3)_{0.2}(SiO_2)_{0.6}$	80	80	120	400	-	680
NAS-Surf →$(Na_2O)_{0.2}(Al_2O_3)_{0.2}(SiO_2)_{0.6}$	80	80	120	400	-	680
NAS-Intf→NAS-Surf+223H_2O	80	80	120	623	446	1349

The surface models of AS and NAS glasses are named as AS-Surf and NAS-Surf, respectively. They were created by introducing a vacuum of 15 Å along the positive Z-axis in the bulk models. These models were then annealed at 300 K for 4 ps using NVT ensemble, which allows the relaxation and reformation of some bonds on the surface broken due to cleavage. Next, we simulated the water boxes separately with length and width same as glass surface models and height equal to 15 Å with a density of 1gm/cm^3. The water boxes at 300 K

were equilibrated well, using the NVT ensemble and an ionic motion time step of 0.5 fs. A smaller time step was used to ensure accuracy in integrating the equation of motion, especially for the lighter atom like hydrogen. Finally, the interface models AS-Intf and NAS-Intf were created by substituting the vacuum with a water box. The water box was kept slightly above the glass surface to avoid any initial close contact with the surface atoms and reduce the internal pressure due to NVT simulation. The interface models were then simulated for 50 ps in the NVT ensemble with 0.5 fs time step. The temperature profile during the simulation is shown in **Figure 35**. It fluctuates within ±10 K of 300 K, ensuring the system remains in equilibrium at 300 K. **Table 14** lists the glass composition and the number of atoms in each model. The same naming of systems will be used throughout the text and figures. **Figure 36** is the sketch of the surface and interface model creation. The top and bottom surfaces of glass interact with water due to the periodic boundary conditions.

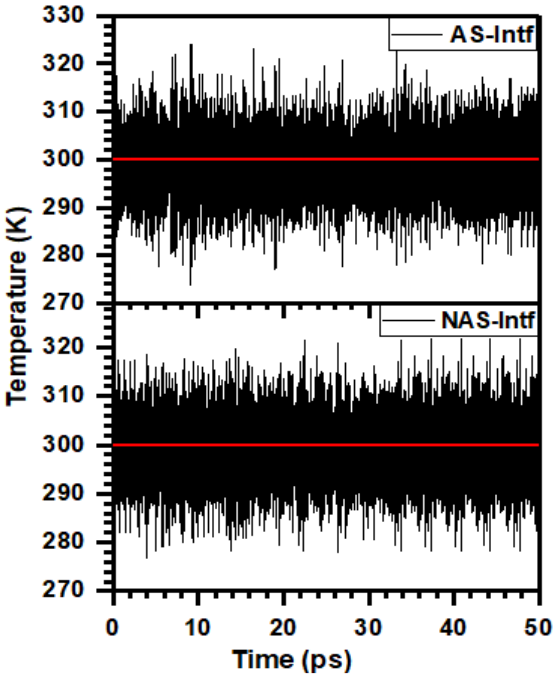

Figure 35. Temperature profile during the simulation of interface models.

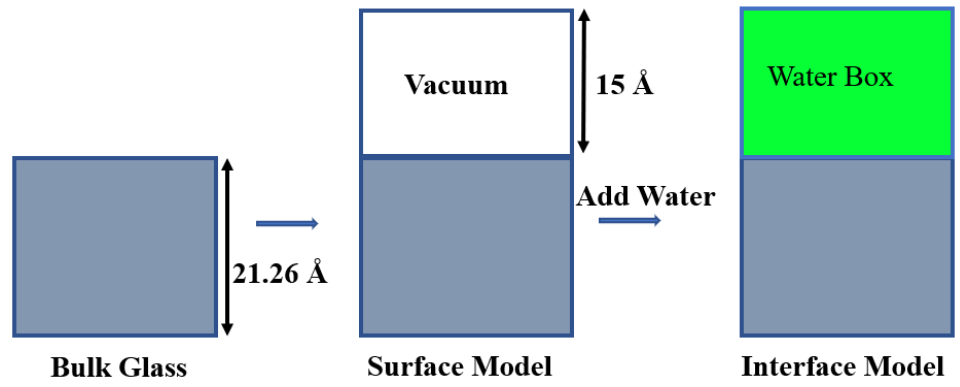

Figure 36. Sketch of glass-water interface model (AS-Intf) creation.

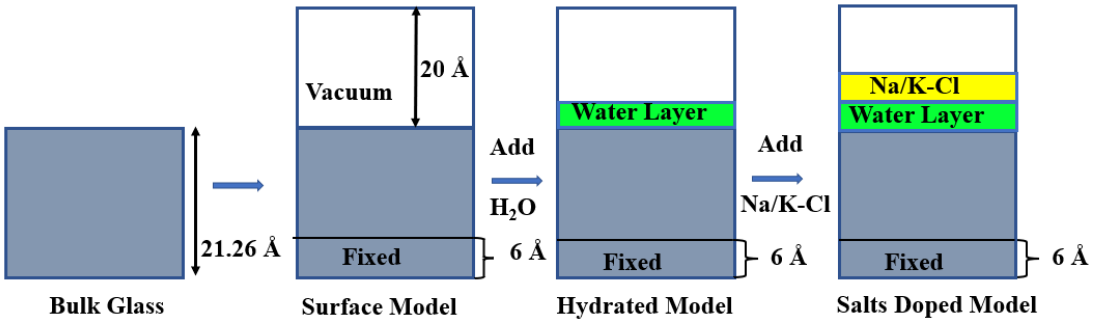

Figure 37. Illustration of salt doped glass models creation.

5.2.3. Simulation of Salt Doped Interface Models

The Na/K-Cl salts doped interface models were created based on the AS-Bulk model discussed above. At first, the surface model, just named Surface, was created from the bulk by inserting a vacuum of 20 Å along the positive Z-axis. On this Surface model, the dangling bonds at the bottom layer were saturated by adding H, and the atoms within ~6 Å layer from the bottom were frozen. This Surface model is slightly different from the AS-Surf model discussed above. The Surface model was equilibrated at 300 K for 4 ps before further proceeding, allowing the bonds on the top surface to readjust. Next, a monolayer of 40 water

molecules was placed on the top layer of the Surface model to create the Surf-W model. This Surf-W model was also equilibrated for 4 ps at 300 K. Finally, we co-doped the hydrated surface with 6, 10, and 14 NaCl, NaCl-KCl, and KCl salt molecules to investigate the effects of salts on the hydrolysis and corrosion of AS glass surface. The salt-doped models are named as mNCl, mNKCl, and mKCl (m = 6, 10, and 14) based on doping of NaCl, NaCl-KCl, and KCl salts, respectively. The AIMD simulation was repeated for salt-doped models for 4 ps at 300 K. All simulations were carried under the NVT ensemble with a time step of 0.5 fs for the ionic motion. After 4 ps run, we switched back to general relaxation as some atoms and molecules at the top layer detach and fly to the vacuum in the long AIMD simulation. Finally, all models were well-optimized without restriction in cell shape and volume. **Figure 37** shows the detailed scheme of model creation. The summary of models is listed in **Table 15**. Unless otherwise stated, the same naming of glass models as listed in **Table 15** will be used throughout this work.

Table 15. Summary of bulk, surface, and salts doped interface models.

Glass Models	Al	Si	O	H	Na	K	Cl	No. of atoms
AS-Bulk →$(Al_2O_3)_{0.4}(SiO_2)_{0.6}$	160	120	480	-	-	-	-	760
Surface →AS-Bulk+17H	160	120	480	17	-	-	-	777
Surf-W →Surface+40H_2O	160	120	520	97	-	-	-	897
6NCl →Surf-W+6NaCl	160	120	520	97	6	-	6	909
6NKCl →Surf-W+3NaCl+3KCl	160	120	520	97	3	3	6	909
6KCl →Surf-W+6KCl	160	120	520	97	-	6	6	909
10NCl →Surf-W+10NaCl	160	120	520	97	10	-	10	917
10NKCl →Surf-W+5NaCl+5KCl	160	120	520	97	5	5	10	917
10KCl →Surf-W+10KCl	160	120	520	97	-	10	10	917
14NCl →Surf-W+14NaCl	160	120	520	97	14	-	14	925
14NKCl →Surf-W+7NaCl+7KCl	160	120	520	97	7	7	14	925
14KCl →Surf-W+14KCl	160	120	520	97	-	14	14	925

Table 16. Structural parameters of the simulated bulk, surface, and interface AS and NAS glass models. (Volume is in $Å^3$ and density in gm/cm^3)

Glass Models	a (Å)	b (Å)	c (Å)	α^0	β^0	γ^0	Volume	Density
AS-Bulk	21.428	21.535	21.264	89.744	90.920	88.837	9809.016	2.604
AS-Surf	21.159	21.382	38.072	90.207	91.303	90.187	17220.633	
AS-Intf	21.159	21.382	37.904	90.000	90.000	90.000	17149.239	
NAS-Bulk	21.323	21.066	21.162	88.834	91.239	90.818	9500.507	2.409
NAS-Surf	21.189	20.907	37.592	88.357	91.563	90.963	16638.177	
NAS-Intf	21.189	20.907	36.178	90.000	90.000	90.000	16026.995	

5.3. Results

5.3.1. Results of Bulk and Interface Models

5.3.1.1. Glass-Water Interface Structures and Reaction Mechanism

The final relaxed interface models of AS and NAS glasses, including the bulk and surface models, are shown in **Figure 38**, and the structural parameters are listed in **Table 16**. It is observed that the glass surface readily gets hydrated in contact with water **(Figure 38 (c),** and **(f))** because the surface becomes more stable with bonded hydroxyl groups rather than having a dangling bond. **Figure 39** shows the snapshot of the glass-water interface at 0 ps and 50 ps. It shows that the initial clear gap on the interface at t = 0 ps disappears, and a significant amount of glass surface is hydrated after 50 ps. The ionized water attacks the glass surface and creates functional groups T-OH (T=Si, Al), breaking the T-O-T bonding network. As a result, the silanol (Si-OH) and aluminol (Al-OH) are formed on the glass surface, which are more stable than having unsaturated dangling bonds. The hydrolysis reaction occurring in the AS glass surface is represented by:

$$\text{T-O-T} + H_2O \rightarrow 2\ \text{T-OH} \qquad (1)$$

The T-OH formation and hydrolysis of glass surface increases with time and propagates into the bulk region. The glass network degrades, and its internal strength reduces because of hydrolysis.

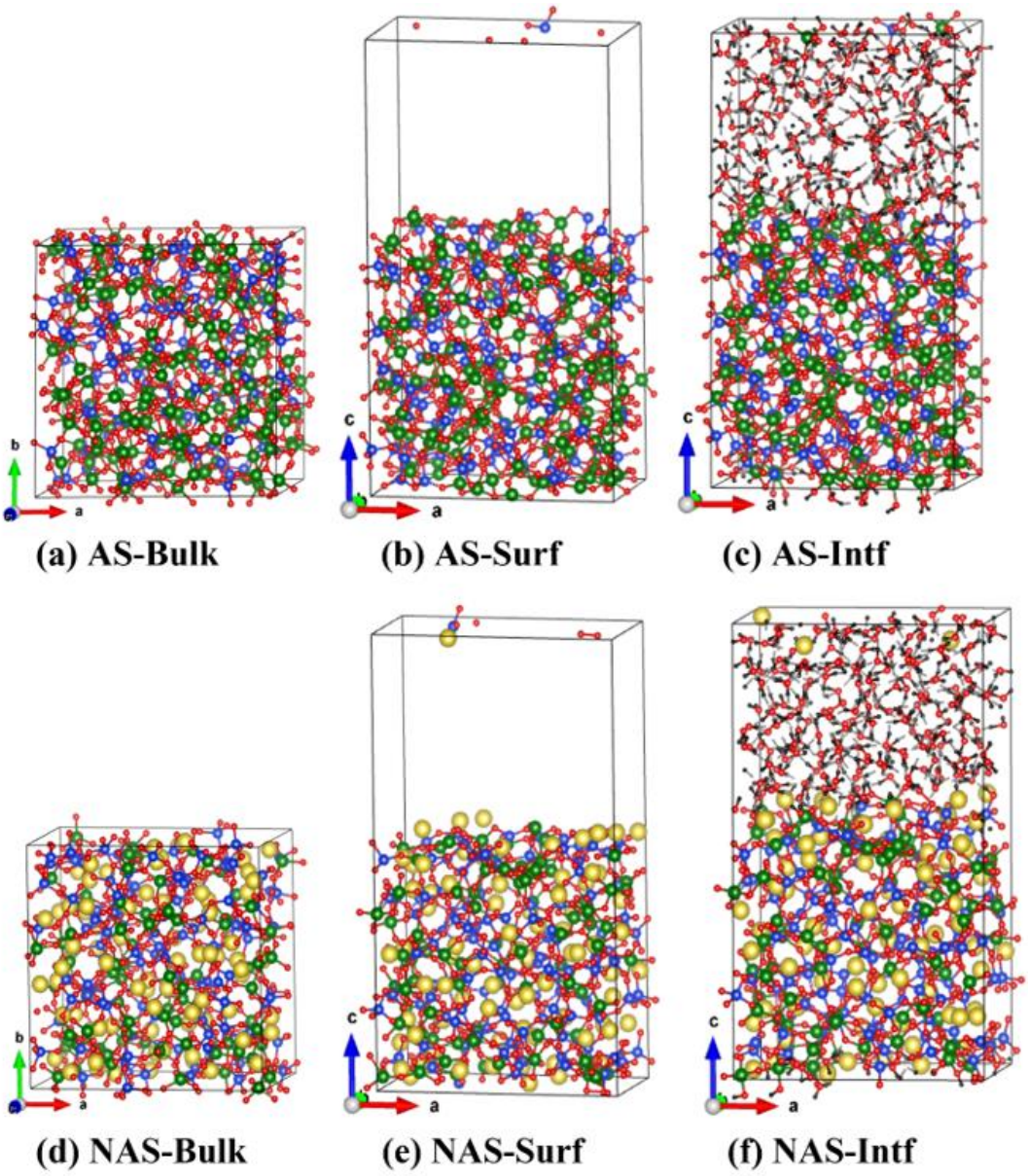

Figure 38. Final relaxed structure of simulated bulk, surface, and interface models. (Si = Blue, Al = Olive, Na = Golden, O = Red, and H = Black)

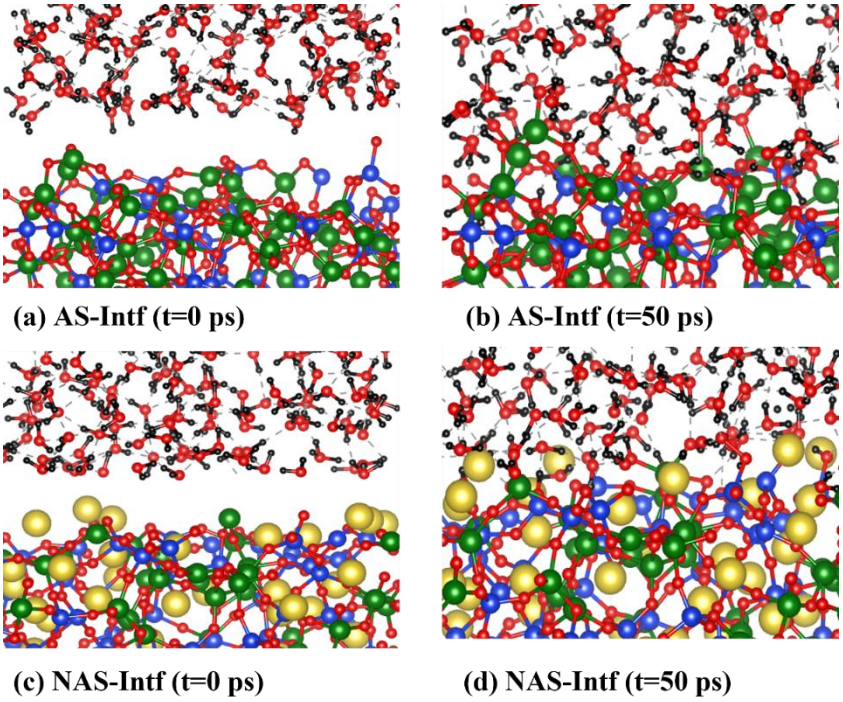

Figure 39. Snapshot of glass-water interfaces for (i) initial configuration (a) and (c) and (ii) after 50 ps AIMD run (b) and (d). (Si = Blue, Al = Olive, Na = Golden, O = Red, and H = Black)

The hydrolysis mechanism in NAS glass is more complicated than pure AS glass due to leachable ion Na. In NAS glass, T-non bridging oxygen (NBO) units easily react with nearby water molecules dissociating them into H^+ and OH^-. The protonation of the NBO site results in the formation of Na-OH and T-OH. The Na-OH dissociates later into Na^+ and OH^- ions. The continuation of this reaction ionizes more water molecules on the surface and propagates hydrolysis into the bulk. The H^+ diffuses into the bulk glass through discrete proton hopping between two adjacent NBO sites. Hence, in NAS glass, in addition to the glass-water reaction (1), the hydrolysis mechanism can be accounted by the following reactions:

$$\text{T-ONa} + H_2O \rightarrow \text{T-OH} + \text{Na-OH} \quad (2)$$

$$\text{Na-OH} \rightarrow Na^+ + OH^- \quad (3)$$

The Na^+ ion is extracted from the glass matrix into the water due to leaching, as shown in **Figure 38 (f)**. The Na in a charge-balanced condition of $[AlO_4]^-$ tetrahedra is less attacked by water than in the NBO position.

Further details on the structure and reaction mechanism of the glass-water interface are achieved by analyzing the different regions of the interface models. **Figure 40** shows the NAS-Intf model after 50 ps AIMD run. The system is divided into three regions: bulk water, interface, and bulk glass. Similar regions are observed in the AS-Intf model also. It is observed that water attacks the glass network from both the top and bottom sides. As a result, some Na ions are leached into the water. The dissolved glass in the interface region is rich in T-OH groups, which propagates to the bulk region with time. The presence of both molecular water H_2O and OH groups in this region implies water can be transported into glass by two mechanisms: proton transfer, i.e., ionic diffusion between network modifying cation and H, and water diffusion. The water diffusion is mostly limited near the surface of the glass, whereas proton transfer goes farthest from the surface. Due to hydrolysis and breaking of the glass network, the interface region becomes weaker than the bulk part. Details about such results and further analysis of structures are elucidated in the interatomic bonding section, where the bond order (BO) value for each bonded pair with corresponding bond length (BL) is analyzed.

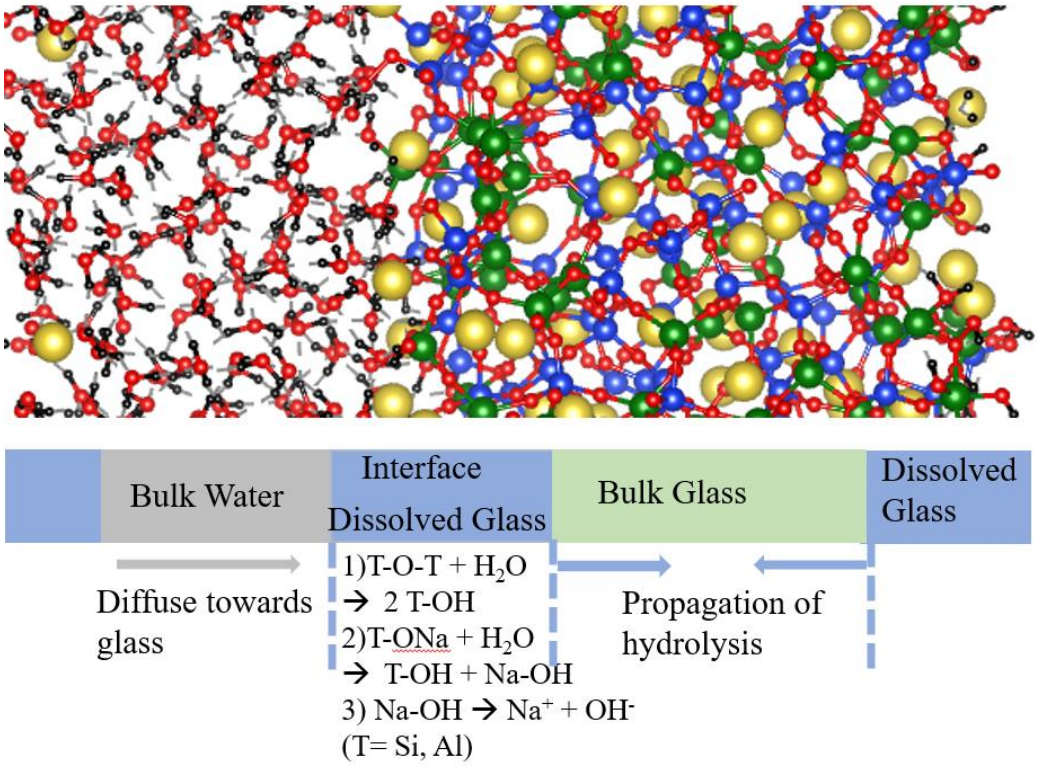

Figure 40. Sodium aluminosilicate glass-water interface model after 50 ps simulation. (Si = Blue, Al = Olive, Na = Golden, O = Red, and H = Black)

5.3.1.2. Pair Distribution Function

The average distance between water and glass components determined by the pair distribution function (PDF) characterizes the glass-water interface. **Figure 41** shows the PDFs between cations (Si, Al, Na) and O from water (O_W), and H from water and O from the glass network (O_N). In the AS-Intf model, the first peak of the Si-O_W pair is at ~1.65 Å, and the Al-O_W pair is at ~1.85 Å. These BLs are longer than the Si-O (~1.62 Å) and Al-O (~1.75 Å) distances in bulk AS glass. In the NAS-Intf model, the Si-O_W and Al-O_W BLs are ~1.65 Å and ~1.76 Å, respectively, while the Si-O and Al-O BLs in bulk NAS glass are at ~1.64 Å and ~1.75 Å, respectively. The large increase in Si-O and Al-O distances in the AS-Intf model than

NAS-Intf implies that the AS network gets easily hydrated than the NAS network with Na/Al = 1.

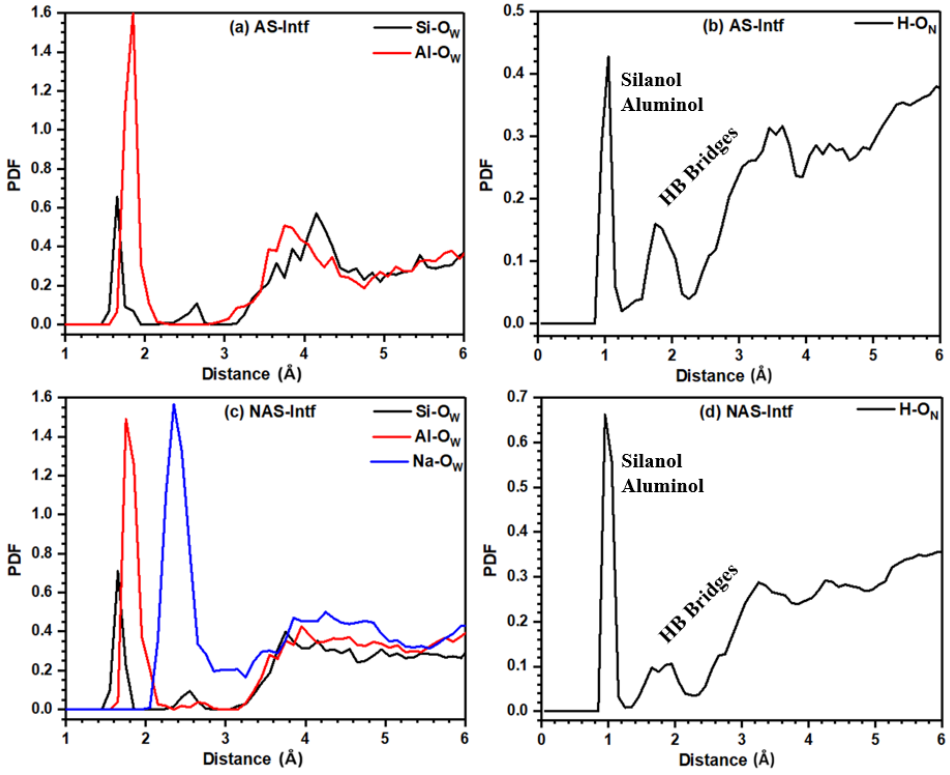

Figure 41. Calculated PDFs in the interface models. (O_W = O from water and O_N = O from glass network)

The sharp first peak for Al-O_W than Si-O_W in **Figure 41 (a)** and **(c)** implies that the Al-O site is more easily attacked by water than the Si-O. i.e., Al is more hydrophilic than Si. Indeed, a near tetrahedral distribution of Si with a smaller number of defects than Al is the main reason for the hydrophobicity of Si. In contrast, either being in a tri-cluster distribution with higher coordination or Na acting as a charge compensator in [AlO_4] tetrahedra, most of the defects are associated with Al which accounts for its hydrophilicity. The existence of a broad second peak

with lower intensity suggests the binding of the first and second solvation shells is via a weak hydrogen bond (HB). The first peak of Na-O_W is at ~2.35 Å, slightly larger than the Na-O distance around 2.30 Å in bulk NAS glass. For H-$O_{N,}$ in both AS-Intf and NAS-Intf models, the first peak lies at ~0.98Å, resulting from the silanol and aluminol, while the second peak centered around 1.9 Å is due to the HB bridges.

Table 17. Calculated CN for cations. The cutoff distances used are Si-O = 2.20 Å, Al-O = 2.40 Å, Na-O = 3.10 Å, and H-O = 1.40 Å.

Glass Models	Si	Al	Na	H
AS-Bulk	4.025	4.356	-	-
AS-Surf	3.967	4.244	-	-
AS-Intf	4.024	4.319	-	0.989
NAS-Bulk	4.000	4.075	5.087	-
NAS-Surf	3.942	3.987	4.625	-
NAS-Intf	3.983	4.150	4.975	0.982

5.3.1.3. Coordination Number and Bond Angle Distribution

The calculated coordination numbers (CNs) for cations are listed in **Table 17**. It shows the distribution of Si is close to tetrahedral in AS-Bulk while perfect tetrahedral in NAS-Bulk glass. Al has CN close to 4 in NAS-Bulk while slightly higher than 4 in AS-Bulk glass. The CN of both ions decreases in the surface models due to the breaking of bonds on the surface. However, its value increases again in the interface models as Si and Al react with water and form hydroxyls. The increase of CN implies the significant hydrolysis of the glass surface. The CN value of Na also decreases from bulk to the surface model but increases again in the interface model. Obviously, the CN of H is close to one.

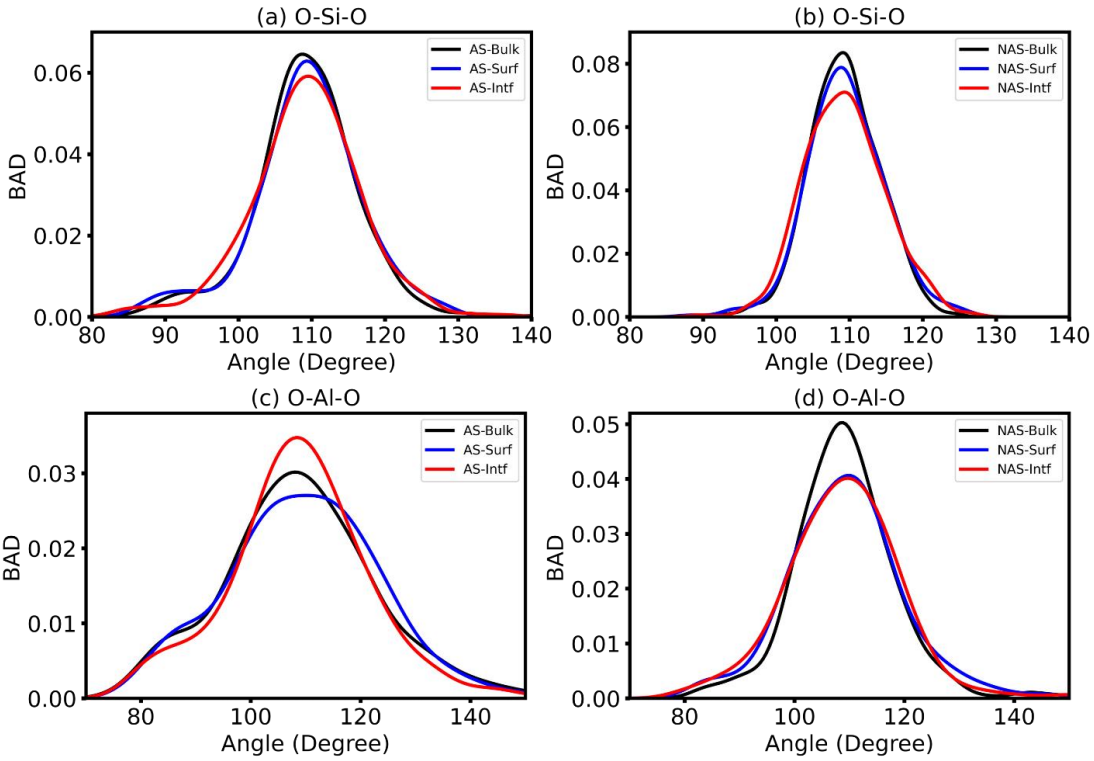

Figure 42. Inter-tetrahedral angles in the simulated bulk, surface and interface models of AS and NAS glasses.

The medium-range order of simulated models is explored by analyzing the bond angle distribution (BAD). **Figure 42** shows the distribution of the inter-tetrahedral angles O-Si-O and O-Al-O. The O-Si-O BAD is centered at ~109^{o} in both AS-Bulk and NAS-Bulk glasses, confirming the mostly tetrahedral distribution of Si atoms in both models. However, the perfect tetrahedral distribution of Si in NAS glass results in higher intensity of O-Si-O in NAS-Bulk than AS-Bulk glass. Compared to the bulk model, the O-Si-O intensity decreases slightly, the peak position shifts to the right, and the distribution becomes broader in AS-Intf and NAS-Intf models. This implies some irregularity in Si tetrahedra distributions due to hydrolysis, which is also reflected by the smaller CN of Si compared to bulk one. The BAD of the O-Al-O angle

is not regular like O-Si-O. In AS and NAS bulk glasses, the O-Al-O peak is centered at ~107^{o}, lower than O-Si-O, and it spreads in a broader range. Due to hydrolysis, the intensity and peak position of O-Al-O change. Overall, the O-Al-O BAD is more irregular, broader, and less intense than O-Si-O in AS and NAS glasses.

The BAD for bridging angles T-O-T (T = Si, and Al) are shown in **Figure 43**. These bridging angles in the bulk glasses have peaks centered in the range of 120^{o}-134^{o} and follow the order of Si-O-Si > Si-O-Al > Al-O-Al. In the interface models, the peak position changes slightly left or right, implying the formation of hydroxyls and changes to the network distribution of Si and Al. These angles in the surface models are broader than the bulk, indicating the irregular distribution of Si and Al on the surface due to bond breaking. The distributions in the interface models are also broader than that of bulk glasses. The intensity of these angles follows the order of Si-O-Si > Si-O-Al > Al-O-Al. The Al-O-Al has the widest distribution followed by Si-O-Al, while Si-O-Si has the sharp distribution among all. The peak position and intensity seem sensitive to the surface model and hydrolysis effect in all three angles. Some of these angles exhibit a bimodal distribution with a small peak centered at ~90^{o} resulting from the small membered rings. The changes observed in the bridging angles distribution, their intensities, and peak position due to hydrolysis are also reflected by varying CN of Si and Al.

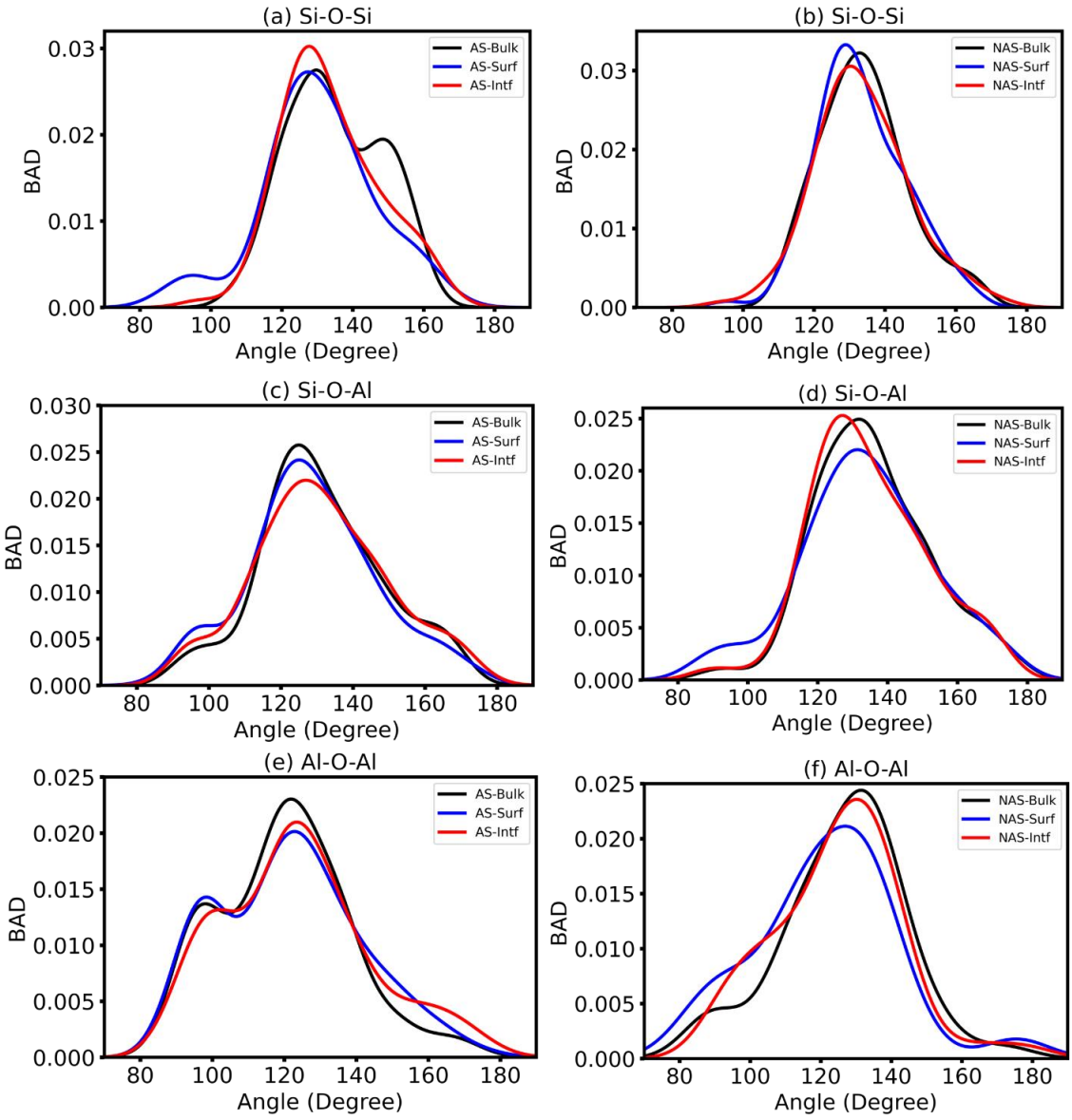

Figure 43. Comparision of bridging angles in the simulated bulk, surface and interface glasses.

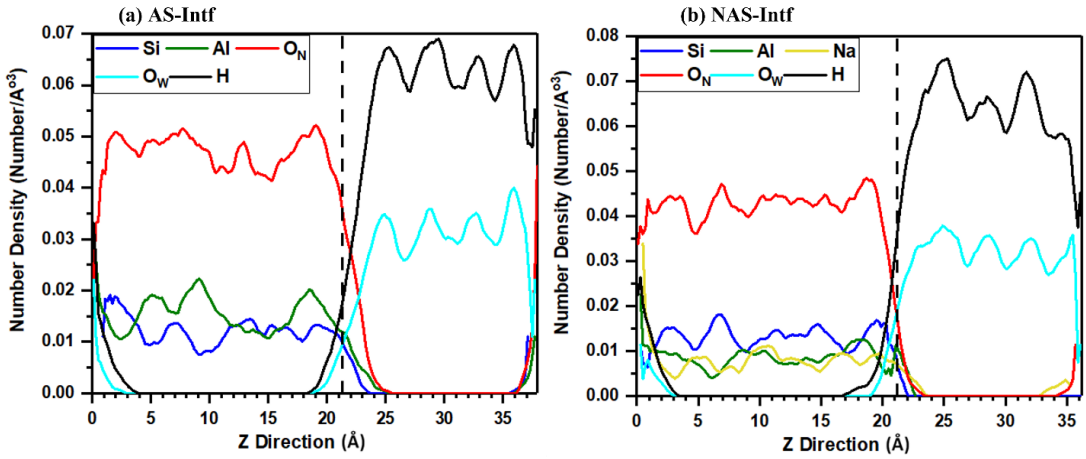

Figure 44. Distribution of number density profile of ions along Z-direction in the interface models. (O_W = O from water, and O_N = O from glass network)

5.3.1.4. Z-Density Profile

The Z-density profile (ZDP) provides information on the distribution of atoms in the perpendicular direction to the interface. **Figure 44** displays the ZDP analyzed in the interface models after the 50 ps simulation. The dashed vertical line separates the top of the surface model from the water medium. It shows a small amount of the network forming ions Si, Al, and O_N penetrates water up to a certain distance in both glasses. The H and O_W from water molecules enter the bulk glass through both sides, and their penetration increases with the simulation progress. In NAS glass, due to the leaching behavior of Na, they dissolve more than Si and Al and diffuse a longer distance into the water from the glass surface. We further provide a deeper analysis of hydrolysis in the interface model, analyzing the averaged ZDP of water components (H^+, OH^-, and H_2O) for 0, 15, 30, and 50 ps. **Figure 45** displays the averaged penetration of water components into the glass from the surface. It shows that water diffusion and hence the propagation of hydrolysis increases with time, implying that a long and

continuous exposure of glass into an aqueous environment causes more degradation of the glass network.

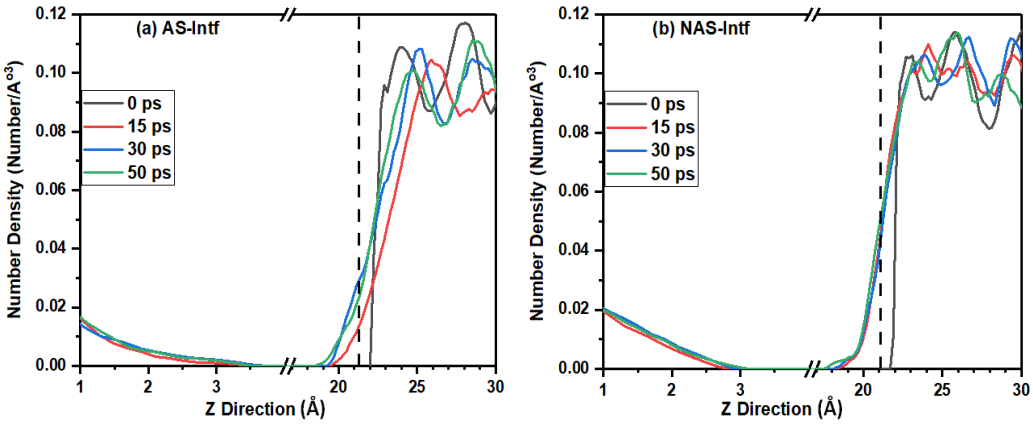

Figure 45. Averaged penetration of water components (H, OH^-, and H_2O) into the bulk glass from the surface as a function of simulation time.

5.3.1.5. Interatomic Bonding

The most important electronic structure result is the internal bonding analysis. The calculated BO provides a complete picture of the internal cohesion and strength in the simulated models. The BO scales with BL in general, but in its quantum mechanical evaluation, the effects of bond angle and bonding distribution of surrounding atoms are also included. The sum of BO values gives the total BO (TBO), a single quantum mechanical metric that characterizes the overall internal cohesion of the material. The calculated TBO and pair-resolved BO (PBO) values are listed in **Table 18**. It shows that the TBO decreases in both AS and NAS glasses from bulk to surface models, but it increases again in the interface models due to a significant contribution on bonding from water molecules. However, the TBO value

Table 18. Calculated TBO and PBO in the bulk, surface, and interface AS and NAS models.

Glass Models	TBO	PBO											
		Si-O	Al-O	H-O	O-O	Na-O	Si-H	Al-H	H-H	Na-H	Si-Na	Al-Na	Na-Na
AS-Bulk	282.04	133.85	148.19	-	-	-	-	-	-	-	-	-	-
AS-Surf	272.97	128.78	144.18	-	-	-	-	-	-	-	-	-	-
AS-Intf	407.51	129.20	144.43	130.19	0.96	-	0.36	0.01	2.35	-	-	-	-
NAS-Bulk	237.69	138.19	76.93	-	-	22.58	-	-	-	-	-	-	-
NAS-Surf	224.73	131.43	72.16	-	0.63	20.09	-	-	-	-	0.12	0.03	0.03
NAS-Intf	360.59	132.89	75.01	126.03	1.27	21.21	0.66	-	3.34	0.02	-	0.04	0.13

for Si-O and Al-O pairs decreases in total from bulk to the interface model, implying the water breaks the glass network and deteriorates its internal strength.

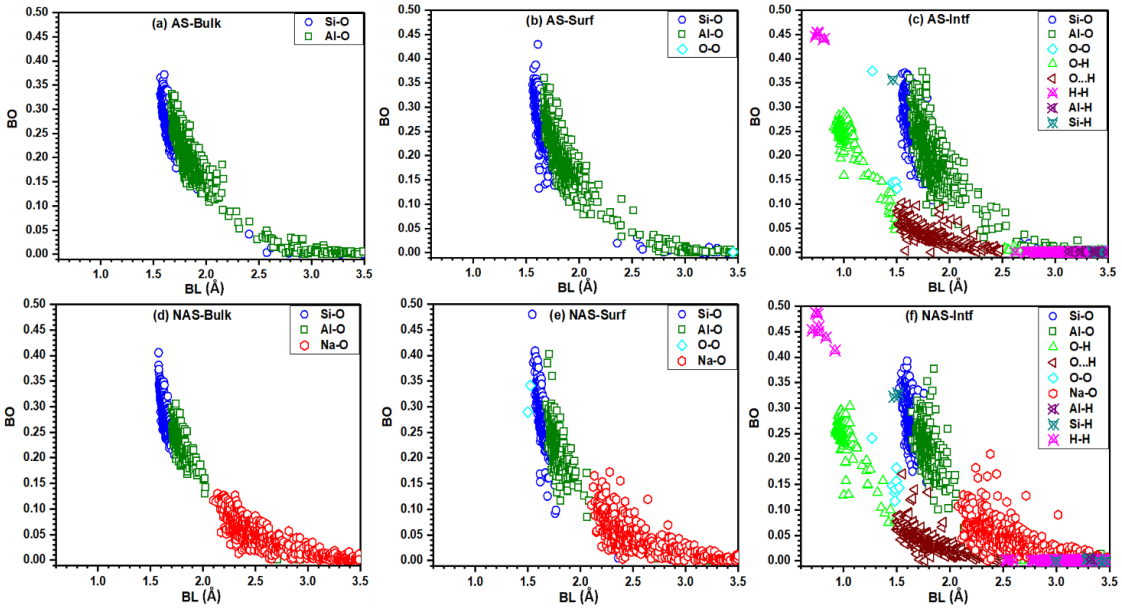

Figure 46. BO versus BL plot in the simulated bulk, surface and interface models.

The BO versus BL distribution in the simulated models is displayed in **Figure 46**. The BO of Si-O and Al-O bonds locates in a narrow BL region in AS-Bulk and NAS-Bulk glasses. These bonds get more scattered in the surface models, and the BO distribution becomes broader. In addition to Si-O and Al-O bonds, there exists O-O pairs in the NAS-Surf model with BO values comparable to the Si-O bonds. The O-O bonds in the AS-Surf model exist only due to the next nearest distribution with BO values close to zero. The BO distribution in the interface models is more complex due to the hydrolysis of the glass network. The covalent O-H bonding within water molecule and due to silanol and aluminol have comparable BO value

with BL ~1 Å. A wide distribution of strong to weak HB appears with BO value 0.02-0.17 e. Some O-O pairs existing in the interface models have BO values comparable to Si-O and Al-O bonds. Compared to surface models, numbers of O-O pairs increase in the interface model. The H-H pairs, mostly existing inside the bulk water, have BO value highest among all bonded pairs with BL ~0.8 Å. The Si-H pairs have BO values comparable to the Si-O, but Al-H pairs have smaller BO values than Al-O pairs. The more scattered and low BO values with elongated BL for network forming ions Si and Al in the interface models imply that the glass-water interaction significantly depolymerizes the glass network and reduces its internal cohesion and strength. These are critical information needed to understand the hydrolysis of a glass surface, which are missing in most of the MD calculations based on geometric parameters.

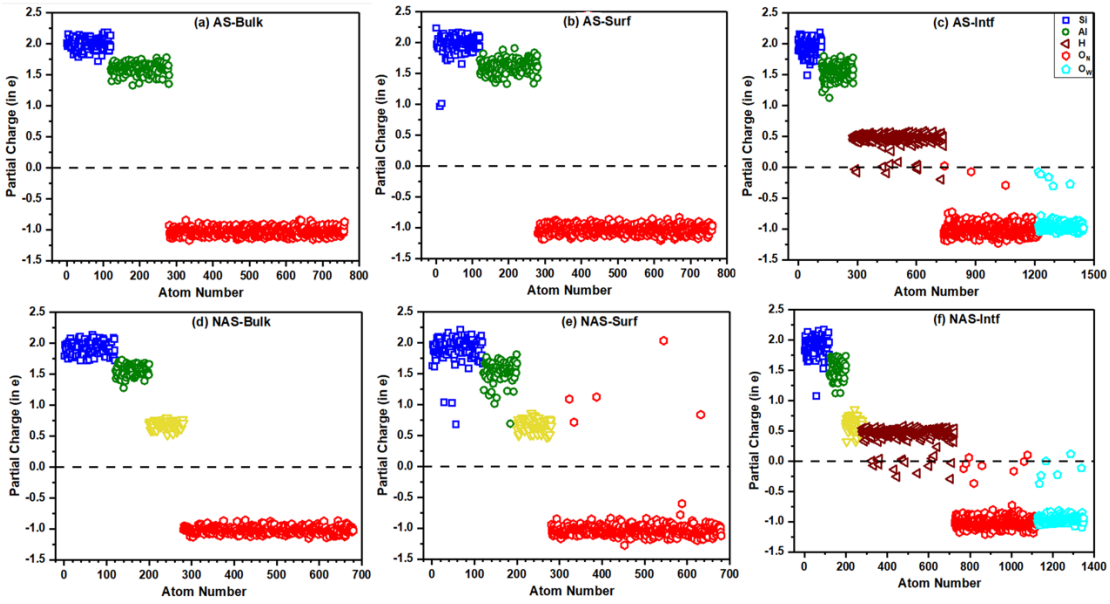

Figure 47. Calculated PC for each atom in the bulk, surface, and interface models of AS and NAS glasses. (O_W = O from water and O_N = O from glass network)

Table 19. Calculated averaged PC (in e) of ions in the simulated bulk, surface, and interface models. (O_N = O from glass network and O_W = O from water)

Glass Models	Si	Al	Na	O_N	O_W	H
AS-Bulk	1.993	1.599	-	-1.032	-	-
AS-Surf	1.963	1.608	-	-1.027	-	-
AS-Intf	1.9450	1.5428	-	-1.010	-0.913	0.466
NAS-Bulk	1.916	1.556	0.682	-1.023	-	-
NAS-Surf	1.900	1.534	0.664	-1.009	-	-
NAS-Intf	1.898	1.514	0.621	-1.001	-0.897	0.452

5.3.1.6. Partial Charge of Ions

Partial charge (PC) is another crucial electronic structure parameter that provides the information of charge transfer between ions in the system. The PC of an atom is defined as the deviation of its effective charge Q* from a neutral charge Q^0 and is given by $\Delta Q^* = Q^0 - Q^*$. The positive PC means a loss of charge, and the negative PC is a gain of charge. The calculated averaged PCs of ions in the simulated models are listed in **Table 19**. It shows that the ions in NAS glass have less averaged PC than that for AS glass. On moving from bulk to the interface model, the averaged PC decreases for each ion. **Figure 47** displays the calculated PC distribution for each atom. It shows Si, Al, and Na lose charge. O from glass network (O_N) gains charge in the bulk model while few of them lose charge in the surface and interface models. O from water (O_W) gains charge in the AS-Intf model while two of them lose charge in the NAS-Intf model. Most of the H lose charge while few of them gain it in both interface models. Our results clearly show that the PC of an atom is not constant, and it strongly depends on the local bonding environments and surroundings of that atom. It also contradicts the conventional MD approach where an atom's predefined constant PC value is used in the simulation. Only the quantum mechanical calculation can account for such effects precisely.

This information on PC is quite helpful in developing and improving the potential for MD study of hydrolysis in a glass.

5.3.2. Results of Salt Doped Interface Models

5.3.2.1. Simulated Glass Structures

The fully relaxed final bulk, surface, and salts-doped glass models are displayed in **Figure 48**, and the structural parameters are listed in **Table 20**. It shows the backbone of the network with Si and Al tetrahedra connected by bridging O. Due to vacuum insertion, some Si and Al at the top of the surface model form dangling bonds, as shown in **Figure 48 (b)**. However, after doping the monolayer water, they interact with water forming silanol and aluminol as shown in **Figure 48 (c),** and convert to a more stable hydroxyl form. In addition, some undercoordinated Si and Al accept proton H^+ forming Si-H and Al-H. With time, the hydrolysis reaction defined by equation (1) propagates towards the bulk glass. However, compared with the interface models discussed above, there are not sufficient water molecules to continue this reaction since only a monolayer of water is present.

Table 20. Final relaxed geometric parameters of the simulated bulk, surface, and salts doped interface glasses.

Glass Models	a (Å)	b (Å)	c (Å)	α^0	β^0	γ^0	Volume (Å^3)
AS-Bulk	21.428	21.535	21.264	89.744	90.920	88.837	9809.016
Surface	21.324	21.409	42.168	89.876	90.653	89.919	19250.054
Surf-W	21.359	21.395	42.289	89.772	90.728	90.013	19323.759
6NCl	21.401	21.364	42.279	90.021	90.979	90.089	19327.690
6NKCl	21.433	21.375	42.283	89.766	91.101	89.984	19367.281
6KCl	21.442	21.365	42.316	89.992	90.912	89.759	19382.590
10NCl	21.395	21.430	42.236	90.225	91.162	89.891	19361.119
10NKCl	21.486	21.356	42.377	89.779	91.089	89.962	19441.474
10KCl	21.428	21.360	42.301	89.779	90.865	90.053	19358.779
14NCl	21.431	21.384	42.315	89.808	91.188	90.105	19387.309
14NKCl	21.428	21.324	42.422	89.844	90.984	90.007	19380.925
14KCl	21.447	21.375	42.359	89.747	91.160	90.043	19414.653

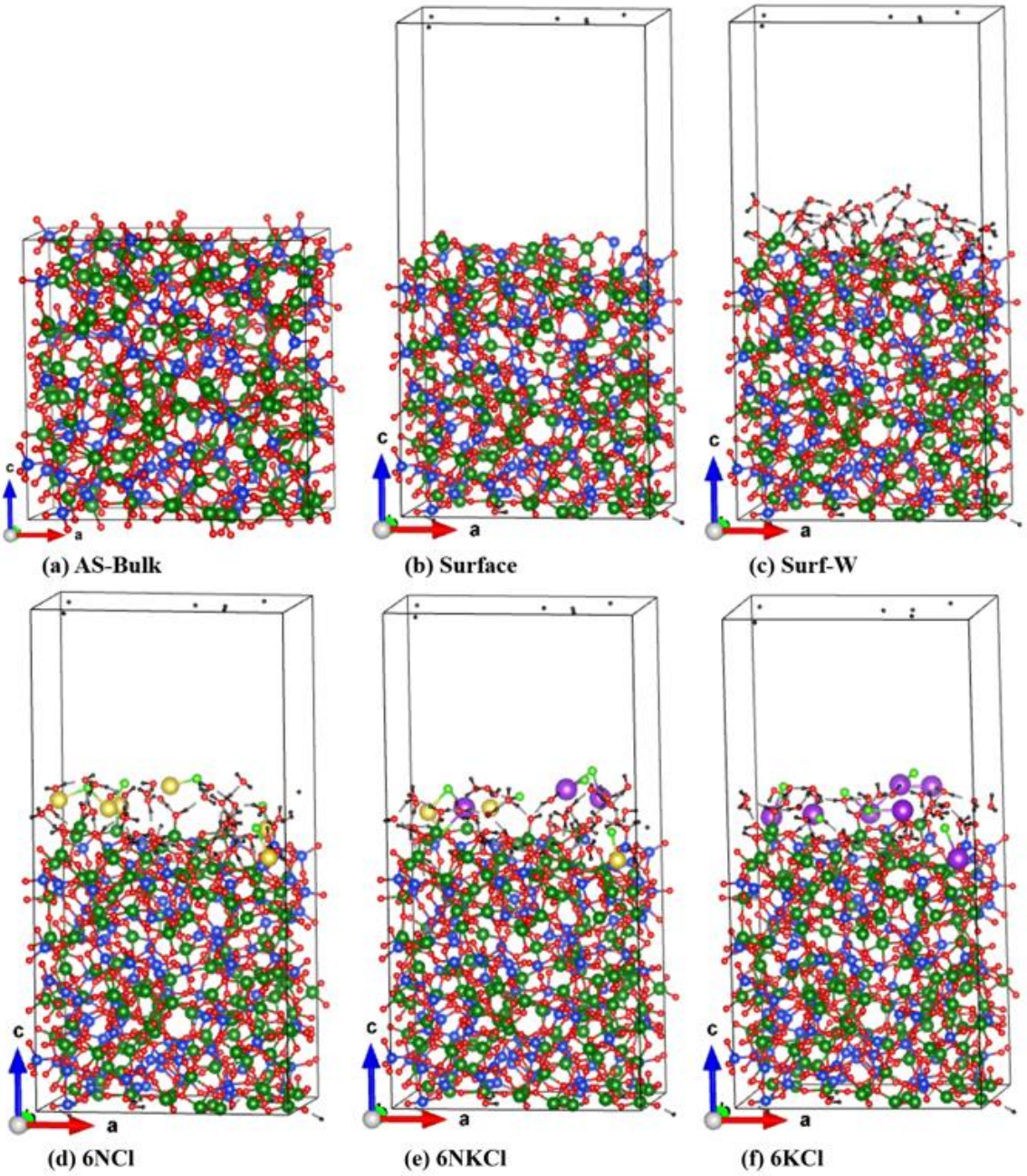
c
a
(a) AS-Bulk
(b) Surface
(c) Surf-W
(d) 6NCl
(e) 6NKCl
(f) 6KCl

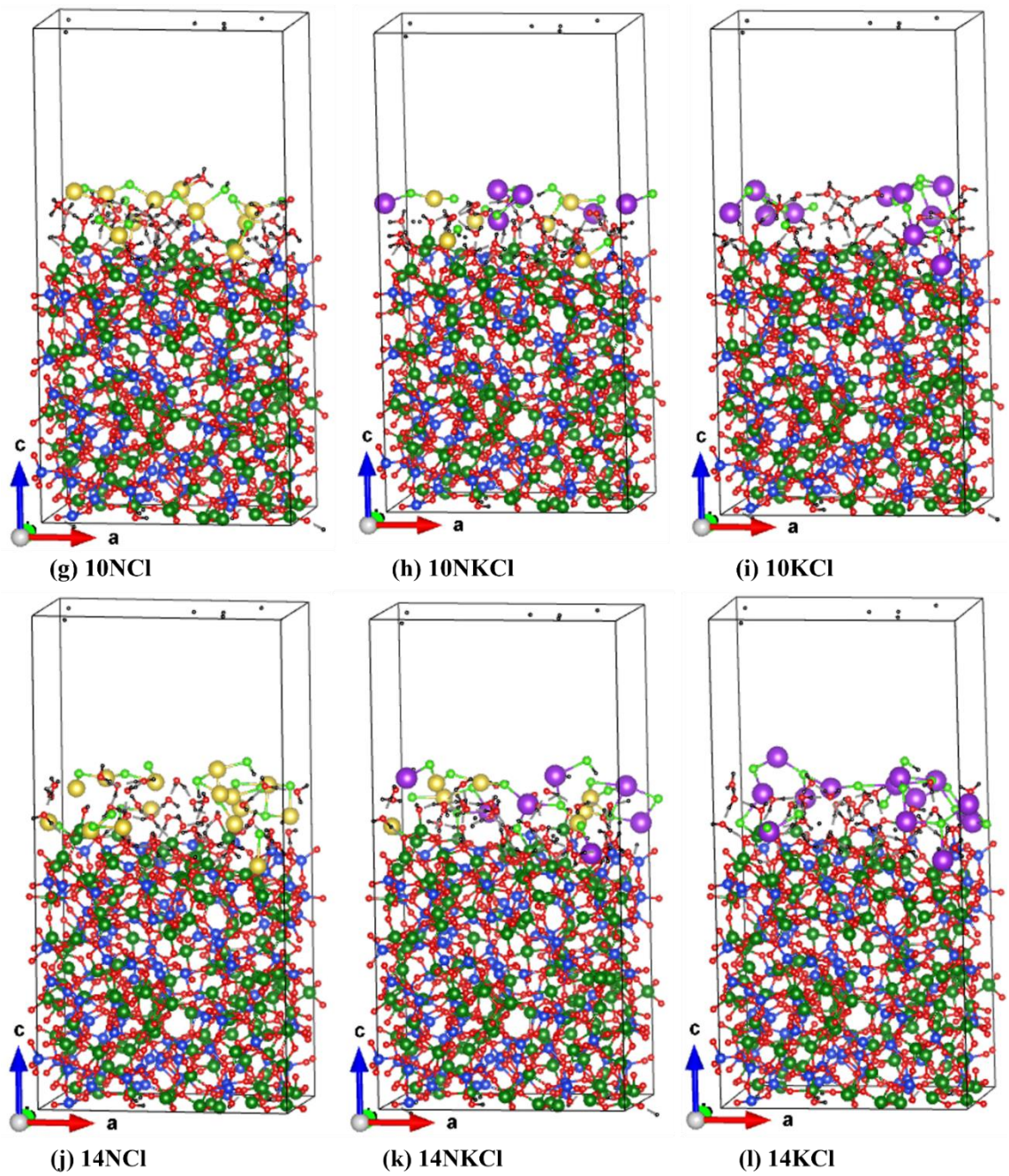

Figure 48. Final relaxed structures of simulated bulk, surface and salts doped models of AS glass. (Si = Blue, Al = Olive, Na = Golden, K = Purple, Cl = Green, O = Red, and H = Black).

The hydrolysis becomes more complicated after doping of salts. The whole system of the salts-doped model can be divided into three regions where the glass-water reaction mechanisms are different: the top water layer with dissolved salts, the water-glass interface, and the bulk glass. Added salts dissolve in water following the reaction mechanism:

$$MCl + H_2O \rightarrow MOH + HCl \quad (M=Na, \text{ and } K) \qquad (4)$$

The MOH will dissociate as M^+ and OH^- following the reaction (3) as discussed in **section 5.3.1.1**. HCl can react further with water producing the hydronium cations H_3O^+ and chloride ion Cl^- following the reversible reaction:

$$HCl + H_2O \rightarrow H_3O^+ + Cl^- \qquad (5)$$

The diffusion of H_3O^+ into the bulk region degrades the glass network. As Cl ions are less soluble in the glass matrix, and due to the leaching of alkali ions, they recombine again to form MCl salts. However, doping of salts increases water ionization, which diffuses towards the glass network and intensifies the glass hydrolysis and corrosion. The hydrolysis increases with the increasing salt concentration. A similar result has been reported in the study of silicate glass dissolution in water in the presence of Na/K-Cl and $CaCl_2$ salts [67]. Due to the larger size of K ions, more water gets dissociated in KCl doped model than NaCl doped one. The following sections will discuss the more detailed effect of salts on the hydrolysis of AS glass surface.

5.3.2.2. Structural Properties

The complexity of short- and medium-range order properties in salt doped AS glasses makes a thorough understanding of hydrolysis very challenging. We analyze the details of PDF, CN, and BAD to explore the effects of structural features on hydrolysis and corrosion of these glasses. The calculated PDFs for cations (Si, Al) and O pairs are shown in **Figure 49**.

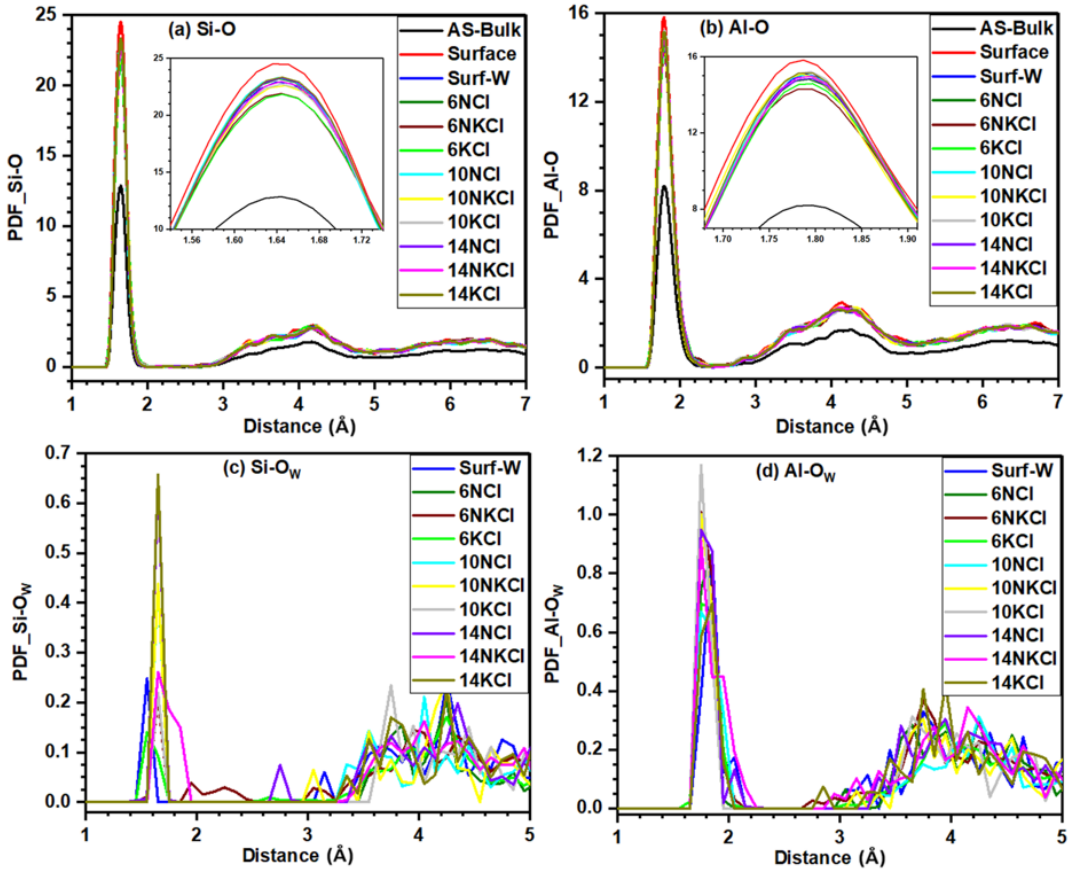

Figure 49. (a, b) Si-O and Al-O total PDFs and (c, d) Si-O_W and Al-O_W partial PDFs in the salts doped models (O_W = O from water).

Figures (a, b) show the PDFs of Si and Al with total O along with the magnified image of the first peak, while (c, d) show the PDFs of Si and Al with O from water. In the bulk glass, the Si-O and Al-O pairs have a primary peak at ~1.62 Å and ~1.80 Å, respectively. However, these peak positions shift slightly right in the surface and salt-doped models, implying the elongation of Si-O and Al-O bonds due to hydrolysis. The intensities of these pairs increase sharply from bulk to the surface model but decrease again in the hydrated and salts doped models. Both distributions do not show any noticeable sharp peaks beyond 2 Å, implying the lack of long-

range properties. A broad secondary peak of lower intensity beyond 4 Å in Si-O and Al-O distributions is the result of the next nearest neighbors. The first sharp peak in Si-O_W and Al-O_W PDFs implies the glass surface is hydrolyzed considerably. The higher intensity of the Al-O_W peak than Si-O_W implies Al is more hydrophilic than Si. The increase in the intensity of peaks with increasing salt concentration indicates glass hydrolysis increases with the increasing content of salts. It does not show any sharp secondary peak, but a broader peak of small intensity appears around 4 Å.

Table 21. Calculated CN for cations. The cutoff distance used are Si-O = 2.20 Å, Al-O = 2.40 Å, H-O = 1.40 Å, Na-O = 3.10 Å, and K-O = 3.80 Å (H_T = total H and H_W = H from water).

Glass Models	Si	Al	H_T	H_W	Na	K
AS-Bulk	4.025	4.356	-	-	-	-
Surface	3.942	4.150	0.471	-	-	-
Surf-W	3.958	4.187	0.907	1.000	-	-
6NCl	4.092	4.193	0.908	1.013	3.500	-
6NKCl	3.957	4.194	0.917	1.025	4.333	3.000
6KCl	3.958	4.169	0.938	1.025	-	3.667
10NCl	3.933	4.181	0.897	1.023	2.500	-
10NKCl	3.967	4.144	0.876	1.020	2.800	2.600
10KCl	3.975	4.194	0.928	1.000	-	2.500
14NCl	3.950	4.206	0.927	1.012	2.357	-
14NKCl	3.966	4.188	0.876	0.997	2.428	2.571
14KCl	3.958	4.150	0.725	0.975	-	2.143

The calculated CN of cations Si, Al, H, Na, and K with O are listed in **Table 21**. As already discussed, Si is near tetrahedrally coordinated in the bulk glass while Al coordination is slightly higher than 4. The CN of Si and Al slightly decreases in the surface model due to bond breaking. However, the CN for these ions increases in the water and salt-doped models due to hydroxyl groups formation. As some of the added H atoms in the surface model are bonded

with Si and Al, the average CN of total H (H_T) with O is less than 1; however, the CN of H from water (H_W) molecules is ~1. The CN of H_W decreases with the increasing concentration of salts, implying that more water dissociates when salt concentration increases. As NaCl and KCl salts are doped at the top of the water layer, they react mainly with the water molecules only and remain bonded to Cl, due to which their CN value is smaller than the typical CN of alkali ions found in glass.

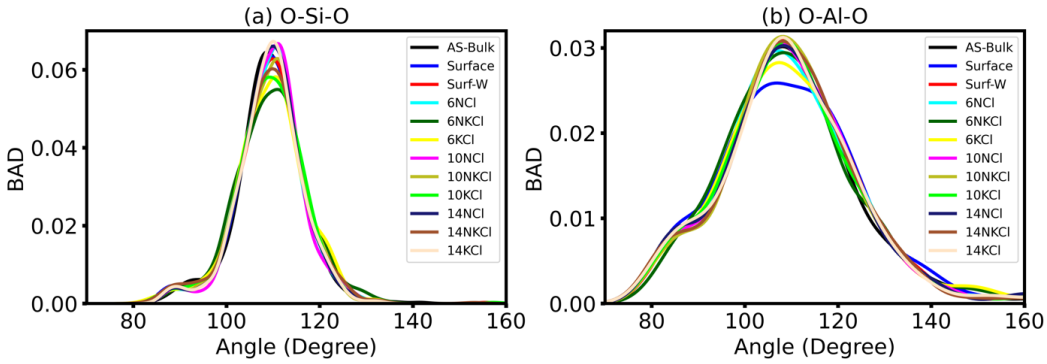

Figure 50. Comparision of (a) O-Si-O and (b) O-Al-O angles in the bulk, surface and salts doped models.

The bond angle analysis presented in **Figures 50** and **51** provides the intermediate range-order information in the simulated models. The inter-tetrahedral angles O-Si-O and O-Al-O distributions (**Figure 50**) show their peak position and intensity changes from bulk to the salts doped models. It implies that due to hydrolysis and the addition of salts, the near tetrahedral distribution of Si and Al is disrupted, and hydroxyl groups are formed. The figure shows O-Al-O angle distribution is broader and less intense than the O-Si-O.

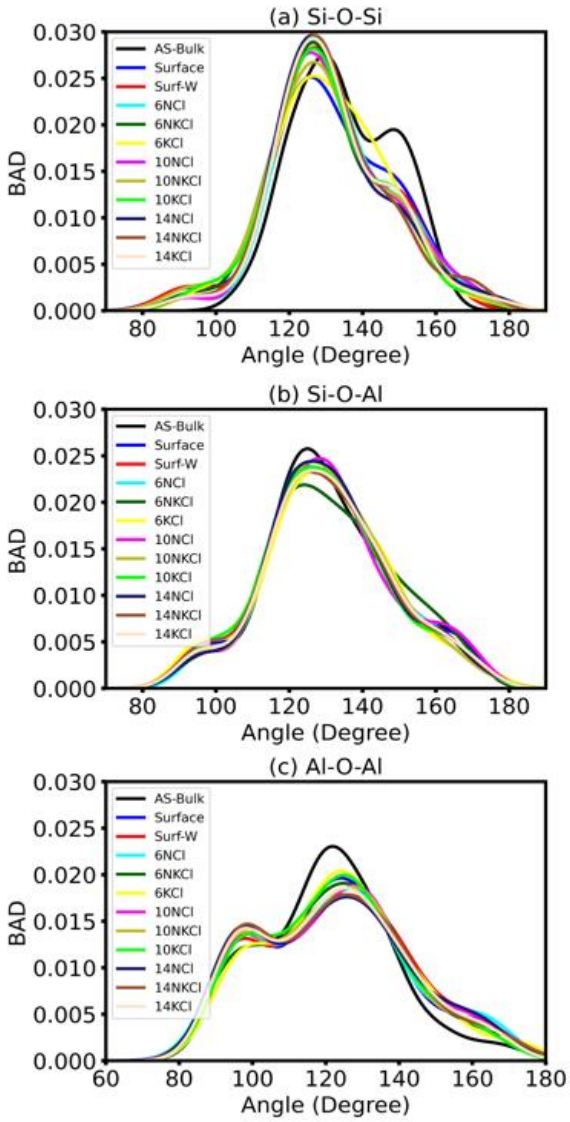

Figure 51. Bridging angle distributions in the bulk, surface and salts doped models.

Figure 51 displays the distribution of bridging angles Si-O-Si, Si-O-Al, and Al-O-Al between two tetrahedra. The main framework geometry of Si-O and Al-O bonds greatly determines the distribution of these angles and the polymerization of the glass network. The peak position and intensity of these angles change due to hydrolysis and doping of salts. The broader distribution in the salt doped models than bulk one implies the breaking of the network

Table 22. Calculated TBO and PBO values for each bonded pair in the simulated bulk, surface, and salts doped interface glass models.

Glass Models	TBO	PBO													
		Si-O	Al-O	H-O	O-O	Na-O	K-O	Si-H	Al-H	H-H	Na-Cl	K-Cl	H-Cl	Si-Cl	Al-Cl
AS-Bulk	282.14	135.48	146.66	-	-	-	-	-	-	-	-	-	-	-	-
Surface	274.08	129.89	140.35	2.31	-	-	-	1.53	-	-	-	-	-	-	-
Surf-W	300.11	130.95	142.99	25.88	-	-	-	0.26	-	0.02	-	-	-	-	-
6NCl	301.48	131.52	141.77	24.22	0.45	1.24	-	0.32	0.03	0.46	0.66	-	0.58	-	0.23
6NKCl	300.87	130.87	142.92	24.75	-	0.55	0.22	0.26	-	0.02	0.32	0.27	0.69	-	-
6KCl	300.08	130.66	142.68	24.74	-	-	0.59	0.34	-	0.01	-	0.48	0.58	-	-
10NCl	302.62	131.24	141.86	24.13	0.38	1.49	-	0.32	0.03	0.49	1.55	-	0.89	0.24	-
10NKCl	301.02	131.14	139.66	22.95	1.08	0.78	0.54	0.78	0.33	1.38	0.89	0.53	0.96	-	-
10KCl	300.79	131.42	143.23	24.95	-	-	0.97	0.29	-	0.01	-	1.00	0.92	-	-
14NCl	305.51	131.32	142.96	25.08	-	2.05	-	0.31	-	0.01	2.21	-	1.08	-	0.48
14NKCl	302.85	131.53	140.85	23.48	0.62	0.87	0.55	0.43	0.08	0.92	1.23	0.82	0.76	-	0.72
14KCl	302.74	131.79	142.17	24.09	0.34	-	0.77	0.34	0.01	0.46	-	1.51	1.09	-	0.39

and its depolymerization due to hydrolysis. The intensity of these angles follows an order of Si-O-Si > Si-O-Al > Al-O-Al. The Al-O-Al is the broadest among the bridging angles distributions. The broader distribution of this angle implies the co-existence of higher coordinated Al along with four coordinated Al. A secondary peak of small intensity appears in some of these angles due to the bimodal distributions.

5.3.2.3. Interatomic Bonding Analysis

The calculated TBO and PBO values of the salt-doped models are listed in **Table 22**. It shows that TBO decreases sharply from bulk to the surface model due to the cleavage of bonds on the surface. However, this value increases again in the water and salts doped models due to the bonding contribution from glass-water interaction. For the same concentration of slats, the TBO decreases from NaCl doped to KCl doped model due to the larger size effect of K ion.

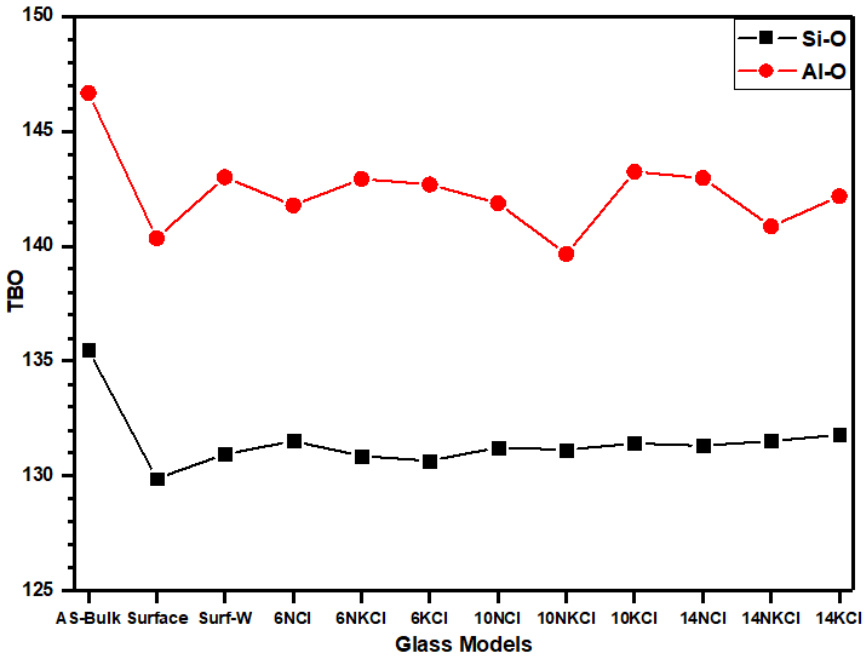

Figure 52. Comparision of TBO for Si-O and Al-O pairs in the simulated bulk and surface modes to salts doped models.

Figure 52 shows the effect of hydrolysis on the TBO for Si-O and Al-O bonds. The TBO for both pairs decreases sharply from bulk to the surface model and increases again in the hydrated model. In the case of salts-doped models, the TBO for Al-O seems to be far more sensitive to the alkali ion size and the concentration of salts. Also, the TBO for the Al-O pair exhibits MAE when NaCl and KCl salts are mixed. Compared to Al-O, the TBO for Si-O is less sensitive to the size of alkali ions and the salt concentration.

The BO versus BL distribution displayed in **Figure 53** helps to dig deeper into the effects of salts on the hydrolysis of AS glass surface. It is a complex display that shows details of the hydrolysis effect on internal bonding. Si-O and Al-O are the main contributors to the bonding with high BO values. In the bulk glass, these bonds are distributed in a sharp region. Due to network breaking and the formation of hydroxyl groups, both bonds scatter somewhat, lowering the averaged BO value in the surface and salts doped models. In the surface model, the added H binds with O from the glass network making strong covalent bonds O_N-H of BL ~1 Å with BO in the range of 0.25 e - 0.33 e. The HBs (O···H) in the surface model are very weak, with BO values close to zero. The undercoordinated Si and Al form Si-H and Al-H bonds and transform into tetrahedral distribution. The Si-H bonds have BO comparable to O_N-H, while Al-H bonds have BO close to zero. The O_{NN}-H bonds beyond 2.5 Å with BO close to zero are due to the next nearest pairs. In the hydrated surface model, the number of HBs increases with BO values varying from 0.01-0.13 e. The O-H bonding from the water molecule (O_W-H) and silanol and aluminol (O_N-H) have comparable BO with BL ~1Å. The O-O, Al-H, and H-H pairs exist beyond 2.5 Å only due to the next nearest neighbors with BO values close to zero. Although the H atoms at the bottom layer are fixed, their position slightly changes due

to the relaxation of shape and volume of the simulation cell. As a result, the Si-H bonds get somewhat elongated, and the BO decreases than the surface model.

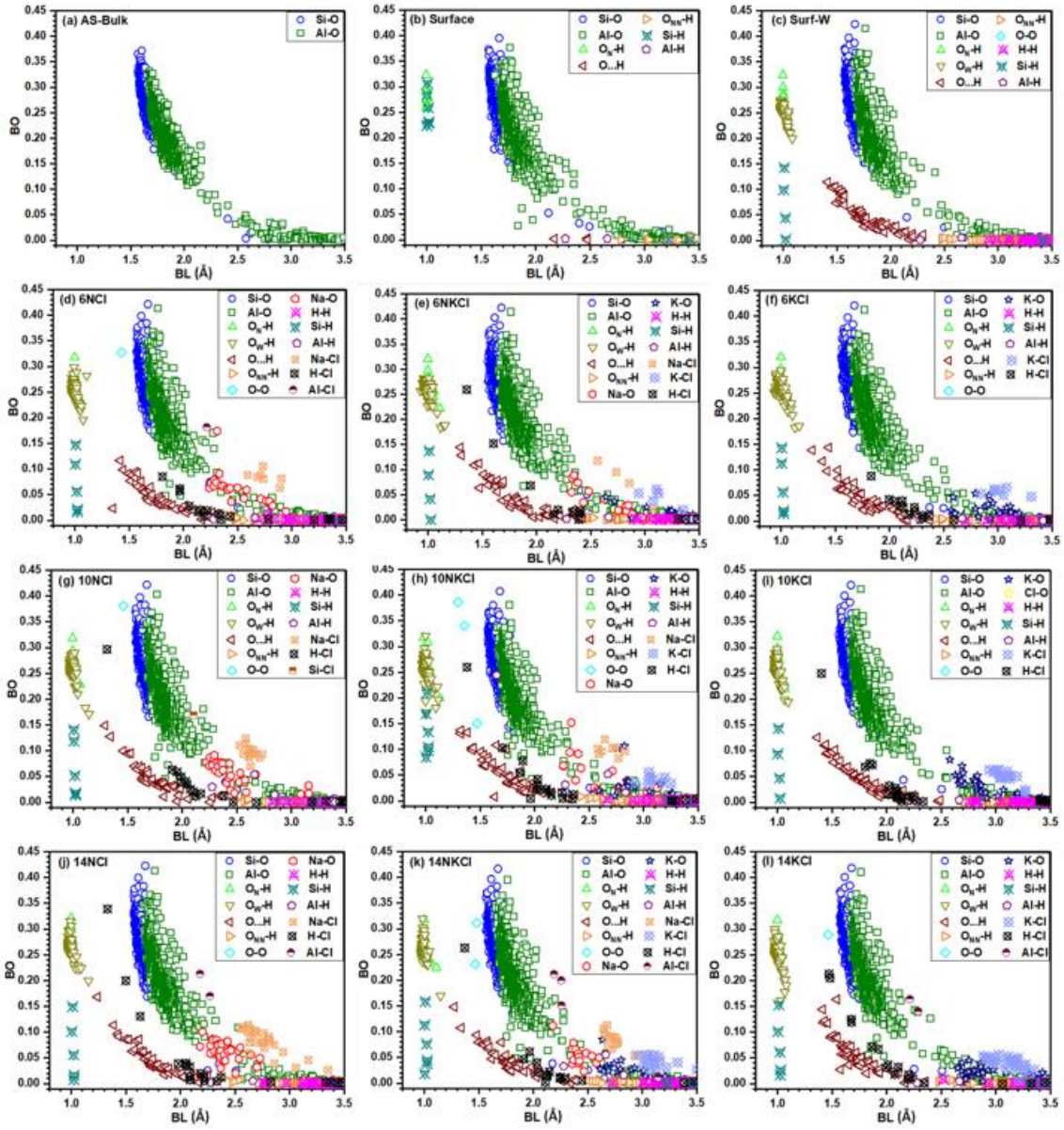

Figure 53. BO versus BL plot in the simulated 12 glass models.

The bonding pattern becomes far more complicated in the salt-doped models due to salt-water interaction and more hydrolysis of the glass network. The Si-O and Al-O bonds become more scattered. The scatteredness increases from NaCl to KCl doped glass due to the larger size of the K ion. It also increases with the increasing concentration of salt, which implies an increase in salt content enhances hydrolysis. The quantity and strength of HBs increase due to more water ionization. The HBs in the salt-doped model have BO values in the range of 0.01-0.17 e. The O_N-H bonds, resulting from silanol and aluminol, and O_W-H from water molecules still have comparable BO values with BL ~1 Å. The O_{NN}-H and H-H pairs result from the next neighbor distribution only beyond 2.5 Å with BO values close to zero. The O-O pairs have BO values comparable to Si-O and Al-O bonds. The Si-H pairs show similar nature as in the Surf-W model. The Al-H bonds have smaller BO than Al-O bonds. The Cl ion detached from the salt makes H-Cl, Si-Cl, and Al-Cl bonds. Some H-Cl has BO values comparable to Si-O and Al-O bonds, while the rest have less than 0.1 e. The Si-Cl and Al-Cl have BO values smaller than Si-O and Al-O bonds. The Na-Cl and K-Cl have BO values less than Si-O and Al-O pairs. The BO values from Na ions in Na-O and Na-Cl are larger than that from K ion in K-O and K-Cl pairs. These details are missing in MD and many other calculations, and only a rigorous quantum mechanical calculation can deal with it. Hence, the bonding analysis result discussed here provides valuable information needed to understand the hydrolysis and corrosion effects of glass surfaces by salts.

Table 23. Calculated averaged PC of each ion in the simulated models. (O_N = O from glass network, O_W = O from water, H_A = Added H, and H_W = H from water)

Glass Models	Si	Al	O_N	O_W	H_A	H_W	Na	K	Cl
AS-Bulk	1.972	1.621	-1.033	-	-	-	-	-	-
Surface	1.952	1.628	-1.028	-	-0.081	-	-	-	-
Surf-W	1.966	1.610	-1.021	-0.924	-0.251	0.468	-	-	-
6NCl	1.969	1.601	-1.026	-0.851	-0.234	0.471	0.645	-	-0.576
6NKCl	1.961	1.600	-1.016	-0.942	-0.246	0.468	0.687	0.747	-0.583
6KCl	1.960	1.602	-1.016	-0.941	-0.235	0.469	-	0.715	-0.661
10NCl	1.967	1.601	-1.026	-0.842	-0.234	0.461	0.662	-	-0.543
10NKCl	1.971	1.620	-1.039	-0.695	-0.199	0.413	0.584	0.627	-0.567
10KCl	1.964	1.608	-1.019	-0.937	-0.242	0.460	-	0.688	-0.606
14NCl	1.964	1.603	-1.018	-0.927	-0.239	0.452	0.653	-	-0.536
14NKCl	1.969	1.599	-1.026	-0.835	-0.226	0.453	0.652	0.683	-0.560
14KCl	1.966	1.604	-1.025	-0.882	-0.230	0.451	-	0.731	-0.559

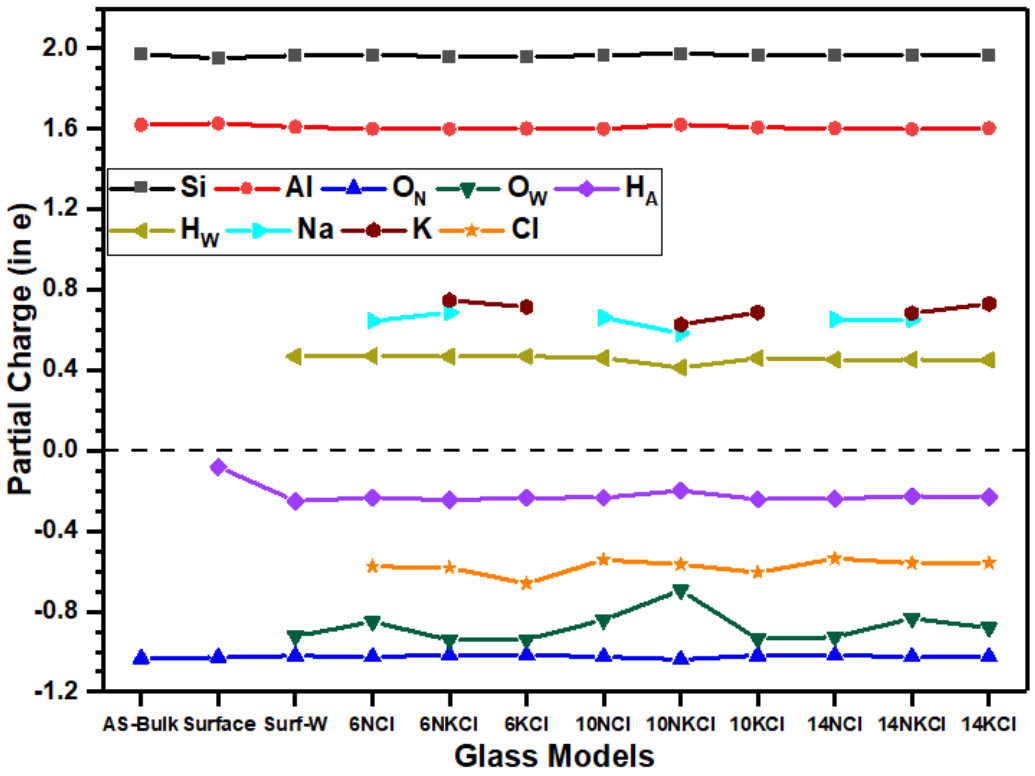

Figure 54. Calculated averaged PC for each ion in the simulated glasses. (H_A = Added H, H_W = H from water, O_W = O from water, and O_N = O from glass network)

5.3.2.4. Partial Charge Analysis

The averaged PC of each atom in the simulated models is listed in **Table 23** and plotted in **Figure 54**. It shows that Si has the highest and O has the lowest PC value. The averaged PC of Si and Al decrease in the salts doped models than the bulk one. The PC of O_W is more sensitive to the alkali ion size and salts concentration than O_N. The PC of added H (H_A) decreases largely from the Surface to the Surf-W model and decreases slightly in the salts doped models. The PC of H from water (H_W) decreases slightly on moving from water doped to the increasing salts doped models. The PC of Cl shows some variation in its averaged value and depends on the PC of alkali ions. We provide further details by analyzing the PC for each atom, as shown in **Figure 55**. It shows that the Si, Al, K, and Na lose charge. The Cl and O atom from the glass network gains charge, except some O in a few models that lose charge. Most O_W gains charge while few of them in some models lose it. The O in O-O configuration loses charge. The H_A and H_W lose or gain charge depending on their bonding configuration and local environment. The H bonded to Si, and Al gains charge while bonded with O loses charge. The PC distribution is congregated in the bulk glass, but it gets scattered in other models. Our results show that the PC of ions is not constant as assumed in most MD calculations, and its value strongly depends on the local bonding environment. This information is quite helpful to develop or improve the potential in MD studies.

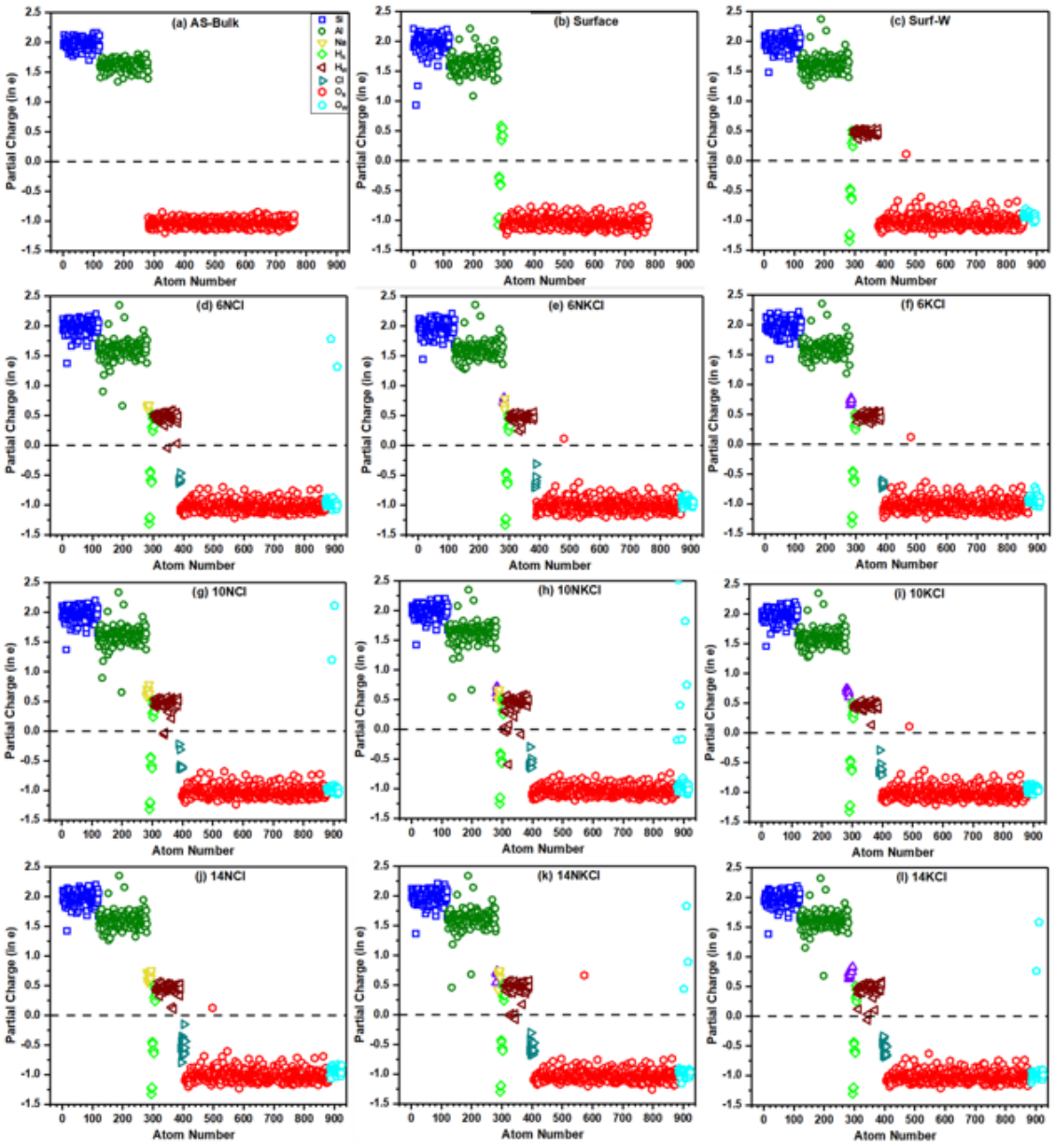

Figure 55. Calculated PC for each ions. (H_A = Added H, H_W = H from water, O_W = O from water, and O_N = O from glass network)

5.4. Summary and Conclusions

The AIMD simulation carried on the AS glass-water interface enhances the knowledge of the hydrolysis mechanism and the effects of Na/K-Cl salts on the aqueous corrosion of this glass. In addition, it provides new insights to better understand the degradation of AS glass surface due to reaction with water. We can sum up our findings in a few points: one of which is the AS glass surface hydrolyzes readily in contact with water forming silanol and aluminol, and the hydrolysis propagates to the bulk region with time. As a result, three distinct regions: bulk water, dissolved glass, and bulk glass, are observed in the glass-water interface system. The AS glass corrodes by water diffusion and H^+ transfer. The H^+ transfer is most effective in alkali AS glass and can go deeper into the bulk glass than water diffusion. The alkali ions in AS network provide a favorable path for protons and water to penetrate the glass surface and accelerate the hydrolysis by leaching. The alkali ions in charge-balanced conditions to Al tetrahedra of AS glass are less prone to water attack than bonded with NBO. Another finding is that Al is more hydrophilic than Si, and water molecules attack the Al-O bonds easily than Si-O. The in-depth bonding analysis provided with BO values for individual bonding pairs depicts the effect of hydrolysis on the internal bonding and cohesion of the simulated models. The most important finding is that the cleavage of bonds on the surface causes drastic changes in glass properties and doping of salts enhances the hydrolysis. The salts with larger alkali ions cause more degradation of the glass network. In addition, an increase in salt concentration intensifies hydrolysis and deterioration of the AS network. Very few studies exist, and little is known in the past about the aqueous corrosion effects of Na/K-Cl salts on AS glass. We

anticipate that our work will motivate glass researchers to carry out more theoretical and experimental works in this direction in the future.

Overall, we have shown that AIMD can effectively investigate hydrolysis and corrosion at atomic resolution in multicomponent AS glasses where the experiment cannot cope alone, and the use of MD is still challenging. Furthermore, our study ensures that it is feasible to use AIMD to study hydrolysis in even more complex and large systems. Such study, including the effect of temperature and pH of a solution that significantly affects glass corrosion, is our next target in the endeavor to study glass corrosion, which looks promising.

CHAPTER 6

FINAL REMARKS

DFT-based VASP and OLCAO are combined to study the hydrolysis and aqueous corrosion of silicate and AS glasses. The hydrated models of bulk SiO_2 and single and mixed alkali ions (Li, Na, and K)-doped alkali silicate glasses are constructed and analyzed the hydrolysis mechanism in them. Both molecular water H_2O and hydroxyl group OH exist in hydrated alkali-silicate glasses. The molecular water itself is not detrimental to the mechanical property, but the ionized water and hydroxyl group attack the glass network lowering its mechanical strength. In addition, due to hydrolysis, the Si-O-Si bonding breaks, and the glass network gets depolymerized. The Li-doped hydrated silicate is the strongest glass than Na-, and K-doped silicate glasses with higher TBOD value. The mechanical property and refractive index show MAE in the case of mixed alkali ions doped glasses.

Furthermore, the hydrolysis effects in single and mixed alkali ions doped bulk alkali AS glasses are analyzed. The hydrolysis mechanism in alkali AS is more complicated. In alkali AS glass also, the water exists as molecular water H_2O and hydroxyl group OH. Hydrolysis depolymerizes the glass network breaking the framework geometry made up of T-O-T (T = Si, and Al). The TBOD and mechanical properties of alkali AS glasses decrease due to hydrolysis. Due to the larger size of potassium, the potassium-doped AS glass is weaker than sodium-doped.

Finally, the hydrolysis and aqueous corrosion of AS surface is analyzed. The glass surface hydrolyzes readily in contact with water, which propagates towards the bulk glass with time. Due to hydrolysis, the glass network depolymerizes, and the internal strength deteriorates.

Presence of leachable alkali ions in the AS network accelerates the glass hydrolysis. Addition of salts Na/K-Cl enhances the glass hydrolysis. Hydrolysis increases with increasing concentration of salts. The results presented in this dissertation provide a new platform of knowledge to understand the aqueous corrosion mechanism of silicate and AS glasses and help design strong and durable glass products. This work shows AIMD can effectively investigate the hydrolysis and corrosion in multicomponent silicate and AS glasses. Furthermore, this study ensures that it is feasible to use AIMD to study hydrolysis in even more complex and large systems. Such studies, including the effect of temperature and pH of solution that significantly affects glass corrosion, can be the next step to study multi-component glass corrosion.

APPENDIX

A typical INCAR file for NVT simulation

System = Al160Si120O709H458

ISMEAR = 0 ! Use 0 for KPOINTS less than 4 otherwise -5.

PREC = Accurate ! low, medium, normal are other options.

ENCUT = 600 eV ! cutoff energy, depends on the system size and accuracy we want.

EDIFF = 1.0E-5 ! enegy difference covergence limit for electronic optimization.

EDIFFG = -1.0E-3 ! enegy difference covergence limit for ionic optimization.

IBRION = 0 ! 0 for MD, 1 best, 2 for diff relaxation problems.

NSW = 5000 ! total number of ionic steps.

ISIF = 2 ! 2 and 4 ionic, 7 volume and 3 both.

NELMIN = 4 ! minimum number of SC steps

NBLOCK = 1 ! frequency of ionic configuration is written to the XDATCAR-file

MDALGO = 2 ! Nose-Hoover thermostat

SIGMA = 0.1 ! specifies the width of the smearing in eV.

ISYM = 0 ! determines the way VASP treats symmetry.

POTIM = 0.5 ! time steps in fs

TEBEG = 300 ! initial temperature

TEEND = 300 ! final temperature

SMASS = 0 ! controls the velocities during an AIMD run.

ISTART = 0 ! determines whether to read the WAVECAR file or not; 1 = if WAVECAR exists.

```
LREAL  = Auto        ! projection on real space. use FALSE (default) for reciprocal space.
NPAR   = 32          ! best sqrt of NCPUs used.
ALGO   = VeryFast    ! default is Normal.
LCHARG = F           ! do not write in CHG and CHGCAR files
LWAVE  = F           ! do not write in WAVECAR file
```

REFERENCES

[1] M. Smirniou and T. Rehren, "Direct evidence of primary glass production in Late Bronze Age Amarna, Egypt," *Archaeometry,* vol. 53, no. 1, pp. 58-80, 2011.

[2] D. Young, *Computational chemistry: a practical guide for applying techniques to real world problems*. John Wiley & Sons, 2004.

[3] R. G. Parr, "Density functional theory of atoms and molecules," in *Horizons of quantum chemistry*: Springer, 1980, pp. 5-15.

[4] W. H. Zachariasen, "The atomic arrangement in glass," *Journal of the American Chemical Society,* vol. 54, no. 10, pp. 3841-3851, 1932.

[5] G. Greaves, "EXAFS and the structure of glass," *Journal of Non-Crystalline Solids,* vol. 71, no. 1-3, pp. 203-217, 1985.

[6] G. Henderson, "A Si K-edge EXAFS/XANES study of sodium silicate glasses," *Journal of non-crystalline solids,* vol. 183, no. 1-2, pp. 43-50, 1995.

[7] R. Dupree, D. Holland, P. W. McMillan, and R. Pettifer, "The structure of soda-silica glasses: a MAS NMR study," *Journal of Non-Crystalline Solids,* vol. 68, no. 2-3, pp. 399-410, 1984.

[8] U. Voigt, H. Lammert, H. Eckert, and A. Heuer, "Cation clustering in lithium silicate glasses: quantitative description by solid-state NMR and molecular dynamics simulations," *Physical Review B,* vol. 72, no. 6, p. 064207, 2005.

[9] J. Zhao, P. Gaskell, M. Cluckie, and A. Soper, "A neutron diffraction, isotopic substitution study of the structure of Li2O· 2SiO2 glass," *Journal of Non-Crystalline Solids,* vol. 232, pp. 721-727, 1998.

[10] B. M. Lee, H. K. Baik, B. S. Seong, S. Munetoh, and T. Motooka, "Generation of glass SiO2 structures by various cooling rates: A molecular-dynamics study," *Computational materials science,* vol. 37, no. 3, pp. 203-208, 2006.

[11] S. K. Mitra, "Molecular dynamics simulation of silicon dioxide glass," *Philosophical Magazine B,* vol. 45, no. 5, pp. 529-548, 1982.

[12] H. Rawson, *Properties and applications of glass*. Elsevier Science & Technology, 1980.

[13] G. Greaves, A. Fontaine, P. Lagarde, D. Raoux, and S. Gurman, "Local structure of silicate glasses," *Nature,* vol. 293, no. 5834, pp. 611-616, 1981.

[14] G. Greaves, "Structure and ionic transport in disordered silicates," *Mineralogical Magazine,* vol. 64, no. 3, pp. 441-446, 2000.

[15] M. I. Ojovan, "The Modified Random Network (MRN) Model within the Configuron Percolation Theory (CPT) of Glass Transition," *Ceramics,* vol. 4, no. 2, pp. 121-134, 2021.

[16] E. Riebling, "Structure of sodium aluminosilicate melts containing at least 50 mole% SiO2 at 1500° C," *The Journal of Chemical Physics,* vol. 44, no. 8, pp. 2857-2865, 1966.

[17] M. J. Toplis, S. C. Kohn, M. E. Smith, and I. J. Poplett, "Fivefold-coordinated aluminum in tectosilicate glasses observed by triple quantum MAS NMR," *American Mineralogist,* vol. 85, no. 10, pp. 1556-1560, 2000.

[18] S. H. Risbud, R. J. Kirkpatrick, A. P. Taglialavore, and B. Montez, "Solid-state NMR Evidence of 4-, 5, and 6-Fold Aluminum Sites in Roller-Quenched SiO2-A12O3 Glasses," *Journal of the American Ceramic Society,* vol. 70, no. 1, 1987.

[19] M. J. Toplis, D. B. Dingwell, and T. Lenci, "Peraluminous viscosity maxima in Na2O□ Al2O3□ SiO2 liquids: The role of triclusters in tectosilicate melts," *Geochimica et Cosmochimica Acta,* vol. 61, no. 13, pp. 2605-2612, 1997.

[20] E. Lacy, "Aluminum in glasses and melts," *Phys. Chem. Glasses,* vol. 4, no. 6, pp. 234-238, 1963.

[21] D. M. Zirl and S. H. Garofalini, "Structure of sodium aluminosilicate glasses," *Journal of the American Ceramic Society,* vol. 73, no. 10, pp. 2848-2856, 1990.

[22] D. E. Day and G. E. Rindone, "Properties of soda aluminosilicate glasses: I, refractive index, density, molar refractivity, and infrared absorption spectra," *Journal of the American Ceramic Society,* vol. 45, no. 10, pp. 489-496, 1962.

[23] D. E. DAY and G. E. Rindone, "Properties of soda aluminosilicate glasses: II, internal friction," *Journal of the American Ceramic Society,* vol. 45, no. 10, pp. 496-504, 1962.

[24] P. I. Onorato, M. N. Alexander, C. W. Struck, G. W. Tasker, and D. Uhlmann, "Bridging and nonbridging oxygen atoms in alkali aluminosilicate glasses," *Journal of the American Ceramic Society,* vol. 68, no. 6, 1985.

[25] G. Tasker, D. Uhlmann, P. Onorato, M. Alexander, and C. Struck, "Structure of sodium aluminosilicate glasses: X-ray photoelectron spectroscopy," *Le Journal de Physique Colloques,* vol. 46, no. C8, pp. C8-273-C8-280, 1985.

[26] H. Maekawa, T. Maekawa, K. Kawamura, and T. Yokokawa, "Silicon-29 MAS NMR investigation of the sodium oxide-alumina-silica glasses," *The Journal of Physical Chemistry,* vol. 95, no. 18, pp. 6822-6827, 1991.

[27] J. F. Stebbins and Z. Xu, "NMR evidence for excess non-bridging oxygen in an aluminosilicate glass," *Nature,* vol. 390, no. 6655, p. 60, 1997.

[28] B. Smets and T. Lommen, "Incorporation of aluminum oxide and boron oxide in sodium silicate glasses, studied by X-ray photoelectron spectroscopy," *Physics and Chemistry of Glasses,* vol. 22, pp. 158-62, 1981.

[29] D. M. Zirl and S. H. Garofalini, "Structure of sodium aluminosilicate glass surfaces," *Journal of the American Ceramic Society,* vol. 75, no. 9, pp. 2353-2362, 1992.

[30] J. Isard, "The mixed alkali effect in glass," *Journal of Non-Crystalline Solids,* vol. 1, no. 3, pp. 235-261, 1969.

[31] M. D. Ingram, "The mixed alkali effect revisited-a new look at an old problem," *Glastechnische Berichte,* vol. 67, no. 6, pp. 151-155, 1994.

[32] J. Swenson and S. Adams, "Mixed alkali effect in glasses," *Physical review letters,* vol. 90, no. 15, p. 155507, 2003.

[33] P. Hayward, "Mixed-alkali effect in aluminosilicate glasses: II, The effect of nonbridging oxygen content," *Physics and Chemistry of Glasses,* vol. 18, no. 1, pp. 1-6, 1977.

[34] A. Rodrigues, S. Fearn, and M. Vilarigues, "Mixed reactions: glass durability and the mixed-alkali effect," *Journal of the American Ceramic Society*.

[35] P. Maass, "Towards a theory for the mixed alkali effect in glasses," *Journal of non-crystalline solids,* vol. 255, no. 1, pp. 35-46, 1999.

[36] J. Kjeldsen, M. M. Smedskjaer, J. C. Mauro, R. E. Youngman, L. Huang, and Y. Yue, "Mixed alkaline earth effect in sodium aluminosilicate glasses," *Journal of Non-Crystalline Solids,* vol. 369, pp. 61-68, 2013.
[37] E. Rysiakiewicz-Pasek, "The measurements of ionic conductivity in mixed alkali-aluminosilicate glasses," in *[1992] Proceedings of the 4th International Conference on Conduction and Breakdown in Solid Dielectrics*, 1992: IEEE, pp. 107-110.
[38] D. E. Day, "Mixed alkali glasses—their properties and uses," *Journal of Non-Crystalline Solids,* vol. 21, no. 3, pp. 343-372, 1976.
[39] C. J. Wilkinson *et al.*, "Topological origins of the mixed alkali effect in glass," *The Journal of Physical Chemistry B,* vol. 123, no. 34, pp. 7482-7489, 2019.
[40] M. Tomozawa, "Water in glass," *Journal of Non-Crystalline Solids,* vol. 73, no. 1-3, pp. 197-204, 1985.
[41] M. Tomozawa, D. Cherniak, and P. Lezzi, "Hydrogen-to-alkali ratio in hydrated alkali aluminosilicate glass surfaces," *Journal of Non-Crystalline Solids,* vol. 358, no. 24, pp. 3546-3550, 2012.
[42] J. Acocella, M. Tomozawa, and E. Watson, "The nature of dissolved water in sodium silicate glasses and its effect on various properties," *Journal of Non-Crystalline Solids,* vol. 65, no. 2-3, pp. 355-372, 1984.
[43] R. F. Bartholomew, "Water in glass," *Treatise on Materials Science & Technology,* vol. 22, pp. 75-127, 1982.
[44] G. HATHERINGTON, "Water in vitreous silica Part 1. Influence of water content on the properties of vitreous silica," *Physics and Chemistry of Glasses,* vol. 3, pp. 129-133, 1962.
[45] H. Scholze, "Gasses and water in glass," *Glass Ind,* vol. 47, no. 10, pp. 546-51, 1966.
[46] H. Scholze, *Glass: nature, structure, and properties*. Springer Science & Business Media, 2012.
[47] J. Shelby and G. McVay, "Influence of water on the viscosity and thermal expansion of sodium trisilicate glasses," *Journal of Non-Crystalline Solids,* vol. 20, no. 3, pp. 439-449, 1976.
[48] M. Takata, J. Acocella, M. Tomozawa, and E. Watson, "Effect of Water Content on the Electrical Conductivity of Na2O≅ 3SiO2 Glass," *Journal of the American Ceramic Society,* vol. 64, no. 12, pp. 719-724, 1981.
[49] L. Wondraczek *et al.*, "Towards ultrastrong glasses," ed: Wiley Online Library, 2011.
[50] C. M. Jantzen, K. G. Brown, and J. B. Pickett, "Durable glass for thousands of years," *International Journal of Applied Glass Science,* vol. 1, no. 1, pp. 38-62, 2010.
[51] J. Du and A. N. Cormack, "Molecular dynamics simulation of the structure and hydroxylation of silica glass surfaces," *Journal of the American Ceramic Society,* vol. 88, no. 9, pp. 2532-2539, 2005.
[52] C. J. Wilkinson *et al.*, "Topological control of water reactivity on glass surfaces: evidence of a chemically stable intermediate phase," *The journal of physical chemistry letters,* vol. 10, no. 14, pp. 3955-3960, 2019.
[53] L. Deng *et al.*, "Reaction mechanisms and interfacial behaviors of sodium silicate glass in an aqueous environment from reactive force field-based molecular dynamics

simulations," *The Journal of Physical Chemistry C,* vol. 123, no. 35, pp. 21538-21547, 2019.
[54] G. S. Frankel *et al.*, "A comparative review of the aqueous corrosion of glasses, crystalline ceramics, and metals," *npj Materials Degradation,* vol. 2, no. 1, pp. 1-17, 2018.
[55] D. E. Clark, M. Dilmore, E. Ethridge, and L. Hench, "Aqueous corrosion of soda-silica and soda-lime-silica glass," *Journal of the American Ceramic Society,* vol. 59, no. 1-2, pp. 62-65, 1976.
[56] C. Cailleteau *et al.*, "Insight into silicate-glass corrosion mechanisms," *Nature materials,* vol. 7, no. 12, p. 978, 2008.
[57] S. Aryal, M. Gao, L. Ouyang, P. Rulis, and W. Ching, "Ab initio studies of Mo-based alloys: Mechanical, elastic, and vibrational properties," *Intermetallics,* vol. 38, pp. 116-125, 2013.
[58] T. Geisler, A. Janssen, D. Scheiter, T. Stephan, J. Berndt, and A. Putnis, "Aqueous corrosion of borosilicate glass under acidic conditions: a new corrosion mechanism," *Journal of Non-Crystalline Solids,* vol. 356, no. 28-30, pp. 1458-1465, 2010.
[59] S. Gin, "Open scientific questions about nuclear glass corrosion," *Procedia Materials Science,* vol. 7, pp. 163-171, 2014.
[60] R. Hellmann *et al.*, "Nanometre-scale evidence for interfacial dissolution–reprecipitation control of silicate glass corrosion," *Nature materials,* vol. 14, no. 3, p. 307, 2015.
[61] J. Du and J. M. Rimsza, "Atomistic computer simulations of water interactions and dissolution of inorganic glasses," *npj Materials Degradation,* vol. 1, no. 1, pp. 1-12, 2017.
[62] M. Takata, M. Tomozawa, and E. Watson, "Effect of water content on mechanical properties of Na2O-SiO2 glasses," *Journal of the American Ceramic Society,* vol. 65, no. 9, pp. c156-c157, 1982.
[63] K. Davis and M. Tomozawa, "Water diffusion into silica glass: structural changes in silica glass and their effect on water solubility and diffusivity," *Journal of Non-Crystalline Solids,* vol. 185, no. 3, pp. 203-220, 1995.
[64] M. Takata, M. Tomozawa, and E. Watson, "Effect of Water Content on Mechanical Properties of Na2O-SiO2 Glasses," *Journal of the American Ceramic Society,* vol. 65, no. 9, 1982.
[65] W.-T. Han and M. Tomozawa, "Effect of residual water in silica glass on static fatigue," *Journal of non-crystalline solids,* vol. 127, no. 1, pp. 97-104, 1991.
[66] S. H. Hahn and A. C. van Duin, "Surface Reactivity and Leaching of a Sodium Silicate Glass Under Aqueous Environment: A ReaxFF Molecular Dynamics Study," *The Journal of Physical Chemistry C,* 2019.
[67] C. Wickert, A. Vieira, J. Dehne, X. Wang, D. Wilder, and A. Barkatt, "Effects of salts on silicate glass dissolution in water: kinetics and mechanisms of dissolution and surface cracking," *Physics and chemistry of glasses,* vol. 40, no. 3, pp. 157-170, 1999.
[68] N. Zotov and H. Keppler, "The influence of water on the structure of hydrous sodium tetrasilicate glasses," *Am. Mineral.,* vol. 83, no. 7-8, pp. 823-834, 1998.

[69] H. Masui, D. Chen, T. Akai, and T. Yazawa, "Hydration in alkali-silicate glasses studied by two dimensional multi-quantum magic angle spinning," *Zeitschrift für Naturforschung A,* vol. 57, no. 6-7, pp. 473-478, 2002.
[70] J. Kuemmerlen, L. H. Merwin, A. Sebald, and H. Keppler, "Structural role of water in sodium silicate glasses: results from silicon-29 and proton NMR spectroscopy," *The Journal of Physical Chemistry,* vol. 96, no. 15, pp. 6405-6410, 1992.
[71] T. Schaller and A. Sebald, "One-and two-dimensional 1 H magic-angle spinning experiments on hydrous silicate glasses," *Solid State Nucl. Magn. Reson.,* vol. 5, no. 1, pp. 89-102, 1995.
[72] N. Zotov, H. Keppler, A. Hannon, and A. Soper, "The effect of water on the structure of silicate glasses—A neutron diffraction study," *Journal of Non-Crystalline Solids,* vol. 202, no. 1-2, pp. 153-163, 1996.
[73] N. Pandya, D. W. Muenow, S. K. Sharma, and B. L. Sherriff, "The speciation of water in hydrated alkali silicate glasses," *Journal of non-crystalline solids,* vol. 176, no. 2-3, pp. 140-146, 1994.
[74] H. Maekawa, T. Saito, and T. Yokokawa, "Water in silicate glass: 17O NMR of hydrous silica, albite, and Na2Si4O9 glasses," *The Journal of Physical Chemistry B,* vol. 102, no. 39, pp. 7523-7529, 1998.
[75] A. Shchukarev, J. Rosenqvist, and S. Sjöberg, "XPS study of the silica–water interface," *Journal of electron spectroscopy and related phenomena,* vol. 137, pp. 171-176, 2004.
[76] A. L. Barnette and S. H. Kim, "Coadsorption of n-propanol and water on SiO2: Study of thickness, composition, and structure of binary adsorbate layer using attenuated total reflection infrared (ATR-IR) and sum frequency generation (SFG) vibration spectroscopy," *The Journal of Physical Chemistry C,* vol. 116, no. 18, pp. 9909-9916, 2012.
[77] E. A. Leed and C. G. Pantano, "Computer modeling of water adsorption on silica and silicate glass fracture surfaces," *Journal of Non-Crystalline Solids,* vol. 325, no. 1, pp. 48-60, 2003.
[78] M. Aertsens and P. Van Iseghem, "Modelling glass dissolution with a Monte Carlo technique," *MRS Online Proceedings Library Archive,* vol. 412, 1995.
[79] S. B. Santra, B. Sapoval, P. Barboux, and F. Devreux, "Pseudo-equilibrium between a random system and a solution: a Monte-Carlo study of glass dissolution in water," *Comptes Rendus de l'Académie des Sciences-Series IIB-Mechanics-Physics-Chemistry-Astronomy,* vol. 326, no. 2, pp. 129-134, 1998.
[80] A. A. Hassanali and S. J. Singer, "Model for the water− amorphous silica interface: The undissociated surface," *The Journal of Physical Chemistry B,* vol. 111, no. 38, pp. 11181-11193, 2007.
[81] J. C. Fogarty, H. M. Aktulga, A. Y. Grama, A. C. Van Duin, and S. A. Pandit, "A reactive molecular dynamics simulation of the silica-water interface," *The Journal of chemical physics,* vol. 132, no. 17, p. 174704, 2010.
[82] S. H. Garofalini, "Molecular dynamics computer simulations of silica surface structure and adsorption of water molecules," *Journal of Non-Crystalline Solids,* vol. 120, no. 1-3, pp. 1-12, 1990.

[83] Á. Cimas, F. Tielens, M. Sulpizi, M.-P. Gaigeot, and D. Costa, "The amorphous silica–liquid water interface studied by ab initio molecular dynamics (AIMD): local organization in global disorder," *Journal of Physics: Condensed Matter,* vol. 26, no. 24, p. 244106, 2014.
[84] M. Pfeiffer-Laplaud, D. Costa, F. Tielens, M.-P. Gaigeot, and M. Sulpizi, "Bimodal acidity at the amorphous silica/water interface," *The Journal of Physical Chemistry C,* vol. 119, no. 49, pp. 27354-27362, 2015.
[85] K. Baral, A. Li, and W.-Y. Ching, "Ab initio modeling of structure and properties of single and mixed alkali silicate glasses," *The Journal of Physical Chemistry A,* vol. 121, no. 40, pp. 7697-7708, 2017.
[86] K. Baral, A. Li, and W. Y. Ching, "Understanding the atomistic origin of hydration effects in single and mixed bulk alkali-silicate glasses," *Journal of the American Ceramic Society,* vol. 102, no. 1, pp. 207-221, 2019.
[87] K. Baral, A. Li, and W.-Y. Ching, "Ab initio molecular dynamics simulation of Na-doped aluminosilicate glasses and glass-water interaction," *AIP Advances,* vol. 9, no. 7, p. 075218, 2019.
[88] K. Baral, A. Li, and W.-Y. Ching, "Ab Initio Study of Hydrolysis Effects in Single and Ion-Exchanged Alkali Aluminosilicate Glasses," *The Journal of Physical Chemistry B,* vol. 124, no. 38, pp. 8418-8433, 2020.
[89] P. Hohenberg and W. Kohn, "Inhomogeneous electron gas," *Physical review,* vol. 136, no. 3B, p. B864, 1964.
[90] W. Kohn and L. J. Sham, "Self-consistent equations including exchange and correlation effects," *Physical review,* vol. 140, no. 4A, p. A1133, 1965.
[91] G. Kresse and J. Furthmüller, "Vienna ab-initio simulation package (VASP)," *Vienna: Vienna University,* 2001.
[92] G. Kresse and D. Joubert, "From ultrasoft pseudopotentials to the projector augmented-wave method," *Physical review b,* vol. 59, no. 3, p. 1758, 1999.
[93] W.-Y. Ching and P. Rulis, *Electronic Structure Methods for Complex Materials: The orthogonalized linear combination of atomic orbitals*. Oxford University Press, 2012.
[94] S. Blinder, "Basic concepts of self-consistent-field theory," *American journal of physics,* vol. 33, no. 6, pp. 431-443, 1965.
[95] C. Møller and M. S. Plesset, "Note on an approximation treatment for many-electron systems," *Physical review,* vol. 46, no. 7, p. 618, 1934.
[96] L. Hedin, "New method for calculating the one-particle Green's function with application to the electron-gas problem," *Physical Review,* vol. 139, no. 3A, p. A796, 1965.
[97] C. Hampel, K. A. Peterson, and H.-J. Werner, "A comparison of the efficiency and accuracy of the quadratic configuration interaction (QCISD), coupled cluster (CCSD), and Brueckner coupled cluster (BCCD) methods," *Chemical physics letters,* vol. 190, no. 1-2, pp. 1-12, 1992.
[98] K. Capelle, "A bird's-eye view of density-functional theory," *Brazilian journal of physics,* vol. 36, pp. 1318-1343, 2006.
[99] E. Teller, "On the stability of molecules in the Thomas-Fermi theory," *Reviews of Modern Physics,* vol. 34, no. 4, p. 627, 1962.

[100] J. P. Perdew, K. Burke, and M. Ernzerhof, "Generalized gradient approximation made simple," *Physical review letters*, vol. 77, no. 18, p. 3865, 1996.
[101] A. D. Becke, "Density-functional exchange-energy approximation with correct asymptotic behavior," *Physical review A*, vol. 38, no. 6, p. 3098, 1988.
[102] C. Lee, W. Yang, and R. G. Parr, "Development of the Colle-Salvetti correlation-energy formula into a functional of the electron density," *Physical review B*, vol. 37, no. 2, p. 785, 1988.
[103] G. Kresse and J. Furthmüller, "Software VASP, vienna (1999)," *Phys. Rev. B*, vol. 54, no. 11, p. 169, 1996.
[104] P. E. Blöchl, "Projector augmented-wave method," *Physical review B*, vol. 50, no. 24, p. 17953, 1994.
[105] D. Vanderbilt, "Soft self-consistent pseudopotentials in a generalized eigenvalue formalism," *Physical review B*, vol. 41, no. 11, p. 7892, 1990.
[106] G. Kresse and J. Hafner, "Norm-conserving and ultrasoft pseudopotentials for first-row and transition elements," *Journal of Physics: Condensed Matter*, vol. 6, no. 40, p. 8245, 1994.
[107] G. Kresse, J. Hafner, and R. Needs, "Optimized norm-conserving pseudopotentials," *Journal of Physics: Condensed Matter*, vol. 4, no. 36, p. 7451, 1992.
[108] D. Bylander, L. Kleinman, and S. Lee, "Self-consistent calculations of the energy bands and bonding properties of B 12 C 3," *Physical Review B*, vol. 42, no. 2, p. 1394, 1990.
[109] E. Davidson, "Methods in computational molecular physics," in *NATO Advanced Study Institute, Series C*, 1983, vol. 113: Plenum New York, p. 95.
[110] D. Wood and A. Zunger, "A new method for diagonalising large matrices," *Journal of Physics A: Mathematical and General*, vol. 18, no. 9, p. 1343, 1985.
[111] J. Hafner and G. Kresse, "The vienna ab-initio simulation program VASP: An efficient and versatile tool for studying the structural, dynamic, and electronic properties of materials," in *Properties of Complex Inorganic Solids*: Springer, 1997, pp. 69-82.
[112] P. Pulay, "Convergence acceleration of iterative sequences. The case of SCF iteration," *Chemical Physics Letters*, vol. 73, no. 2, pp. 393-398, 1980.
[113] D. D. Johnson, "Modified Broyden's method for accelerating convergence in self-consistent calculations," *Physical Review B*, vol. 38, no. 18, p. 12807, 1988.
[114] R. Stadler, W. Wolf, R. Podloucky, G. Kresse, J. Furthmüller, and J. Hafner, "Ab initio calculations of the cohesive, elastic, and dynamical properties of CoSi 2 by pseudopotential and all-electron techniques," *Physical Review B*, vol. 54, no. 3, p. 1729, 1996.
[115] O. Nielsen and R. M. Martin, "First-principles calculation of stress," *Physical Review Letters*, vol. 50, no. 9, p. 697, 1983.
[116] W. Voigt, *Lehrbuch der kristallphysik:(mit ausschluss der kristalloptik)*. BG Teubner, 1910.
[117] A. Reuß, "Berechnung der fließgrenze von mischkristallen auf grund der plastizitätsbedingung für einkristalle," *ZAMM-Journal of Applied Mathematics and Mechanics/Zeitschrift für Angewandte Mathematik und Mechanik*, vol. 9, no. 1, pp. 49-58, 1929.

[118] R. Hill, "The elastic behaviour of a crystalline aggregate," *Proceedings of the Physical Society. Section A*, vol. 65, no. 5, p. 349, 1952.
[119] N. Li and W.-Y. Ching, "Structural, electronic and optical properties of a large random network model of amorphous SiO2 glass," *Journal of non-crystalline solids*, vol. 383, pp. 28-32, 2014.
[120] N. Li, R. Sakidja, S. Aryal, and W.-Y. Ching, "Densification of a continuous random network model of amorphous SiO 2 glass," *Physical Chemistry Chemical Physics*, vol. 16, no. 4, pp. 1500-1514, 2014.
[121] K. Baral, P. Adhikari, and W. Y. Ching, "Ab initio Modeling of the Electronic Structures and Physical Properties of a-Si1− xGexO2 Glass (x= 0 to 1)," *Journal of the American Ceramic Society*, vol. 99, no. 11, pp. 3677-3684, 2016.
[122] K. Baral and W.-Y. Ching, "Electronic structures and physical properties of Na2O doped silicate glass," *Journal of Applied Physics*, vol. 121, no. 24, p. 245103, 2017.
[123] L. Liang, P. Rulis, L. Ouyang, and W. Ching, "Ab initio investigation of hydrogen bonding and network structure in a supercooled model of water," *Physical Review B*, vol. 83, no. 2, p. 024201, 2011.
[124] L. Poudel, N. F. Steinmetz, R. H. French, V. A. Parsegian, R. Podgornik, and W.-Y. Ching, "Implication of the solvent effect, metal ions and topology in the electronic structure and hydrogen bonding of human telomeric G-quadruplex DNA," *Physical Chemistry Chemical Physics*, vol. 18, no. 31, pp. 21573-21585, 2016.
[125] J. Eifler, R. Podgornik, N. F. Steinmetz, R. H. French, V. A. Parsegian, and W. Y. Ching, "Charge distribution and hydrogen bonding of a collagen α2-chain in vacuum, hydrated, neutral, and charged structural models," *International Journal of Quantum Chemistry*, vol. 116, no. 9, pp. 681-691, 2016.
[126] B. Jawad, L. Poudel, R. Podgornik, N. F. Steinmetz, and W.-Y. Ching, "Molecular mechanism and binding free energy of doxorubicin intercalation in DNA," *Physical Chemistry Chemical Physics*, vol. 21, no. 7, pp. 3877-3893, 2019.
[127] R. S. Mulliken, "Electronic population analysis on LCAO–MO molecular wave functions. I," *The Journal of Chemical Physics*, vol. 23, no. 10, pp. 1833-1840, 1955.
[128] R. Mulliken, "Electronic population analysis on LCAO–MO molecular wave functions. II. Overlap populations, bond orders, and covalent bond energies," *The Journal of Chemical Physics*, vol. 23, no. 10, pp. 1841-1846, 1955.
[129] R. Mulliken, "Electronic population analysis on LCAO-MO molecular wave functions. IV. Bonding and antibonding in LCAO and valence-bond theories," *The Journal of Chemical Physics*, vol. 23, no. 12, pp. 2343-2346, 1955.
[130] T. Bakos, S. Rashkeev, and S. Pantelides, "H 2 O and O 2 molecules in amorphous SiO 2: defect formation and annihilation mechanisms," *Physical Review B*, vol. 69, no. 19, p. 195206, 2004.
[131] G. Hetherington and K. Jack, "Water in Vitreous Silica–Part I: Influence of," *Water" Content on the Properties of Vitreous Silica," Phys. Chem. Glasses*, vol. 3, no. 4, pp. 129-33, 1962.
[132] H. Eckert, J. P. Yesinowski, L. A. Silver, and E. M. Stolper, "Water in silicate glasses: quantitation and structural studies by proton solid echo and magic angle spinning NMR methods," *The Journal of Physical Chemistry*, vol. 92, no. 7, pp. 2055-2064, 1988.

[133] R. Bartholomew and J. Schreurs, "Wide-line NMR study of protons in hydrosilicate glasses of different water content," *Journal of Non-Crystalline Solids,* vol. 38, pp. 679-684, 1980.
[134] R. Bartholomew, B. Butler, H. Hoover, and C. Wu, "Infrared spectra of a water-containing glass," *Journal of the American Ceramic Society,* vol. 63, no. 9-10, pp. 481-485, 1980.
[135] S. M. Wiederhorn, T. Fett, G. Rizzi, M. J. Hoffmann, and J.-P. Guin, "Water penetration—its effect on the strength and toughness of silica glass," *Metallurgical and Materials Transactions A,* vol. 44, no. 3, pp. 1164-1174, 2013.
[136] T. Fett, G. Rizzi, M. J. Hoffmann, S. Wagner, and S. M. Wiederhorn, "Effect of water on the inert strength of silica glass: Role of water penetration," *Journal of the American Ceramic Society,* vol. 95, no. 12, pp. 3847-3853, 2012.
[137] R. M. Van Ginhoven, H. Jonsson, B. Park, and L. R. Corrales, "Cleavage and recovery of molecular water in silica," *The Journal of Physical Chemistry B,* vol. 109, no. 21, pp. 10936-10945, 2005.
[138] H. Franek, G. Frischat, and H. Knödler, "Reactions between aqueous solutions and glass surfaces," *Journal of Non-Crystalline Solids,* vol. 42, no. 1-3, pp. 561-567, 1980.
[139] L. L. Hench, "Physical chemistry of glass surfaces," *Journal of non-crystalline solids,* no. 26, pp. 343-369, 1977.
[140] J. Rimsza and J. Du, "Ab initio molecular dynamics simulations of the hydroxylation of nanoporous silica," *Journal of the American Ceramic Society,* vol. 98, no. 12, pp. 3748-3757, 2015.
[141] M. Tomozawa, "Alkali ionic transport in mixed alkali glasses," *Journal of non-crystalline solids,* vol. 152, no. 1, pp. 59-69, 1993.
[142] J. Habasaki and K. L. Ngai, "The mixed alkali effect in ionically conducting glasses revisited: A study by molecular dynamics simulation," *Physical Chemistry Chemical Physics,* vol. 9, no. 33, pp. 4673-4689, 2007.
[143] S. Balasubramanian and K. Rao, "A molecular dynamics study of the mixed alkali effect in silicate glasses," *Journal of non-crystalline solids,* vol. 181, no. 1-2, pp. 157-174, 1995.
[144] W. Ching, "Microscopic calculation of localized electron states in an intrinsic glass," *Physical review letters,* vol. 46, no. 9, p. 607, 1981.
[145] K. Baral, A. Li, and W.-Y. Ching, "Ab Initio Modeling of Structure and Properties of Single and Mixed Alkali Silicate Glasses," *The Journal of Physical Chemistry A,* 2017.
[146] N. Li and W.-Y. Ching, "Structural, electronic and optical properties of a large random network model of amorphous SiO 2 glass," *Journal of Non-Crystalline Solids,* vol. 383, pp. 28-32, 2014.
[147] B. Walker, C. C. Dharmawardhana, N. Dari, P. Rulis, and W.-Y. Ching, "Electronic structure and optical properties of amorphous GeO 2 in comparison to amorphous SiO 2," *Journal of Non-Crystalline Solids,* vol. 428, pp. 176-183, 2015.
[148] R. Dupree, D. Holland, P. W. McMillan, and R. Pettifer, "The structure of soda-silica glasses: a MAS NMR study," *Journal of Non-Crystalline Solids,* vol. 68, no. 2, pp. 399-410, 1984.

[149] G. Kresse and J. Furthmuller, "Vienna ab-initio simulation package (VASP): The guide," *Universität Wien, VASP-Guide*, 2002.
[150] G. Kresse, "Software vasp, vienna, 1999; g. kresse, j. furthmüller," *Phys. Rev. B*, vol. 54, no. 11, p. 169, 1996.
[151] W. Ching, "Theoretical studies of the electronic properties of ceramic materials," *Journal of the American Ceramic Society*, vol. 73, no. 11, pp. 3135-3160, 1990.
[152] H. Yao, L. Ouyang, and W. Y. Ching, "Ab initio calculation of elastic constants of ceramic crystals," *Journal of the American Ceramic Society*, vol. 90, no. 10, pp. 3194-3204, 2007.
[153] W. Voigt, "Lehrbuch der Kristallphysik (mit Ausschluss der Kristalloptik), edited by BG Teubner and JW Edwards, Leipzig Berlin," *Ann Arbor, Mich*, 1928.
[154] A. Reuss, "Berechnung der fließgrenze von mischkristallen auf grund der plastizitätsbedingung für einkristalle," *ZAMM-Journal of Applied Mathematics and Mechanics/Zeitschrift für Angewandte Mathematik und Mechanik*, vol. 9, no. 1, pp. 49-58, 1929.
[155] J. Eifler, P. Rulis, R. Tai, and W.-Y. Ching, "Computational Study of a Heterostructural Model of Type I Collagen and Implementation of an Amino Acid Potential Method Applicable to Large Proteins," *Polymers*, vol. 6, no. 2, pp. 491-514, 2014.
[156] P. C. Martin, "Sum Rules, Kramers-Kronig Relations, and Transport Coefficients in Charged Systems," *Physical Review*, vol. 161, no. 1, pp. 143-155, 1967, doi: 10.1103/PhysRev.161.143.
[157] S. Aryal, R. Sakidja, M. W. Barsoum, and W. Y. Ching, "A genomic approach to the stability, elastic, and electronic properties of the MAX phases," *physica status solidi (b)*, vol. 251, no. 8, pp. 1480-1497, 2014.
[158] C. Dharmawardhana, A. Misra, and W.-Y. Ching, "Quantum mechanical metric for internal cohesion in cement crystals," *Scientific reports*, vol. 4, 2014.
[159] C. Dharmawardhana, M. Bakare, A. Misra, and W. Y. Ching, "Nature of Interatomic Bonding in Controlling the Mechanical Properties of Calcium Silicate Hydrates," *Journal of the American Ceramic Society*, vol. 99, no. 6, pp. 2120-2130, 2016.
[160] B. Hunca, C. Dharmawardhana, R. Sakidja, and W.-Y. Ching, "Ab initio calculations of thermomechanical properties and electronic structure of vitreloy Z r 41.2 T i 13.8 C u 12.5 N i 10 B e 22.5," *Physical Review B*, vol. 94, no. 14, p. 144207, 2016.
[161] P. Adhikari, C. C. Dharmawardhana, and W. Y. Ching, "Structure and properties of Hydrogrossular mineral series," *Journal of the American Ceramic Society*.
[162] L. Poudel, C. Tamerler, A. Misra, and W.-Y. Ching, "Atomic-Scale Quantification of Interfacial Binding Between Peptides and Inorganic Crystals: The Case of Calcium Carbonate Binding Peptide on Aragonite," *The Journal of Physical Chemistry C*, 2017.
[163] P. C. Martin, "Sum rules, Kramers-Kronig relations, and transport coefficients in charged systems," *Physical Review*, vol. 161, no. 1, p. 143, 1967.
[164] A. Paul, "Chemical durability of glass," in *Chemistry of glasses*: Springer, 1982, pp. 108-147.
[165] N. P. Bansal and R. H. Doremus, *Handbook of glass properties*. Elsevier, 2013.
[166] H. Franz, "Durability and corrosion of silicate glass surfaces," *Journal of Non-Crystalline Solids*, vol. 42, no. 1-3, pp. 529-534, 1980.

[167] M. Tomozawa, C. Erwin, M. Takata, and E. Watson, "Effect of Water Content on the Chemical Durability of Na2O 3SiO2 Glass," *Journal of the American Ceramic Society,* vol. 65, no. 4, pp. 182-183, 1982.
[168] R. Jagdt, "Relaxation phenomena in alkali silicate glasses," *Glastech. Ber.,* vol. 33, no. 1, pp. 10-19, 1960.
[169] K. Matusita, S. Sakka, A. Osaka, N. Soga, and M. Kunugi, "Elastic modulus of mixed alkali glass," *Journal of Non Crystalline Solids,* vol. 16, no. 2, pp. 308-312, 1974.
[170] L. M. Thompson and J. F. Stebbins, "Non-bridging oxygen and high-coordinated aluminum in metaluminous and peraluminous calcium and potassium aluminosilicate glasses: High-resolution 17O and 27Al MAS NMR results," *American Mineralogist,* vol. 96, no. 5-6, pp. 841-853, 2011.
[171] C. Le Losq, M. R. Cicconi, G. N. Greaves, and D. R. Neuville, "Silicate glasses," in *Springer Handbook of Glass*: Springer, 2019, pp. 441-503.
[172] R. Gy, "Ion exchange for glass strengthening," *Materials Science and Engineering: B,* vol. 149, no. 2, pp. 159-165, 2008.
[173] A. K. Varshneya, "The physics of chemical strengthening of glass: room for a new view," *Journal of non-crystalline solids,* vol. 356, no. 44-49, pp. 2289-2294, 2010.
[174] A. K. Varshneya, "Chemical strengthening of glass: lessons learned and yet to be learned," *International Journal of Applied Glass Science,* vol. 1, no. 2, pp. 131-142, 2010.
[175] J. C. Mauro, C. S. Philip, D. J. Vaughn, and M. S. Pambianchi, "Glass science in the United States: current status and future directions," *International Journal of Applied Glass Science,* vol. 5, no. 1, pp. 2-15, 2014.
[176] V. Piovesan *et al.*, "Chemical durability of peraluminous glasses for nuclear waste conditioning," *npj Materials Degradation,* vol. 2, no. 1, p. 7, 2018.
[177] B. O. Mysen, "Role of Al in depolymerized, peralkaline aluminosilicate melts in the systems Li 2 O-Al 2 O 3-SiO 2, Na 2 O-Al 2 O 3-SiO 2, and K 2 O-Al 2 O 3-SiO 2," *American Mineralogist,* vol. 75, no. 1-2, pp. 120-134, 1990.
[178] C. Le Losq, D. R. Neuville, P. Florian, G. S. Henderson, and D. Massiot, "The role of Al3+ on rheology and structural changes in sodium silicate and aluminosilicate glasses and melts," *Geochimica et Cosmochimica Acta,* vol. 126, pp. 495-517, 2014.
[179] T. K. Bechgaard *et al.*, "Structure and mechanical properties of compressed sodium aluminosilicate glasses: Role of non-bridging oxygens," *Journal of Non-Crystalline Solids,* vol. 441, pp. 49-57, 2016.
[180] D. Käfer *et al.*, "Ultra-Smooth and Ultra-Strong Ion-Exchanged Glass as Substrates for Organic Electronics," *Advanced Functional Materials,* vol. 23, no. 25, pp. 3233-3238, 2013.
[181] J. D. Musgraves, J. Hu, and L. Calvez, *Springer Handbook of Glass*. Springer Nature, 2019.
[182] B. O. Mysen and M. J. Toplis, "Structural behavior of Al3+ in peralkaline, metaluminous, and peraluminous silicate melts and glasses at ambient pressure," *American Mineralogist,* vol. 92, no. 5-6, pp. 933-946, 2007.
[183] A. K. Varshneya, *Fundamentals of inorganic glasses*. Elsevier, 2013.

[184] J. F. Stebbins and Z. Xu, "NMR evidence for excess non-bridging oxygen in an aluminosilicate glass," *Nature,* vol. 390, no. 6655, pp. 60-62, 1997.
[185] S. K. Lee and J. F. Stebbins, "Disorder and the extent of polymerization in calcium silicate and aluminosilicate glasses: O-17 NMR results and quantum chemical molecular orbital calculations," *Geochimica et Cosmochimica Acta,* vol. 70, no. 16, pp. 4275-4286, 2006.
[186] D. Giordano and D. B. Dingwell, "Non-Arrhenian multicomponent melt viscosity: a model," *Earth and Planetary Science Letters,* vol. 208, no. 3-4, pp. 337-349, 2003.
[187] S. Luber, "Recent progress in computational exploration and design of functional materials," *Computational Materials Science,* vol. 161, pp. 127-134, 2019.
[188] D. Dingwell, C. Romano, and K.-U. Hess, "The effect of water on the viscosity of a haplogranitic melt under PTX conditions relevant to silicic volcanism," *Contributions to Mineralogy and Petrology,* vol. 124, no. 1, pp. 19-28, 1996.
[189] R. F. Bartholomew, "High-water containing glasses," *Journal of Non-Crystalline Solids,* vol. 56, no. 1-3, pp. 331-342, 1983.
[190] B. C. Schmidt, H. Behrens, T. Riemer, R. Kappes, and R. Dupree, "Quantitative determination of water speciation in aluminosilicate glasses: a comparative NMR and IR spectroscopic study," *Chemical geology,* vol. 174, no. 1-3, pp. 195-208, 2001.
[191] A. Oehler and M. Tomozawa, "Water diffusion into silica glass at a low temperature under high water vapor pressure," *Journal of non-crystalline solids,* vol. 347, no. 1-3, pp. 211-219, 2004.
[192] L. Silver and E. Stolper, "Water in albitic glasses," *Journal of petrology,* vol. 30, no. 3, pp. 667-709, 1989.
[193] K. Davis and M. Tomozawa, "An infrared spectroscopic study of water-related species in silica glasses," *Journal of Non-Crystalline Solids,* vol. 201, no. 3, pp. 177-198, 1996.
[194] D. B. Dingwell and B. O. Mysen, "Effects of water and fluorine on the viscosity of albite melt at high pressure: a preliminary investigation," *Earth and Planetary Science Letters,* vol. 74, no. 2-3, pp. 266-274, 1985.
[195] B. O. Mysen and P. Richet, *Silicate glasses and melts*. Elsevier, 2018.
[196] Q. Zeng, H. Nekvasil, and C. P. Grey, "In support of a depolymerization model for water in sodium aluminosilicate glasses:: Information from NMR spectroscopy," *Geochimica et Cosmochimica Acta,* vol. 64, no. 5, pp. 883-896, 2000.
[197] I. Farnan, S. Kohn, and R. Dupree, "A study of the structural role of water in hydrous silica glass using cross-polarisation magic angle spinning NMR," *Geochimica et Cosmochimica Acta,* vol. 51, no. 10, pp. 2869-2873, 1987.
[198] Z. Xu, H. Maekawa, J. V. Oglesby, and J. F. Stebbins, "Oxygen speciation in hydrous silicate glasses: An oxygen-17 NMR study," *Journal of the American Chemical Society,* vol. 120, no. 38, pp. 9894-9901, 1998.
[199] S. Kohn, R. Dupree, and M. Smith, "Proton environments and hydrogen-bonding in hydrous silicate glasses from proton NMR," *Nature,* vol. 337, no. 6207, p. 539, 1989.
[200] S. Kohn, R. Dupree, and M. Smith, "A multinuclear magnetic resonance study of the structure of hydrous albite glasses," *Geochimica et Cosmochimica Acta,* vol. 53, no. 11, pp. 2925-2935, 1989.

[201] S. Kohn, M. E. Smith, P. Dirken, E. R. van Eck, A. Kentgens, and R. Dupree, "Sodium environments in dry and hydrous albite glasses: improved 23Na solid state NMR data and their implications for water dissolution mechanisms," *Geochimica et Cosmochimica Acta,* vol. 62, no. 1, pp. 79-87, 1998.
[202] S. C. Kohn, R. Dupree, and M. G. Mortuza, "The interaction between water and aluminosilicate magmas," *Chemical Geology,* vol. 96, no. 3-4, pp. 399-409, 1992.
[203] B. Schmidt, T. Riemer, S. Kohn, H. Behrens, and R. Dupree, "Different water solubility mechanisms in hydrous glasses along the Qz-Ab join:: Evidence from NMR spectroscopy," *Geochimica et Cosmochimica Acta,* vol. 64, no. 3, pp. 513-526, 2000.
[204] D. Sykes, B. T. Poe, P. F. McMillan, R. W. Luth, and R. K. Sato, "A spectroscopic investigation of anhydrous KAlSi3O8 and NaAlSi3O8 glasses quenched from high pressure," *Geochimica et Cosmochimica Acta,* vol. 57, no. 8, pp. 1753-1759, 1993.
[205] X. Xue and M. Kanzaki, "Depolymerization effect of water in aluminosilicate glasses: Direct evidence from 1H-27Al heteronuclear correlation NMR," *American Mineralogist,* vol. 91, no. 11-12, pp. 1922-1926, 2006.
[206] X. Xue, "Water speciation in hydrous silicate and aluminosilicate glasses: Direct evidence from 29Si-1H and 27Al-1H double-resonance NMR," *American Mineralogist,* vol. 94, no. 2-3, pp. 395-398, 2009.
[207] D. Sykes and J. Kubicki, "A model for H2O solubility mechanisms in albite melts from infrared spectroscopy and molecular orbital calculations," *Geochimica et Cosmochimica Acta,* vol. 57, no. 5, pp. 1039-1052, 1993.
[208] W. J. Malfait and X. Xue, "The nature of hydroxyl groups in aluminosilicate glasses: Quantifying Si–OH and Al–OH abundances along the SiO2–NaAlSiO4 join by 1H, 27Al–1H and 29Si–1H NMR spectroscopy," *Geochimica et Cosmochimica Acta,* vol. 74, no. 2, pp. 719-737, 2010.
[209] W. J. Malfait, "The nearly complete dissociation of water in glasses with strong aluminum avoidance," *American Mineralogist,* vol. 99, no. 8-9, pp. 1648-1652, 2014.
[210] A. Mohajerani and J. Zwanziger, "Mixed alkali effect on Vickers hardness and cracking," *Journal of Non-Crystalline Solids,* vol. 358, no. 12-13, pp. 1474-1479, 2012.
[211] J. C. Lapp and J. E. Shelby, "The mixed alkali effect in lithium-sodium aluminosilicate glasses," *Journal of Non-Crystalline Solids,* vol. 95, pp. 889-896, 1987.
[212] A. H. Dietzel, "On the so-called mixed alkali effect," *Physics and chemistry of glasses,* vol. 24, no. 6, pp. 172-180, 1983.
[213] V. Belostotsky, "Defect model for the mixed mobile ion effect," *Journal of Non-Crystalline Solids,* vol. 353, no. 11-12, pp. 1078-1090, 2007.
[214] F. Lodesani, M. C. Menziani, H. Hijiya, Y. Takato, S. Urata, and A. Pedone, "Structural origins of the Mixed Alkali Effect in Alkali Aluminosilicate Glasses: Molecular Dynamics Study and its Assessment," *Scientific reports,* vol. 10, no. 1, pp. 1-18, 2020.
[215] J. Du, "Molecular Dynamics Simulations of Oxide Glasses," in *Springer Handbook of Glass*: Springer, 2019, pp. 1131-1155.
[216] R. Dongol, L. Wang, A. Cormack, and S. Sundaram, "Molecular dynamics simulation of sodium aluminosilicate glass structures and glass surface-water reactions using the reactive force field (ReaxFF)," *Applied Surface Science,* vol. 439, pp. 1103-1110, 2018.

[217] Y. Xiang, J. Du, M. M. Smedskjaer, and J. C. Mauro, "Structure and properties of sodium aluminosilicate glasses from molecular dynamics simulations," *The Journal of chemical physics*, vol. 139, no. 4, p. 044507, 2013.
[218] Y. Zhao *et al.*, "Ionic self-diffusion of Na2O–Al2O3–SiO2 glasses from molecular dynamics simulations," *Journal of Non-Crystalline Solids*, vol. 527, p. 119734, 2020.
[219] R. T. Neilson, F. J. Spera, and M. S. Ghiorso, "Thermodynamics, self-diffusion, and structure of liquid NaAlSi3O8 to 30 GPa by classical molecular dynamics simulations," *American Mineralogist*, vol. 101, no. 9, pp. 2029-2040, 2016.
[220] M. Montorsi, M. C. Menziani, C. Leonelli, G. C. Pellacani, and A. Cormack, "Molecular dynamics simulations of alumina addition in sodium silicate glasses," *Molecular Simulation*, vol. 24, no. 1-3, pp. 157-165, 2000.
[221] A. Atila, S. Ouaskit, and A. Hasnaoui, "Ionic Self-Diffusion and the Glass Transition Anomaly in Aluminosilicates," *arXiv preprint arXiv:2004.11117*, 2020.
[222] A. Atila, E. M. Ghardi, S. Ouaskit, and A. Hasnaoui, "Atomistic insights into the impact of charge balancing cations on the structure and properties of aluminosilicate glasses," *Physical Review B*, vol. 100, no. 14, p. 144109, 2019.
[223] H. Liu *et al.*, "Searching for correlations between vibrational spectral features and structural parameters of silicate glass network," *Journal of the American Ceramic Society*, vol. 103, no. 6, pp. 3575-3589, 2020.
[224] A. Tandia, K. D. Vargheese, and J. C. Mauro, "Elasticity of ion stuffing in chemically strengthened glass," *Journal of non-crystalline solids*, vol. 358, no. 12-13, pp. 1569-1574, 2012.
[225] G. Kresse and J. Furthmüller, "Vienna ab initio simulation package (VASP)," *Vienna: Vienna University*, 2001.
[226] R. J. Eagan and J. Swearekgen, "Effect of composition on the mechanical properties of aluminosilicate and borosilicate glasses," *Journal of the American Ceramic Society*, vol. 61, no. 1-2, pp. 27-30, 1978.
[227] W. Loewenstein, "The distribution of aluminum in the tetrahedra of silicates and aluminates," *Am. Mineral.*, vol. 39, pp. 92-96, 1954.
[228] G. Gutierrez and B. Johansson, "Molecular dynamics study of structural properties of amorphous Al 2 O 3," *Physical Review B*, vol. 65, no. 10, p. 104202, 2002.
[229] J. R. Allwardt, J. F. Stebbins, B. C. Schmidt, D. J. Frost, A. C. Withers, and M. M. Hirschmann, "Aluminum coordination and the densification of high-pressure aluminosilicate glasses," *American Mineralogist*, vol. 90, no. 7, pp. 1218-1222, 2005.
[230] J. R. Allwardt, B. T. Poe, and J. F. Stebbins, "The effect of fictive temperature on Al coordination in high-pressure (10 GPa) sodium aluminosilicate glasses," *American Mineralogist*, vol. 90, no. 8-9, pp. 1453-1457, 2005.
[231] M. Ren *et al.*, "Composition–structure–property relationships in alkali aluminosilicate glasses: A combined experimental–computational approach towards designing functional glasses," *Journal of Non-Crystalline Solids*, vol. 505, pp. 144-153, 2019.
[232] M. J. Toplis, D. B. Dingwell, K.-U. Hess, and T. Lenci, "Viscosity, fragility, and configurational entropy of melts along the join SiO2-NaAlSiO4," *American Mineralogist*, vol. 82, no. 9-10, pp. 979-990, 1997.

[233] Q. Zheng, M. M. Smedskjaer, R. E. Youngman, M. Potuzak, J. C. Mauro, and Y. Yue, "Influence of aluminum speciation on the stability of aluminosilicate glasses against crystallization," *Applied Physics Letters,* vol. 101, no. 4, p. 041906, 2012.
[234] H. Moore and P. McMillan, "Study of Glasses Consisting of the Oxides of Elements of Low Atomic Weight: II, Absorptions Characteristic of Certain of the Experimental Glasses," *J. Soc. Glass Technol.,* vol. 40, no. 193, pp. 97-138T, 1956.
[235] J. F. Stebbins, J. Wu, and L. M. Thompson, "Interactions between network cation coordination and non-bridging oxygen abundance in oxide glasses and melts: Insights from NMR spectroscopy," *Chemical Geology,* vol. 346, pp. 34-46, 2013.
[236] J. F. Stebbins, E. V. Dubinsky, K. Kanehashi, and K. E. Kelsey, "Temperature effects on non-bridging oxygen and aluminum coordination number in calcium aluminosilicate glasses and melts," *Geochimica et Cosmochimica Acta,* vol. 72, no. 3, pp. 910-925, 2008.
[237] I. Haslingerova, "Estimation of bond energies from mulliken overlap populations," *Czechoslovak Journal of Physics B,* vol. 27, no. 12, pp. 1389-1393, 1977.
[238] V. R. Bhardwaj *et al.*, "Femtosecond laser-induced refractive index modification in multicomponent glasses," *Journal of applied physics,* vol. 97, no. 8, p. 083102, 2005.
[239] J. F. Schairer and N. L. Bowen, "The system Na 2 O-Al 2 O 3-SiO 2," *American Journal of Science,* vol. 254, no. 3, pp. 129-195, 1956.
[240] A. Pedone, G. Malavasi, A. N. Cormack, U. Segre, and M. C. Menziani, "Insight into elastic properties of binary alkali silicate glasses; prediction and interpretation through atomistic simulation techniques," *Chemistry of Materials,* vol. 19, no. 13, pp. 3144-3154, 2007.
[241] T. Rouxel, "Elastic properties and short-to medium-range order in glasses," *Journal of the American Ceramic Society,* vol. 90, no. 10, pp. 3019-3039, 2007.
[242] C. L. Allred, X. Yuan, M. Z. Bazant, and L. W. Hobbs, "Elastic constants of defected and amorphous silicon with the environment-dependent interatomic potential," *Physical Review B,* vol. 70, no. 13, p. 134113, 2004.
[243] C. Weigel *et al.*, "Elastic moduli of XAlSiO4 aluminosilicate glasses: effects of charge-balancing cations," *Journal of Non-Crystalline Solids,* vol. 447, pp. 267-272, 2016.
[244] S. Gin, P. Jollivet, M. Fournier, F. Angeli, P. Frugier, and T. Charpentier, "Origin and consequences of silicate glass passivation by surface layers," *Nature communications,* vol. 6, no. 1, pp. 1-8, 2015.
[245] C. Cailleteau *et al.*, "Insight into silicate-glass corrosion mechanisms," *Nature materials,* vol. 7, no. 12, pp. 978-983, 2008.
[246] Y. Zhou *et al.*, "Strategies to direct vascularisation using mesoporous bioactive glass-based biomaterials for bone regeneration," *International Materials Reviews,* vol. 62, no. 7, pp. 392-414, 2017.
[247] H. Liu, D. Ngo, M. Ren, J. Du, and S. H. Kim, "Effects of surface initial condition on aqueous corrosion of glass—A study with a model nuclear waste glass," *Journal of the American Ceramic Society,* vol. 102, no. 4, pp. 1652-1664, 2019.
[248] H. Kaya, D. Ngo, N. J. Smith, S. Gin, and S. H. Kim, "Network structure in alteration layer of boroaluminosilicate glass formed by aqueous corrosion," *Journal of Non-Crystalline Solids,* vol. 553, p. 120494, 2021.

[249] L. Deng *et al.*, "Ion-exchange mechanisms and interfacial reaction kinetics during aqueous corrosion of sodium silicate glasses," *npj Materials Degradation,* vol. 5, no. 1, pp. 1-13, 2021.
[250] R. Hellmann, "Mechanisms of Glass Corrosion by Aqueous Solutions," *Encyclopedia of Glass Science, Technology, History, and Culture,* vol. 1, pp. 647-662, 2021.
[251] N. Stone-Weiss, R. E. Youngman, R. Thorpe, N. J. Smith, E. M. Pierce, and A. Goel, "An insight into the corrosion of alkali aluminoborosilicate glasses in acidic environments," *Physical Chemistry Chemical Physics,* vol. 22, no. 4, pp. 1881-1896, 2020.
[252] M. Dathe *et al.*, "Dissolution of sodium silicate glasses for the production of water glass–part IV: characterisation of reaction layer and glass surface," *Glass Technology-European Journal of Glass Science and Technology Part A,* vol. 62, no. 1, pp. 9-23, 2021.
[253] S. Gin *et al.*, "Insights into the mechanisms controlling the residual corrosion rate of borosilicate glasses," *Npj Materials Degradation,* vol. 4, no. 1, pp. 1-9, 2020.
[254] T. S. Mahadevan and J. Du, "Hydration and reaction mechanisms on sodium silicate glass surfaces from molecular dynamics simulations with reactive force fields," *Journal of the American Ceramic Society,* vol. 103, no. 6, pp. 3676-3690, 2020.
[255] S. Gin, J.-M. Delaye, F. Angeli, and S. Schuller, "Aqueous alteration of silicate glass: state of knowledge and perspectives," *npj Materials Degradation,* vol. 5, no. 1, pp. 1-20, 2021.
[256] H. Jabraoui, S. Gin, T. Charpentier, R. Pollet, and J.-M. Delaye, "Leaching and Reactivity at the Sodium Aluminosilicate Glass–Water Interface: Insights from a ReaxFF Molecular Dynamics Study," *The Journal of Physical Chemistry C,* 2021.
[257] H. Mei *et al.*, "Effects of water on the mechanical properties of silica glass using molecular dynamics," *Acta Materialia,* vol. 178, pp. 36-44, 2019.
[258] A. R. Potter, C. J. Wilkinson, S. H. Kim, and J. C. Mauro, "Effect of water on topological constraints in silica glass," *Scripta Materialia,* vol. 160, pp. 48-52, 2019.
[259] B. Bunker, "Molecular mechanisms for corrosion of silica and silicate glasses," *Journal of Non-Crystalline Solids,* vol. 179, pp. 300-308, 1994.
[260] W. Zhao, K. Li, P. Lin, K. Xu, and S. Tan, "Dissolution of Cl in alkaline earth (Ca, Sr, Ba) aluminosilicate glasses," *Journal of Non-Crystalline Solids,* vol. 516, pp. 56-62, 2019.
[261] J. Webster, R. Kinzler, and E. Mathez, "Chloride and water solubility in basalt and andesite melts and implications for magmatic degassing," *Geochimica et Cosmochimica Acta,* vol. 63, no. 5, pp. 729-738, 1999.
[262] D. E. Perea *et al.*, "Tomographic mapping of the nanoscale water-filled pore structure in corroded borosilicate glass," *npj Materials Degradation,* vol. 4, no. 1, pp. 1-7, 2020.
[263] S. Ong, X. Zhao, and K. B. Eisenthal, "Polarization of water molecules at a charged interface: second harmonic studies of the silica/water interface," *Chemical Physics Letters,* vol. 191, no. 3-4, pp. 327-335, 1992.
[264] J. Rimsza and J. Du, "Interfacial structure and evolution of the water–silica gel system by reactive force-field-based molecular dynamics simulations," *The Journal of Physical Chemistry C,* vol. 121, no. 21, pp. 11534-11543, 2017.

[265] S. Aryal, P. Rulis, and W. Y. Ching, "Mechanical properties and electronic structure of mullite phases using first-principles modeling," *Journal of the American Ceramic Society*, vol. 95, no. 7, pp. 2075-2088, 2012.
[266] S. Hasan, P. Adhikari, K. Baral, and W.-Y. Ching, "Conspicuous interatomic bonding in chalcogenide crystals and implications on electronic, optical, and elastic properties," *AIP Advances*, vol. 10, no. 7, p. 075216, 2020.
[267] S. Hasan, K. Baral, N. Li, and W.-Y. Ching, "Structural and physical properties of 99 complex bulk chalcogenides crystals using first-principles calculations," *Scientific reports*, vol. 11, no. 1, pp. 1-18, 2021.
[268] B. Jawad, L. Poudel, R. Podgornik, and W.-Y. Ching, "Thermodynamic dissection of the intercalation binding process of doxorubicin to dsDNA with implications of ionic and solvent effects," *The Journal of Physical Chemistry B*, vol. 124, no. 36, pp. 7803-7818, 2020.
[269] L. Poudel, C. Tamerler, A. Misra, and W.-Y. Ching, "Atomic-scale quantification of interfacial binding between peptides and inorganic crystals: The case of calcium carbonate binding peptide on aragonite," *The Journal of Physical Chemistry C*, vol. 121, no. 51, pp. 28354-28363, 2017.
[270] W.-Y. Ching, P. Adhikari, B. Jawad, and R. Podgornik, "Ultra-large-scale ab initio quantum chemical computation of bio-molecular systems: The case of spike protein of SARS-CoV-2 virus," *Computational and Structural Biotechnology Journal*, vol. 19, pp. 1288-1301, 2021.
[271] S. Nosé, "A unified formulation of the constant temperature molecular dynamics methods," *The Journal of chemical physics*, vol. 81, no. 1, pp. 511-519, 1984.
[272] S. Nosé, "A molecular dynamics method for simulations in the canonical ensemble," *Molecular physics*, vol. 52, no. 2, pp. 255-268, 1984.
[273] G. A. Rosales-Sosa, A. Masuno, Y. Higo, and H. Inoue, "Crack-resistant Al 2 O 3–SiO 2 glasses," *Scientific reports*, vol. 6, no. 1, pp. 1-7, 2016.

VITA

Khagendra Baral was born on 1980 in Jhapa, Nepal. He completed his schooling from Janata Higher Secondary School. He completed his Bachelor of Science (B.Sc.) and Master of Science (M.Sc.) from Tribhuvan University, Nepal.

In 2014, Mr. Baral came to the United States as a graduate student in the Department of Physics and Astronomy at the University of Missouri-Kansas City. In the same year, he started his Interdisciplinary Ph.D. program in Physics with Chemistry as a co-discipline. While studying IPhD degree, Mr. Baral worked as a Graduate Teaching Assistant in the Physics Department for his initial two years. After that, he worked as a Graduate Research Assistant in the Electronic Structure Group under the supervision of Professor Wai-Yim Ching.

Mr. Baral is a member of the American Ceramic Society (ACerS), Biophysical Society (BPS), Nepal Physical Society (NPS), and Association of Nepali Physicists in America (ANPA). Mr. Baral has authored or co-authored 12 scientific papers in peer-reviewed journals. In addition, he has presented three posters and four conference talks.

PUBLICATIONS

1. Y. Li, K. Shetye, K. Baral, L. Jin, J. D. Oster, D.-M. Zhu, and Z. Peng., "Main-chain polyoxometalate-containing donor–acceptor conjugated copolymers: synthesis, characterization, morphological studies and applications in single-component photovoltaic cells," *RSC advances*, vol. 6, no. 36, pp. 29909-29919, 2016.
2. K. Baral, P. Adhikari, and W. Y. Ching, "Ab initio Modeling of the Electronic Structures and Physical Properties of a-Si1− xGexO2 Glass (x= 0 to 1)," *Journal of the American Ceramic Society*, vol. 99, no. 11, pp. 3677-3684, 2016.
3. K. Baral and W.-Y. Ching, "Electronic structures and physical properties of Na2O doped silicate glass," *Journal of Applied Physics*, vol. 121, no. 24, p. 245103, 2017.
4. K. Baral, A. Li, and W.-Y. Ching, "Ab initio modeling of structure and properties of single and mixed alkali silicate glasses," *The Journal of Physical Chemistry A*, vol. 121, no. 40, pp. 7697-7708, 2017.
5. K. Baral, A. Li, and W. Y. Ching, "Understanding the atomistic origin of hydration effects in single and mixed bulk alkali-silicate glasses," *Journal of the American Ceramic Society*, vol. 102, no. 1, pp. 207-221, 2019.
6. K. Baral, A. Li, and W.-Y. Ching, "Ab initio molecular dynamics simulation of Na-doped aluminosilicate glasses and glass-water interaction," *AIP Advances*, vol. 9, no. 7, p. 075218, 2019.
7. W.-Y. Ching, L. Poudel, S. San, and K. Baral, "Interfacial interaction between suolunite crystal and silica binding peptide for novel bioinspired cement," *ACS combinatorial science*, vol. 21, no. 12, pp. 794-804, 2019.
8. S. Hasan, P. Adhikari, K. Baral, and W.-Y. Ching, "Conspicuous interatomic bonding in chalcogenide crystals and implications on electronic, optical, and elastic properties," *AIP Advances*, vol. 10, no. 7, p. 075216, 2020.
9. K. Baral, A. Li, and W.-Y. Ching, "Ab Initio Study of Hydrolysis Effects in Single and Ion-Exchanged Alkali Aluminosilicate Glasses," *The Journal of Physical Chemistry B*, vol. 124, no. 38, pp. 8418-8433, 2020.
10. K. Baral, S. San, R. Sakidja, A. Couet, K. Sridharan, and W.-Y. Ching, "Temperature-dependent properties of molten Li2BeF4 Salt using Ab initio molecular dynamics," *ACS omega*, vol. 6, no. 30, pp. 19822-19835, 2021.
11. S. Hasan, K. Baral, N. Li, and W.-Y. Ching, "Structural and physical properties of 99 complex bulk chalcogenides crystals using first-principles calculations," *Scientific reports*, vol. 11, no. 1, pp. 1-18, 2021.
12. K. Baral, P. Adhikari, B. Jawad, R. Podgornik, and W.-Y. Ching, "Solvent Effect on the Structure and Properties of RGD Peptide (1FUV) at Body Temperature (310 K) Using Ab Initio Molecular Dynamics," *Polymers*, vol. 13, no. 19, p. 3434, 2021.